



universität
uulm

Institute of Physiological Chemistry, Ulm University

Head: Prof. Dr. Thomas Wirth

Cyclin D3 is essential for the maintenance of B-cell acute lymphoblastic leukemia

DISSERTATION

**Dissertation submitted in partial fulfillment of the requirements for the
degree of „Doctor rerum naturalium” (Dr. rer. nat.) of the
International Graduate School in Molecular Medicine Ulm**

Franz Ketzer

Born in Landshut

2022

Current dean of the medical faculty:

Prof. Dr. Thomas Wirth

Current chairman of the International Graduate School in
Molecular Medicine Ulm:

Prof. Dr. Bernd Knöll

Thesis Advisory Committee:

First supervisor:

Prof. Dr. Thomas Wirth, Institute of Physiological Chemistry
Ulm University

Second supervisor:

Prof. Dr. Ralf Marienfeld, Institute of Pathology
University Clinic Ulm

Third supervisor:

Prof. Dr. Markus Müschen, Center of Molecular and Cellular Oncology
Yale School of Medicine

External reviewer:

Prof. Dr. Lars-Oliver Klotz, Nutrigenomics Section
Friedrich-Schiller-University Jena

Day doctorate awarded:

24.03.2022

Copyright notification

Results gained from my thesis have been published in the article

CCND3 is indispensable for the maintenance of B-cell acute lymphoblastic leukemia

by Franz Ketzer, Hend Abdelrasoul, Mona Vogel, Ralf Marienfeld, Markus Müschen, Hassan Jumaa, Thomas Wirth & Alexey Ushmorov.

Oncogenesis **11**, 1 (2022).

DOI: <https://doi.org/10.1038/s41389-021-00377-0>

License: Creative Commons Attribution 4.0 International License,
<http://creativecommons.org/licenses/by/4.0/>

Acknowledgments

Aus Datenschutzgründen entfernt.

Aus Datenschutzgründen entfernt.

Contents

Table of contents	VII
List of abbreviations	VIII
1 Introduction	1
1.1 B-cell development	1
1.2 B-cell acute lymphoblastic leukemia (B-ALL)	8
1.2.1 Risk-factors for B-ALL	9
1.2.2 Pathophysiology of B-ALL	10
1.2.3 Therapy of B-ALL	12
1.3 Forkhead Box Class O1 (FOXO1)	14
1.4 Cyclin D3 (CCND3)	17
1.4.1 Cell cycle as a therapeutic target in cancer	20
1.5 Aim of the thesis	23
2 Materials and Methods	24
2.1 Materials	24
2.1.1 Reagents	24
2.1.2 Plasticware	29
2.1.3 Technical laboratory equipment	29
2.1.4 Websites and software	30
2.1.5 Vectors	30
2.1.6 Antibodies	32
2.2 Methods	32
2.2.1 Bioinformatical methods	32
2.2.2 Cell culture	36
2.2.3 Molecular biological methods	40
2.2.4 Gene expression analysis	49

3	Results	53
3.1	CCND3 is the highest expressed D-type Cyclin in B-ALL . . .	53
3.1.1	CCND3 is distinctly highly expressed in lymphoid cells	53
3.1.2	Expression of CCND3 in cell lines resembles that of primary patient samples	56
3.2	<i>CCND3</i> expression is directly regulated by FOXO1	59
3.2.1	Assessment of comparability between <i>FOXO1</i> knockdown in human cells and conditional <i>Foxo1</i> deletion in a murine B-ALL model	59
3.2.2	Genetic <i>Foxo1</i> depletion exclusively reduces expression of <i>Ccnd3</i> but no other D-Cyclin	62
3.2.3	Pharmacological <i>Foxo1</i> inhibition reduces expression of <i>Ccnd3</i>	65
3.2.4	The cytotoxic effects of FOXO1 inhibition cannot be ameliorated by ectopic CCND2 expression	67
3.2.5	<i>Ccnd3</i> expression is neither regulated by MYC nor by E2F	68
3.2.6	FOXO1 directly binds to and activates the <i>CCND3</i> promoter	70
3.3	Depletion of CCND3 is toxic for B-ALL cells	75
3.3.1	CCND3 knockdown in B-ALL cell lines	75
3.3.2	Targeting CCND3 in different <i>ex vivo</i> models	77
3.3.3	Depletion of CCND3 but not inhibition of the enzymatic activity of its associated kinases CDK4/6 induces apoptosis in B-ALL cells	79
3.3.4	Cytotoxicity of <i>CCND3</i> knockdown is not caused by the accumulation of reactive oxygen species	82
3.4	CCND3 upregulation protects B-ALL cells from the cytotoxic effects of CDK4/6 inhibition	84
3.4.1	Upregulation of CCND3 ameliorates growth arrest induced by palbociclib	84

3.4.2	B-ALL cells acquire resistance to palbociclib by increasing CCND3 expression	86
3.5	CCND3 regulates the transcription of a distinct subset of genes independently of CDK4/6 kinase activity	90
3.5.1	Palbociclib and <i>CCND3</i> knockdown induce distinct gene expression dependent on genotype and treatment	90
3.5.2	CCND3 modulates the transcription of genes independently of CDK4/6	94
3.6	CDK8 downregulation partially mediates the cytotoxic effect of CCND3 depletion	99
3.6.1	<i>CDK8</i> expression is decreased only by CCND3 knockdown but not CDK4/6 inhibition	99
3.6.2	Genetic depletion of <i>CDK8</i> is toxic in B-ALL cells of different underlying driver mutations	101
4	Discussion	105
4.1	CCND3 is the highest expressed D-type Cyclin in B-ALL . .	105
4.2	CCND3 expression is directly activated by FOXO1	106
4.3	CCND3 depletion but not CDK4/6 inhibition is toxic to B-ALL cells	108
4.4	CCND3 regulates gene expression independently of CDK4/6	110
4.5	CDK8 contributes to the cytotoxic effects of CCND3 depletion in B-ALL	114
4.6	Conclusion	115
5	Summary	116
6	References	118
7	Statutory Declaration	145

List of abbreviations

4-OHT	4-Hydroxy-Tamoxifen
ACBD7	Acyl-CoA binding domain-containing 7
AID	Activation-induced Cytidine Deaminase
AKT	RAC-alpha Serine/threonine-protein Kinase
AML	acute myeloid leukemia
BACH2	BTB Domain And CNC Homolog 2
B-ALL	B-cell acute lymphoblastic leukemia
BCR	B-cell receptor
BCR-ABL1	Breaking cluster region-Abelson Kinase 1
BIM	BCL2 Like 11
BSA	bovine serum albumin
CBFB	Core-Binding Factor Subunit Beta
CCNC	Cyclin C
CCND1	Cyclin D1
CCND2	Cyclin D2
CCND3	Cyclin D3
CD	Cluster of Differentiation
CDK4	Cyclin-dependent kinase 4
CDK6	Cyclin-dependent kinase 6
CDK8	Cyclin-dependent kinase 8
ChIP	Chromatin immunoprecipitation
CK1	Casein Kinase 1
c-KIT	Tyrosine-Protein kinase kit
CLP	Common Lymphoid Progenitor
CNS	central nervous system
CREB	CAMP Responsive Element Binding Protein
DCF	2',7' –dichlorofluorescein
DCFDA	2',7' – dichlorofluorescein diacetate
DLBCL	diffuse-large B-cell lymphoma
DMP1/DMTF1	Cyclin D Binding Myb Like Transcription Factor 1

DYNLRB1	Dynein Light Chain Roadblock-Type 1
DYRK1	Dual Specificity Tyrosine-Phosphorylation-Regulated Kinase 1
E2A	Transcription Factor 3
EBF1	Early B-cell Factor 1
ELK1	ETS Transcription Factor
EMSA	electrophoretic mobility shift assay
ETV6	ETS Variant Transcription Factor 6
EV	empty vector
FhBox	Forkhead Box
FLT3	Fms Related Receptor Tyrosine Kinase 3
FOXO1	Forkhead Box Class O1
GC	germinal center
GFPT1	Glutamine-Fructose-6-Phosphate Transaminase 1
GSEA	gene set enrichment analysis
GTP	Guanosine-5'-triphosphate
HLF	Hepatic Leukemia Factor
HSD17B10	Hydroxysteroid 17-Beta Dehydrogenase 10
HSC	hematopoietic stem cell
ICMT	Protein-S-isoprenylcysteine O-methyltransferase
Ig	Immunoglobulin
IGH	Immunoglobulin Heavy Locus
Igκ	Immunoglobulin Kappa
Igλ	Immunoglobulin Lambda
IPLL	Immunoglobulin Lambda Like Polypeptide
IKZF1	IKAROS Family Zinc Finger 1
IL3	Interleukin-3
IL7R	Interleukin-7 Receptor
IGF1	Insulin Growth Factor 1
IP3	inositol 1,4,5-trisphosphate
ITAM	immunoreceptor tyrosine-based activation motifs

LEF1	Lymphoid Enhancer Binding Factor 1
MAPK	mitogen-activated protein-kinase
MEIS1	Homeobox Protein Meis1
MHC	major histocompatibility complex
MLLr	mixed-lineage leukemia rearranged
mTOR	mechanistic Target of Rapamycin
NEK7	Never In Mitosis A-Related Kinase 7
NF-κB	nuclear factor 'kappa-light-chain-enhancer' of activated B-cells
OBF1	Octamer-binding Transcription Factor 1
PAX5	Paired Box Protein 5
PBX1	PBX Homeobox 1
PCA	principal component analysis
PDAC	pancreatic ductal adenocarcinoma
PDX	patient-derived xenograft
PI3K	phosphatidylinositol 3-kinases
PIP₂	phosphatidylinositol-(4,5)-bisphosphate
PKA	Protein Kinase A
PLCγ	Phospholipase C gamma
PPARγ	Peroxisome Proliferator-activated Receptor Gamma
PRDX3	Peroxiredoxin 3
PROTAC	Proteolysis-Targeting Chimera
RAS	Rat Sarcoma Virus
RB1	Retinoblastoma protein 1
RENBP	Renin binding protein
ROS	reactive oxygen species
RUNX1	RUNX Family Transcription Factor 1
SCA	Stem cells antigen
shRNA	small-hairpin RNA
SIRT1	Sirtuin 1
SLC	surrogate light chain

SLP65	SH2-domain-containing leukocyte protein of 65 kDa
SOX4	SRY-Box Transcription Factor 4
STAT	Signal transducer and activator of transcription
STR	short tandem-repeat
SYK	Spleen Associated Tyrosine Kinase
T-ALL	T-cell acute lymphoblastic leukemia
tBHP	tert-butyl hydroperoxide
TCF3/E2A	Transcription Factor 3
TDT	Terminal Deoxynucleotidyltransferase
TGF-β	Transforming Growth Factor beta
TSS	transcriptional start site
VDJ	Variable-Diversity-Joining
VPREB	V-Set Pre-B Cell Surrogate Light Chain 1

Chapter 1

Introduction

1.1 B-cell development

Hematopoiesis is a widely branched, complex process that starts 18 days post-conception in the yolk sac in humans, is independently initiated two weeks later in the aorta-gonad-mesonephros, and then moves to the fetal liver and bone marrow at around five weeks post-conception (Jackson et al., 2021). The start of lymphopoiesis by differentiation of self-renewing multipotent hematopoietic stem cell (HSC)s to early lymphoid progenitor cells has first been observed six weeks post-conception in human embryos, while further differentiated early B-cell progenitors have been found as early as seven weeks post-conception (Nuñez et al., 1996; Asma et al., 1984). The shift of the lymphopoiesis from the fetal liver to the bone marrow occurs at around ten weeks post-conception and stays this way throughout life (Tavian et al., 2010). Henceforth, the earlier stages of B-cell development until the expression of a functional B-cell receptor (BCR) take place in the bone marrow. It is only after the successful selection of non-autoreactive, mature BCRs that B-cells leave the bone marrow and migrate to the periphery. In general, lymphopoiesis is characterized by cycles of proliferation and differentiation. This process is orchestrated by an intricate network of surface receptors, downstream signaling molecules and transcription factors. Depending on the developmental stage of B-cells, the expression and activity of these molecules vary (Figure 1).

Lymphopoiesis begins with the rare and quiescent long-term HSCs residing in the bone marrow niche. They are also called LSK cells, defined as the $(Lin)^-$, Stem cells antigen (SCA)-1⁺ and Tyrosine-Protein kinase kit (c-KIT)⁺ subset of multipotent stem cells. Long-term HSCs differentiate

into short-term HSCs upon expression of Cluster of Differentiation (CD)34. Short-term HSCs can reconstitute themselves only for up to one month, while long-term HSCs are capable of reconstitution up to 4 months after generation (Cheng et al., 2020). Induced by Transcription Factor 3 (E2A) and IKAROS Family Zinc Finger 1 (IKZF1), short-term HSCs are primed to give rise to Common Lymphoid Progenitor (CLP) cells (Tavian et al., 2010; Jackson et al., 2021). The CLP compartment is characterized by high Fms Related Receptor Tyrosine Kinase 3 (FLT3) expression, expression of Interleukin-7 Receptor (IL7R) as well as early Terminal Deoxynucleotidyltransferase (TDT) activity (DeKoter et al., 2002; Pang et al., 2018). Already at this early stage of B-lymphopoiesis, Forkhead Box Class O1 (FOXO1) transcriptionally activates RAG1/2, thereby initiating Variable-Diversity-Joining (VDJ)-recombination, the crucial process underlying antibody specificity and diversity (Igarashi et al., 2002). Successful V(D)J-recombination during lymphopoiesis will first enable pre-B-cells to express the pre-BCR. After further recombination, the pre-BCR will be replaced by the mature BCR (IgM). During this time before the expression of a functional pre-BCR, IL7R activity provides early B-cell progenitors with proliferation and survival signals (Buchner and Müschen, 2014).

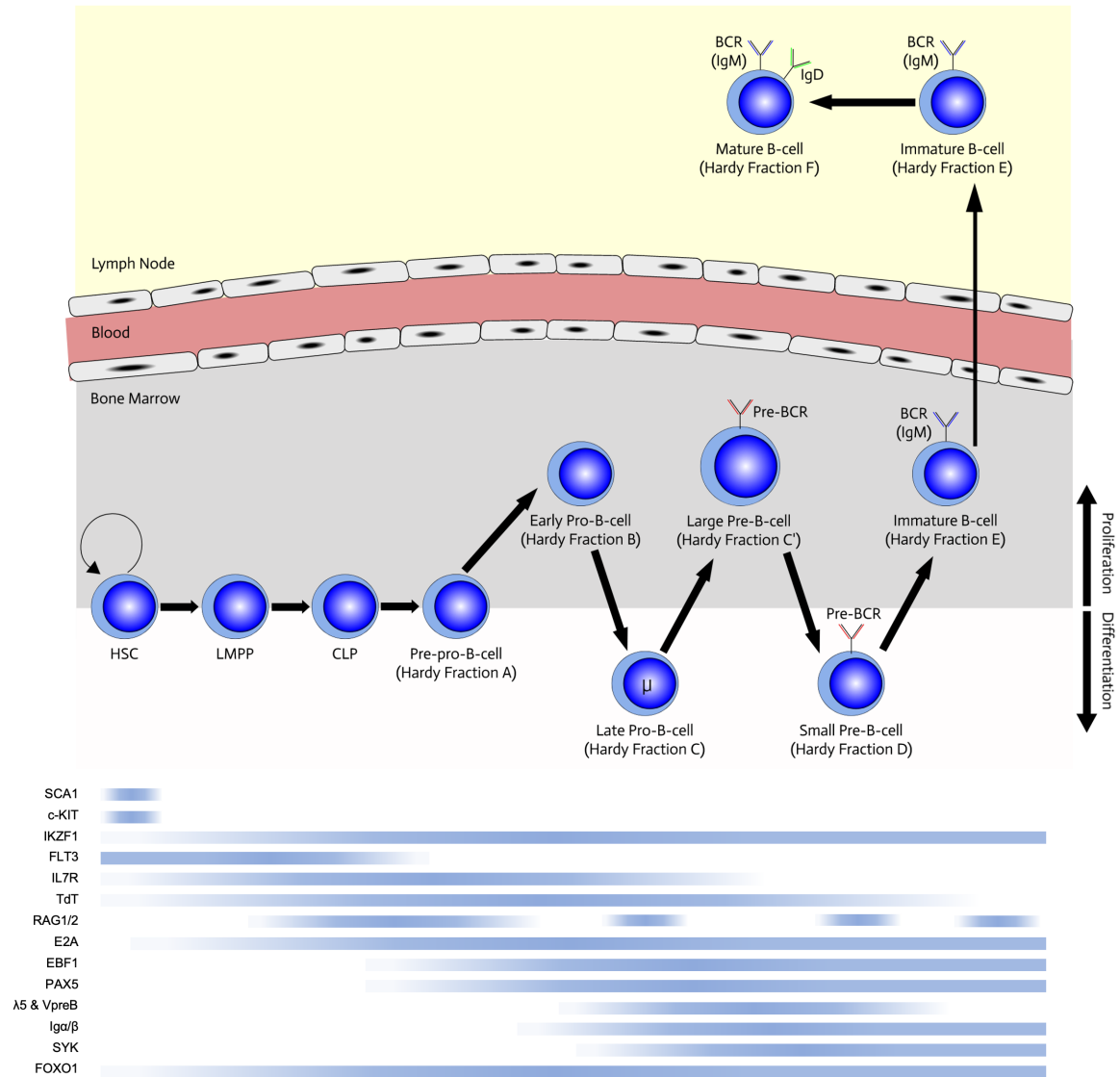


Figure 1: B-cell development

After Clark et al. (2014); Matthias and Rolink (2005); Cheng et al. (2020)

HSC: Hematopoietic stem cell; LMPP: Lymphoid-primed multipotent progenitor; CLP: Common lymphoid progenitor; BCR: B-cell receptor; Ig: Immunoglobulin

The differentiation of CLPs to the pre-pro-B-cell stage (Hardy fraction A, (Hardy and Hayakawa, 2001)) is induced by the activation of the transcription factors Transcription Factor 3 (TCF3/E2A), Early B-cell Factor 1 (EBF1), and Paired Box Protein 5 (PAX5). Since the lack of just one of these genes causes a stop in differentiation in the early B-cell stages, they are considered the master regulators of B-cell differentiation (Matthias and Rolink, 2005). The ensuing B-cell commitment is signified by the surface expression of CD19, a co-stimulatory molecule that regulates the signaling

threshold of the pre-BCR as well as the mature BCR (Otero and Rickert, 2003; Xu et al., 2014). Surface expression of CD19 is typically first found on pro-B-cells and is further expressed on B-cells until the end of their life span.

Amongst others, the transcription factors SRY-Box Transcription Factor 4 (SOX4), Lymphoid Enhancer Binding Factor 1 (LEF1), FOXO1, BTB Domain And CNC Homolog 2 (BACH2), and Octamer-binding Transcription Factor 1 (OBF1) are crucially involved in the regulation of successful, in-frame recombination of the V(D)J segments during the pro-B-cell stages (Hardy fractions B/C). This produces a functional, membrane-bound Immunoglobulin (Ig) μ -heavy chain, the first component of the (pre-)BCR. Subsequently, a surrogate light chain (SLC) is expressed from the V-Set Pre-B Cell Surrogate Light Chain 1 (VPREB) and an Immunoglobulin Lambda Like Polypeptide (IGLL) ($V\lambda 5$) locus, completing the assembly of the pre-BCR (Sakaguchi and Melchers, 1986; Kudo and Melchers, 1987). Together with its co-receptors CD79A and CD79B, the pre-BCR is first found on the surface of large cycling pre-B-cells (Hardy fraction C') and provides survival and proliferation signals (Matthias and Rolink, 2005).

The signal transduction pathways activated by the pre-BCR are very similar to those of B-cells expressing a mature BCR (IgM) (Herzog et al., 2009) (Figure 2). It has been demonstrated that tonic pre-BCR signaling is induced by auto-crosslinking of pre-BCRs, mediated by the $\lambda 5$ surrogate light chain (Ohnishi and Melchers, 2003). During the proliferative stages of early B-cell development, activation of the pre-BCR leads to phosphorylation of immunoreceptor tyrosine-based activation motifs (ITAM) by SRC-family kinases like LYN. This activates Spleen Associated Tyrosine Kinase (SYK) which transfers phosphate groups to the scaffold protein SH2-domain-containing leukocyte protein of 65 kDa (SLP65), a central junction of (pre-)BCR signaling. Additionally, SYK activates Phospholipase C gamma (PLC γ) which cleaves

phosphatidylinositol-(4,5)-bisphosphate (PIP₂) to inositol 1,4,5-trisphosphate (IP₃), which acts as a second messenger, inducing calcium release from the endoplasmic reticulum. Furthermore, PIP₂ is converted into PIP₃ by phosphatidylinositol 3-kinases (PI3K), in turn activating RAC-alpha Serine/threonine-protein Kinase (AKT). Furthermore, the Rat Sarcoma Virus (RAS) pathway, culminating in the activation of multiple transcription factors like ETS Transcription Factor (ELK1) or CAMP Responsive Element Binding Protein (CREB), can be activated via phosphorylation mediated by SLP65. Apart from the pre-BCR, activation of the interleukin 7-receptor has also been shown to contribute to the proliferation program of pre-B-cells via activation of STAT5, in turn inducing the transcription of the proto-oncogene MYC. It has been thoroughly shown that *Il7ra* deficient mice are unable to develop functional T- and B-cell compartments and that IL7 is essential for the survival of early B-cell precursors *in vivo* as well as *ex vivo*. In human B-cell precursors, the role of IL7R is still controversial, with data pointing to other possible receptor systems that might be able to replace IL7R (Clark et al., 2014). The main transcription factors regulating the expression of genes needed for proliferation (i.e. MYC, CCND2) or differentiation (i.e. RAG1/2) are STAT5, FOXO1, BCL6, ELK1, and CREB. Activation of these signaling pathways by pre-BCR engagement steers the cycling between differentiation/recombination and proliferation. For example, activated AKT phosphorylates FOXO1, which subsequently gets exported from the nucleus and is proteasomally degraded. This leads to no further RAG1/2 activation by FOXO1, enabling the stop of recombination and initiation of proliferation (Nemazee, 2017). With no or weak activation of the pre-BCR, B-lymphoblasts are negatively selected by either undergoing a new cycle of V(D)J-recombination or death by neglect. Importantly, (pre-)BCR signaling strength needs to be tightly regulated, with too much as well as too little signaling leading to failure of B-cell maturation (Müschen, 2018). This mechanism safeguards the generation of B-cells with faulty or auto-reactive

BCRs (Pelandra and Torres, 2012).

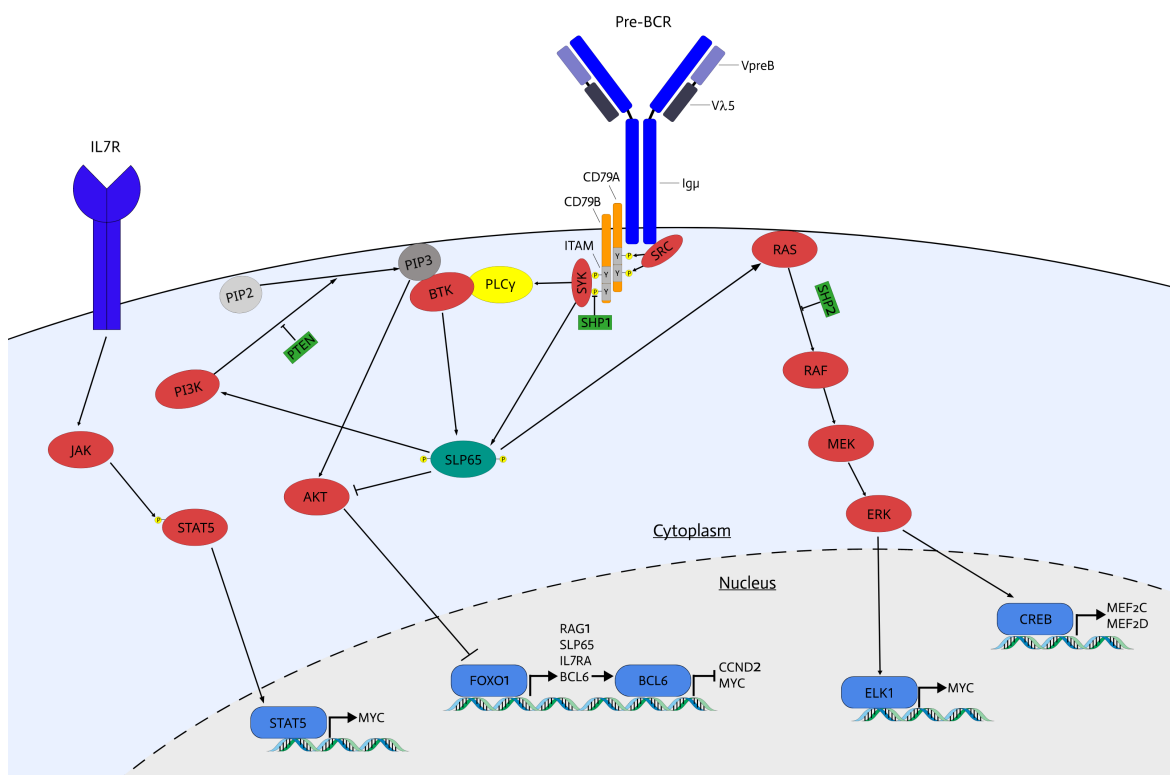


Figure 2: Pre-BCR signaling

After Monroe (2006); Herzog et al. (2009); Rickert (2013); Buchner and Müschen (2014)

After multiple cycles of proliferation and successful VDJ-recombination (Hardy fractions A-D), immature B-cells (Hardy fraction E) express the first complete BCR (IgM), consisting of the Igμ heavy chain and the recombined light chain products of either *Immunoglobulin Kappa (Igκ)* or *Immunoglobulin Lambda (Igλ)* (Collins and Watson, 2018). The successful pairing of light and heavy chains initiates tonic BCR signaling and enables immature B-cells to leave the bone marrow if the BCR is non-autoreactive. Positively selected immature B-cells migrate to the periphery, where they additionally start expressing IgD on their surface (Nemazee, 2017). After egress from the bone marrow, peripheral tolerance mechanisms like induction of anergy or desensitization of the BCR function as the last safeguard against auto-reactivity. However, opposed to positive and negative selection processes in the bone marrow, most peripheral tolerance

mechanisms can be reverted, in order to provide an antibody repertoire against pathogens with auto-antigen-like structures (Cerutti et al., 2013; Nemazee, 2017).

Matured naïve B-cells reside in secondary lymphoid organs, such as the spleen and lymph nodes, where they are presented with antigens through lymph flow and antigen-presenting cells, such as dendritic cells (Gatto and Brink, 2010; Katikaneni and Jin, 2019). B-cells take up antigens by receptor-mediated endocytosis, process, and present peptide-fragments of the antigen on their surface on a major histocompatibility complex (MHC) II molecule to the T-cell receptor of a CD4⁺ T-helper cell. Upon binding, the T-helper cell expresses CD40L on its surface, which binds to a CD40 molecule on the B-cell membrane. This triggers the B-cell to either exit the follicle and to differentiate into short-lived plasmablasts, which first proliferate and then differentiate into antibody-secreting plasma cells, or to form a germinal center (GC) within the lymphoid follicle (Lebien and Tedder, 2008). Short-lived plasma cells survive for three days and serve as a first-line defense against rapidly dividing pathogens such as viruses, but produce lower-affinity antibodies than those derived from the germinal center reaction (Dal Porto et al., 2002; Lebien and Tedder, 2008).

In order to produce higher affinity antibodies as well as a stable B-cell memory, activated B-cells form a GC within the follicle. First, in the dark zone of the GC, clonal expansion of centroblasts and somatic hypermutation of the variable region of the BCR is initiated by Activation-induced Cytidine Deaminase (AID). Somatic hypermutation is performed by rapid induction of double-strand breaks and single nucleotide exchanges (Gatto and Brink, 2010). The aim of this process is to generate immunoglobulins specific to the antigen (Kuraoka et al., 2011). After somatic hypermutation, centroblasts move to the light zone, where negative selection takes place. Centrocytes in the light zone depend on survival signals through binding to the antigen, presented by follicular dendritic cells. Those centrocytes with a low-affinity BCR are negatively selected and undergo apoptosis or another

round of affinity maturation in the dark zone. Surviving centrocytes that were not negatively selected re-enter the dark zone, either continuing somatic hypermutation to further increase antigen affinity or to undergo class-switch recombination. Of note, class-switch recombination of one immunoglobulin to another isotype does not rely on a germinal center, it has also been shown to occur before the formation of a GC, immediately after B-cell activation by a T-helper cell (Stavnezer et al., 2008). After successful affinity maturation, activated follicular B-cells differentiate into plasma- or memory cells. This complex process ensures the production of a highly specific B-cell response and antibody repertoire while minimizing the emergence of autoreactive antibodies (Mak, 2014). In humans, five classes of antibodies are known: IgA, IgD, IgE, IgG, and IgM. The broad repertoire of antibodies is capable of recognizing up to 5×10^{13} antigen patterns (Pieper et al., 2013). As part of the humoral immune response, the different antibodies fulfill functions such as neutralization, opsonization, antibody-dependent cell-mediated cytotoxicity, and complement activation (Mak, 2014).

1.2 B-cell acute lymphoblastic leukemia (B-ALL)

Leukemia is the umbrella term for proliferative, malignant disorders concerning cells of the hematopoietic system with an incidence of 5.4/100,000 on average worldwide in 2020 (Juliusson and Hough, 2016; Sung et al., 2021). Hematopoietic malignancies accounted for approximately 300,000 deaths worldwide in 2020 (Sung et al., 2021). Among the different types of leukemia, B-cell acute lymphoblastic leukemia (B-ALL) is the most common malignancy in children to date, with approximately 80% of B-ALL cases occurring in minors (Terwilliger and Abdul-Hay, 2017). Its incidence is characterized by an early peak between 0-9 years and a late peak at around 50 years (Yi et al., 2020). Interestingly, the incidence in children seems to have slightly diminished over the last 30

years while the number of elderly people getting diagnosed with B-ALL increased (Yi et al., 2020).

1.2.1 Risk-factors for B-ALL

Several risk factors for B-ALL are known, amongst which only a few, like exposure to chemicals and radiation, have been mechanistically elucidated. Both processes typically lead to DNA damage (Xie et al., 2005). However, the reasons for the higher incidence of B-ALL in males as well as in certain ethnicities and age groups remain poorly understood, although links have been made to various genetic predispositions. For example, prolonged signaling of Insulin Growth Factor 1 (IGF1) and IGF2 has been associated with increased incidence of B-ALL in Hispanic populations and children with higher than average birth weight (Huang et al., 2020). Furthermore, particularly in children, chronic and recurring infections have been linked to the development of B-ALL (Rodríguez-Hernández et al., 2019). Additionally, several genetic disorders have been connected to an increased risk of developing B-ALL (Table 1).

Table 1: Genetic Disorders linked to an increased risk of B-ALL. Inheritance is classified as either autosomal dominant (AD), autosomal recessive (AR), sporadic or X-linked. After Tebbi (2021).

Genetic disorder	Gene	Inheritance
Monosomy 7	7p/q	AD
Thrombocytopenia 5	ETV6	AD
Li-Fraumeni Syndrome	TP53	AD
Familial B-ALL, PAX5-mutation	PAX5	AD
Germline SH2B3	SH2B3	AR
Diamond Blackfan anemia	RPS10, RPL5, RPL11	Sporadic, AD, AR
Shwachman-Diamond syndrome	SBDS	AR
Fanconi anemia	FANC, BRCA2, BRIP1, PALB2, RAD51C, SLX4	AR
Mismatch repair cancer syndrome	PMS2, MSH2/6, MLH1	AR
Ataxia-telangiectasia	ATM	AR
Nijmegen breakage syndrome	NBS1	AR
Bloom syndrome	BLM	AR
Wiskott-Aldrich syndrome	WASP	X-linked
Burton's agammaglobulinemia	BTK	X-linked
Trisomy 21	21q	Sporadic

1.2.2 Pathophysiology of B-ALL

B-ALL patients typically present with diffuse symptoms like anemia, fever, weight loss, splenomegaly, or hepatomegaly (Jabbour et al., 2005). The diagnosis is usually performed by evaluating the number, morphology, immunophenotype, and cytogenetics of lymphoblasts. Typically, a presence of lymphoblasts in the peripheral vascular system and 20% or more lymphoblasts in the bone marrow indicate B-ALL (Alvarnas et al., 2015). The identification of underlying driver mutations has become increasingly important over the last decades, yielding much higher therapeutic success through the development and application of mutation-specific inhibitors (Jabbour et al., 2015). Furthermore, the occurrence of different driver mutations in B-ALL varies greatly between children and adults (Figure 3). For mixed-lineage leukemia rearranged (MLLr) B-ALL, 2 out of 3 infants are affected, but only 7% of older children carry an MLL-translocation. Genetic aberrations in B-ALL are diverse and are associated with different clinical outcomes (Zhang et al., 2017). Hyperdiploid and ETS Variant Transcription Factor 6 (ETV6)-RUNX Family Transcription Factor 1 (RUNX1) (t(12;21)) mutations are associated with favorable prognosis, E2A-PBX Homeobox 1 (PBX1) (t(1;19)) and Interleukin-3 (IL3)-Immunoglobulin Heavy Locus (IGH) (t(5;14)) have an intermediate prognosis and Breaking cluster region-Abelson Kinase 1 (BCR-ABL1) (t(9;22)), MLLr (t(v;11q23)) and hypodiploid cases show poor clinical outcomes (Zhang et al., 2017). Apart from cytogenetic determinants, a commonly used measure for risk stratification is the minimal residual disease, typically analyzed after induction therapy by techniques such as (multidimensional) flow cytometry, PCR-based techniques, and next-generation sequencing (Van Dongen et al., 2015).

Hyperdiploidy is characterized by an increased number of chromosomes, commonly chromosomes 4, 6, 10, 14, 17, 18, 21, and X (Paulsson and Johansson, 2009). Interestingly, depending on which chromosomes are

multiplied, different clinical outcomes have been observed, however mostly favorable.

The ETV6-RUNX1 translocation is widely regarded as insufficient in establishing B-ALL by itself and a "second hit" is needed to induce malignant transformation. The translocation was found to act in a dominant-negative manner, subverting the activity of RUNX1 (Zhang et al., 2017). It is commonly found *in utero* and mostly occurs in pediatric B-ALL (Wiemels et al., 1999).

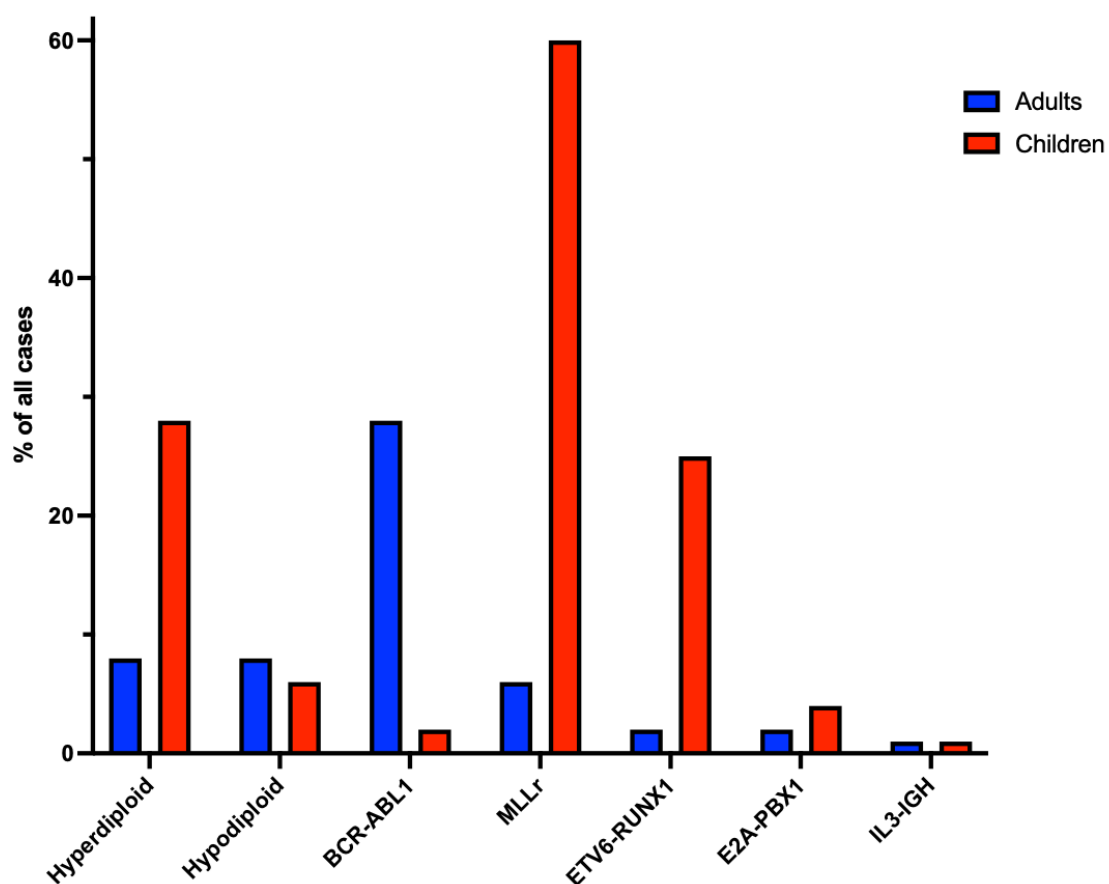


Figure 3: Most common genetic aberrations in B-ALL
After Zhang et al. (2017)

Translocation of (9;22), resulting in the "Philadelphia Chromosome", affects the breaking cluster region on chromosome 22 at q11.2 and the ABL1 gene on chromosome 9, q34.1, producing either a 190 kDa or 210 kDa BCR-ABL1 fusion kinase (Cilloni and Saglio, 2012). It is more commonly found in adult B-ALL patients and was one of the first molecules to be

targeted by a specific kinase inhibitor, imatinib, greatly increasing the overall survival of patients carrying the "Philadelphia Chromosome" (Fielding et al., 2014).

Rearrangements of MLL (KMT2A) with more than 80 different partners have been identified, with AF4 being the most common one (Zhang et al., 2017). MLL is a methyltransferase, inducing malignant transformation by changing the chromatin methylation patterns when translocated. Interestingly, MLLr B-ALL has been found to depend on the expression of BCL6, which represses pro-apoptotic BCL2 Like 11 (BIM) (Hurtz et al., 2019).

Hypodiploidy is typically categorized into high hypodiploidy (42-45 chromosomes), low hypodiploidy (33-39 chromosomes) and near haploidy (23-29 chromosomes) and less number of chromosomes is an indicator of worse clinical outcome (Zhang et al., 2017; Safavi et al., 2013).

E2A is an essential gene for early B-lymphoblastic development and is rarely translocated with Hepatic Leukemia Factor (HLF), which is associated with poor prognosis. It is more commonly found as an E2A-PBX1 fusion gene, which has not been known to impact the initial clinical outcome but was associated with an increased risk of central nervous system involved relapse (Licht, 2020).

Of note, many more subtypes of B-ALL have been identified, like IL3-IGH and other IGH-rearrangements, intrachromosomal amplification of chromosome 21 (iAMP21) B-ALL as well as BCR-ABL1-like B-ALL which is characterized by translocations of various cytokine receptors and tyrosine kinases (Arber et al., 2016).

1.2.3 Therapy of B-ALL

The first modern-day treatment of acute (myeloid) leukemia was described in 1930. The treatment consisted of a combination of radiation, arsenic, and thorium-X (Gloor, 1930). The patient survived the treatment and would live

until the age of 102, 50 years after the diagnosis and treatment. While thorium-X is not used anymore, arsenic has been re-discovered for the therapy of promyelocytic leukemia and radiation is still an important part of today's leukemia treatment regimens (Gurnari et al., 2020). Nowadays, treatment strategies for acute leukemia usually consist of induction, consolidation (intensification), and maintenance therapy, often including preventative measures for central nervous system (CNS) involvement (Figure 4).

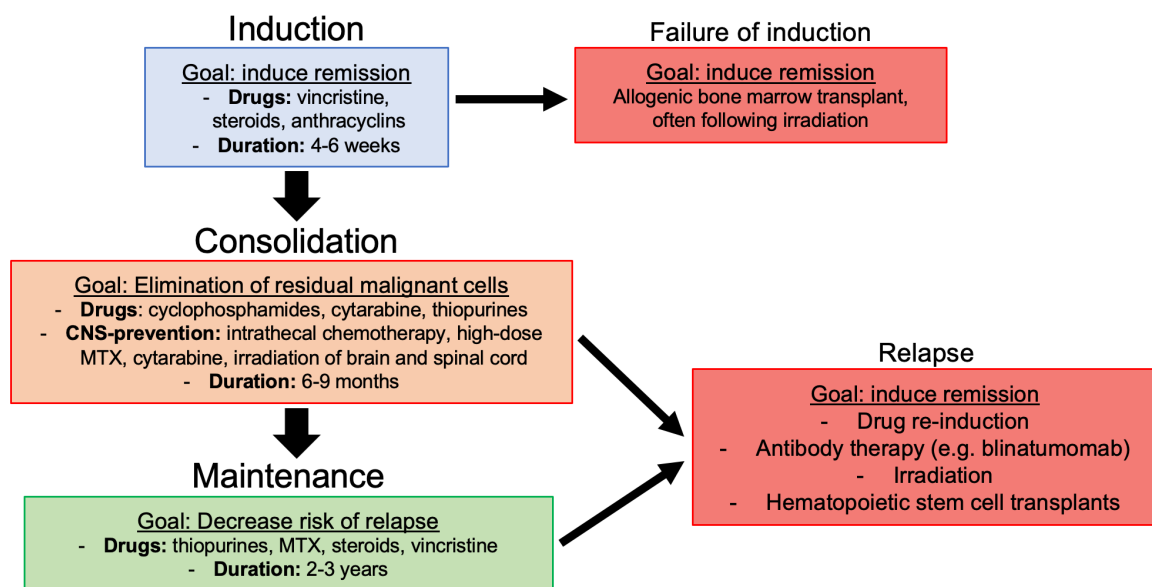


Figure 4: Treatment strategies for B-ALL
After Rudin et al. (2017); Hunger and Raetz (2020)

In case of failed induction or relapse, alternative therapeutic strategies are employed, like CAR-T-cells, bi-specific T-cell engaging (BiTE) antibodies, or bone marrow/hematopoietic stem cell transplants (Goebeler and Bargou, 2020; Hunger and Raetz, 2020).

However, the well-known success story of the small molecular weight inhibitor imatinib, targeting the BCR-ABL1 kinase, paved the way for the search and development of novel targeted therapies specifically inhibiting oncogenic drivers. The introduction of imatinib to the therapy of BCR-ABL1⁺ B-ALL increased the 5-year overall survival in adults by

approximately 50% (Abou Dalle et al., 2019). Other small molecular weight inhibitors for targeted therapy of B-ALL that are either in clinical trials or have been successfully used clinically include dasatinib and ponatinib (BCR-ABL1), ruxolitinib (JAK1/2), and copanlisib (PI3K) (Aldoss and Stein, 2018). Furthermore, monoclonal antibodies have been adopted in B-ALL therapy regimens, like inotuzumab ozogamicin (CD22) and rituximab/ofatumumab (CD20), further improving clinical outcomes for refractory and relapsed B-ALL cases (Aldoss and Stein, 2018).

In general, the search for targeted therapies is ongoing and the continually bad prognosis especially for adults with B-ALL incentivizes pre-clinical research to scan for new targets. New approaches like targeting phosphatases in B-ALL have been discovered and have prospects of eventually making it to clinical trials and improving the outcomes of difficult-to-treat cases (Shojaee et al., 2016; Xiao et al., 2018).

1.3 Forkhead Box Class O1 (FOXO1)

One target that was recently identified as a vulnerability of B-ALL of different genetic backgrounds is the Forkhead Box Class O1 (FOXO1), also referred to as forkhead in rhabdomyosarcoma (FKHR) (Wang et al., 2018). The term "forkhead" refers to the phenotype observed in *Drosophila melanogaster* when FOXO1 was mutated, causing the development of an additional head, while the latter name derives from its tumorigenic fusion with *PAX3*, first identified in solid tumor alveolar rhabdomyosarcoma (Weigel et al., 1989; Roberts et al., 2014). The four known FOXO members that have been identified in mammals, FOXO1, FOXO3, FOXO4, and FOXO6 share a highly conserved, approximately 110 amino acids long sequence called the forkhead domain, which binds to different target genes (Jonsson and Peng, 2005). Additionally, FOXO family members contain a nuclear localization signal, a nuclear export signal, and a C-terminal transactivation domain (Figure 5). However, apart from the structurally

stable forkhead domain, FOXO1 is an intrinsically disordered protein (Obsil and Obsilova, 2008).

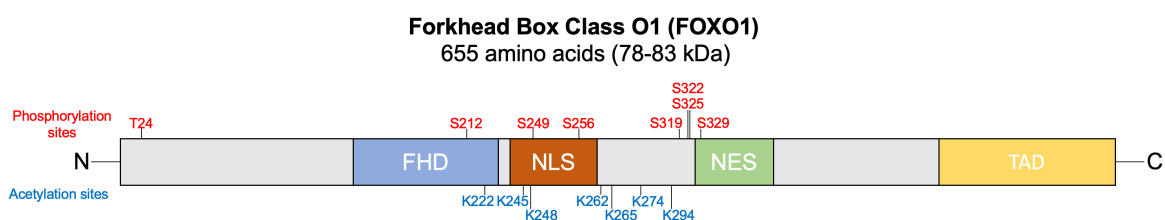


Figure 5: Structure of the FOXO1 protein

FHD=Forkhead domain; NLS=Nuclear localization signal; NES=Nuclear export signal; TAD=Transactivation domain. After Ma et al. (2018).

FOXO1 is post-translationally regulated by AKT-phosphorylation at positions Thr24, Ser253, and Ser316. These phosphorylations enable binding by the adaptor protein 14-3-3, blocking the import of FOXO1 from the cytoplasm to the nucleus and increasing nuclear export, thus decreasing the expression of FOXO1 target genes (Ma et al., 2018). Furthermore, phosphorylation of FOXO1 can also occur, amongst others, by Protein Kinase A (PKA), Dual Specificity Tyrosine-Phosphorylation-Regulated Kinase 1 (DYRK1), and Casein Kinase 1 (CK1). Upon phosphorylation and nuclear export, FOXO1 is ubiquitinated and proteasomally degraded. FOXO1 is also regulated via acetylation by P300 or CREB-binding protein and de-acetylation by Sirtuin 1 (SIRT1) (Ma et al., 2018). FOXO1 controls a host of different cellular processes, ranging from metabolism to cell death, cell cycle, cell differentiation, and reactive oxygen species (ROS) regulation (Ushmorov and Wirth, 2018). Because of its role as a regulator of glucose metabolism, it is of particular interest as a potential target in metabolic disease, like type 2 diabetes or hypertriglyceridemia (Hyun Kim et al., 2011; Ushmorov and Wirth, 2018). While FOXO1 is essential for embryonic angiogenesis and *Foxo1*^{-/-} mice die at E10.5 (Hosaka et al., 2004), multiple inducible *Cre-loxP* mouse models have been investigated in the context of metabolism. For example, inducible knockout of *Foxo1* in murine pancreatic cells induces increased glucose-stimulated insulin secretion as well as increased β -cell proliferation (Miyazaki et al., 2012). Furthermore,

hepatic knockout of *Foxo1* decreased blood glucose levels (Zhang et al., 2012). Mutations of FOXO1 in humans have been observed and are directly associated with different malignancies as well as congenital hypopituitarism (Kapali et al., 2016). In rhabdomyosarcoma, FOXO1 is translocated with PAX3 (Galili et al., 1993). In diffuse large B-cell lymphoma, approximately 9% of patients carry a FOXO1 mutation, predominantly at the AKT phosphorylation site T24, leading to a constitutively active variant of FOXO1 which is associated with worse overall survival (Trinh et al., 2013). Additionally, a rare translocation of FOXO1 with Homeobox Protein Meis1 (MEIS1) has been discovered in B-ALL, which is also associated with a worse clinical outcome (Zheng et al., 2020).

FOXO1 is a master regulator during B-cell development, controlling proliferation and differentiation by inducing immunoglobulin rearrangement through direct transcriptional activation of RAG1 but also its activation of apoptosis-inducing genes like Fas-ligand and BIM. It has been shown that *Foxo1*-deficient mice develop a block in B-lymphoid development at the CLP stage (Lin et al., 2010). Hence, it was hypothesized that increased FOXO1 activity through either AKT hyperactivation or constitutively active FOXO1 would drive B-ALL cells into cell cycle arrest and apoptosis, which was indeed demonstrated to be the case (Matthias and Rolink, 2005; Köhrer et al., 2016). However, it has been shown that FOXO1 is consistently expressed in B-ALL cells, suggesting that it could not be classified as a classical tumor suppressor (Wang et al., 2018). Indeed, not only its overactivation but also its depletion induces apoptosis in B-ALL, suggesting a FOXO1-dependency and dose-dependent or "Goldilocks" regulation of FOXO1 in B-ALL (Köhrer et al., 2016; Wang et al., 2018; Abdelrasoul et al., 2020). The case of FOXO1 in B-cell malignancies becomes all the more intriguing when considering that in classical Hodgkin lymphoma, FOXO1 indeed acts as a tumor suppressor but Burkitt Lymphoma depends on FOXO1 activity (Vogel et al., 2014; Gehringer et al., 2019). Different mechanisms of FOXO1 dependency in B-ALL have been suggested,

including downregulation of Cyclin D3 (CCND3) and IL7R (Wang et al., 2018; Abdelrasoul et al., 2020), but more research is needed to elucidate the complete picture of the role of FOXO1 in B-ALL.

1.4 Cyclin D3 (CCND3)

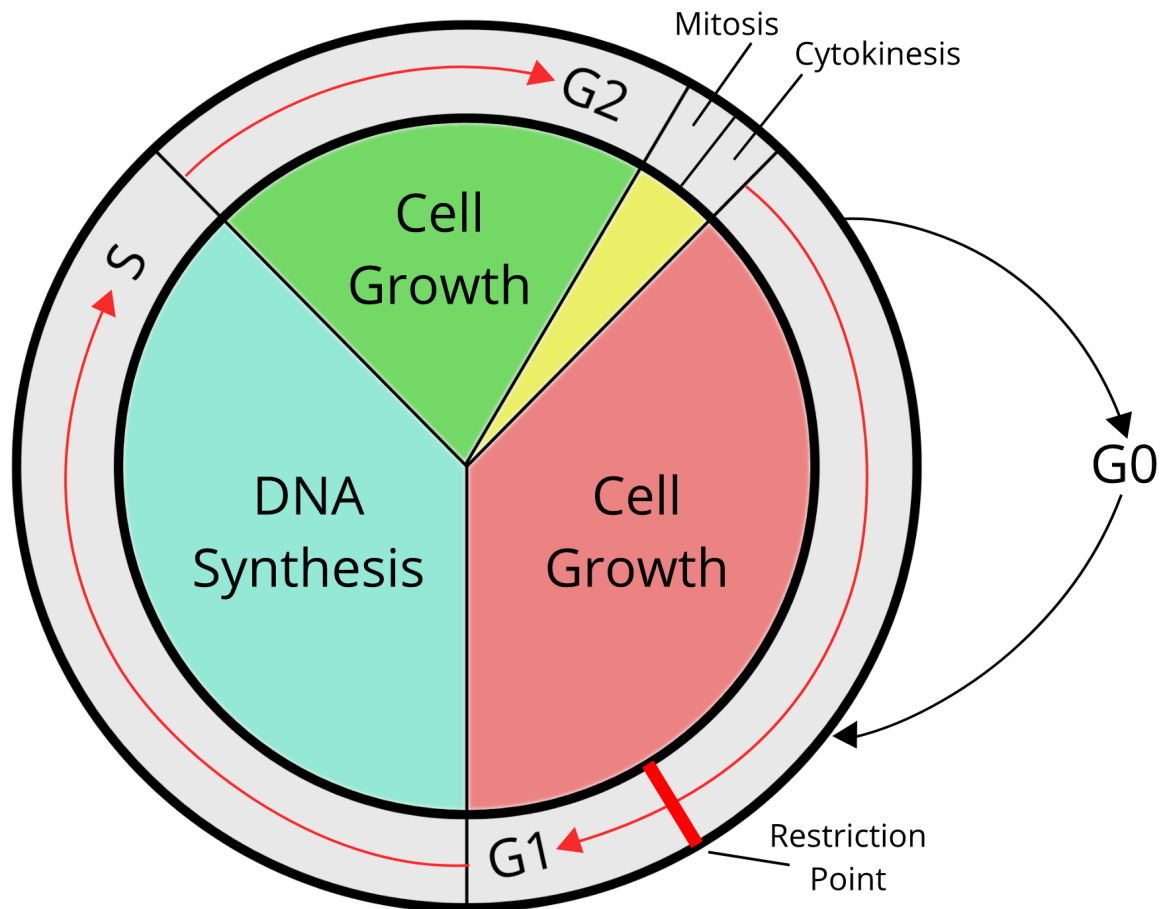


Figure 6: The mammalian cell cycle

After (Malumbres and Barbacid, 2009). Yellow area represents M-Phase, green, red and blue areas represent the interphase.

Cell cycle progression is orchestrated by Cyclin-CDK complexes that activate different gene expression programs, driving cells either into cell division, G0 cell arrest, or cell death (Figure 6). The mammalian cell cycle consists of the interphase, which is subdivided into the G1 growth phase from which cells can enter G0 quiescence and into which cells can also re-enter from G0 upon mitogenic stimulation, the S-phase in which a second

set of DNA is synthesized, and the G2 growth phase which prepares the interphase cells for cell division in the M-phase. In this stage of the cell cycle, the cell divides and spawns a daughter cell through division, sectioned into prophase, metaphase, anaphase, telophase, and subsequent cytokinesis. The cells then either re-enter the cell cycle at G1 or undergo G0 quiescence (Ren et al., 2002). Cyclin D3 (CCND3) is one of the three D-type Cyclins next to CCND1 and CCND2. Canonically, it binds to Cyclin-dependent kinase 4 (CDK4) and Cyclin-dependent kinase 6 (CDK6), activating their enzymatic activity by forming a stabilized holoenzymatic complex (Figure 7). Before entering G1 from G0, Retinoblastoma protein 1 (RB1), the restrictive factor of G1-S progression, is first hypo-phosphorylated by CCND-CDK3. This enables further phosphorylation by other Cyclin-CDK complexes (Ren and Rollins, 2004). Next, during the G1 phase of the cell cycle, the CCND-CDK4/6 complex phosphorylates RB1 at the CDK consensus motif S/T-P-X-K/R (Ubersax and Ferrell, 2007). This constitutes the process of hypo-phosphorylation of RB1 at positions S249, T252, T356, S608, S788, S807, S811, and S826. These phosphorylations alone are not enough to release RB1 from its repression target E2F, thus blocking entry into the S-phase of the cell cycle. This phosphorylation of RB1 by CDK4/6 can be inhibited by the negative cell cycle regulator p16^{INK4A} (Serra and Chetty, 2018). After initial phosphorylations of RB1 by CCND-CDK4/6, CCNE-CDK2 continues hyper-phosphorylation of RB1 at positions T5 (substituted by S364 in mice), T373, and S795 (Zarkowska and Mitnacht, 1997; Ezhevsky et al., 1997; MacDonald and Dick, 2012). At the end of the G1 phase, CCNE-CDK2 finishes RB1 hyper-phosphorylation at S612 and T821, ultimately leading to the release of RB1 from E2F. In the case of DNA damage or other stop signals for proliferation, CDK2 activity is inhibited by p21 or p27 (Karimian et al., 2016; Razavipour et al., 2020). After release of RB1, E2F initiates the transcriptional program leading to the G1-S transition of the cell cycle by facilitating the transcription of positive cell cycle regulators like MYC, A-,

E- and D-type Cyclins, CDKs, and more (Bracken et al., 2004).

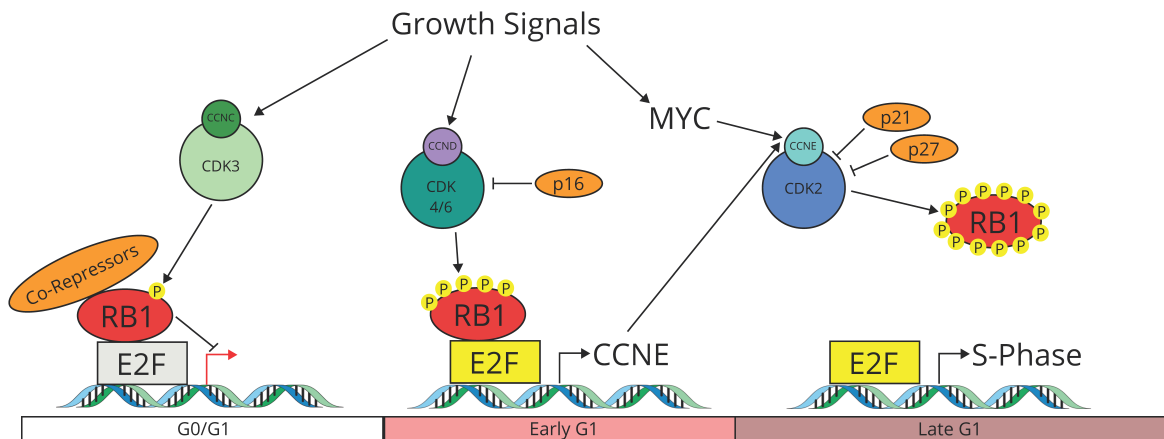


Figure 7: Regulation of G1-S-phase progression by RB1 phosphorylation

CCNC=Cyclin C; CDK=Cyclin dependent kinase; RB1=Retinoblastoma protein 1; CCND=CCND1/2/3; CCNE= Cyclin E. After (Giacinti and Giordano, 2006).

Interestingly, the common perception of redundancy of D-type Cyclins has recently been challenged, particularly in B-cells and their precursors. For example, it has been demonstrated that during B-cell development, CCND2 is almost continually expressed, but the upregulation of CCND3 expression is indispensable for the transition of pre-BCR⁻ progenitor B-cells to pre-BCR⁺ precursor B-cells (Cooper et al., 2006). Additionally, it was found that the three D-type Cyclins associate with either CDK4 or CDK6 or stay unbound, depending on the developmental stage of B-cells, and the different complexes even localize in different, not overlapping compartments within the developing B-cells (Powers et al., 2012). Furthermore, knockout of *Ccnd1*, *Ccnd2*, and/or *Ccnd3* all lead to completely different phenotypes in mice and *Ccnd3*^{-/-} are particularly lacking in the development of the lymphoid cell compartment (Sicinska et al., 2003).

Interestingly, D-type Cyclins have been implicated in non-canonical activities apart from cell cycle regulation, both in complex and without CDK4/6 (Hydbring et al., 2016). All three D-Cyclins bind to Cyclin D Binding Myb Like Transcription Factor 1 (DMP1/DMTF1), which activates p53 via physical binding as well as via ARF-activation (Fry and Inoue, 2019). Furthermore, CCND3 competes with Core-Binding Factor Subunit

Beta (CBFB) for binding to RUNX1, modulating its transcriptional program (Peterson et al., 2005). In complex with CDK4, CCND3 has been demonstrated to stimulate the activity of Peroxisome Proliferator-activated Receptor Gamma (PPAR γ), thus promoting adipogenesis (Sarruf et al., 2005). Conclusively, the role of D-Cyclins in healthy and malignant cells is not restricted to their canonical functions within the CCND-CDK4/6 holoenzymatic complex and attention should be paid to their non-canonical roles as well when describing the functions of D-type Cyclins.

1.4.1 Cell cycle as a therapeutic target in cancer

CCND3 in complex with CDK4/6 is an essential part of the G1 restriction point of the cell cycle which is frequently deregulated in cancer (Moser et al., 2018). The escape from negative cell cycle regulation by circumventing cell cycle restriction points, thus enabling massively increased proliferation is a classical hallmark of cancer (Hanahan and Weinberg, 2011). Frequently mutated components of cell cycle regulation are *RBI*, *TP53*, E- and D-type Cyclins, CDKs, and CDK inhibitors like p16, p21, and p27 (Suski et al., 2021). Since Cyclins and CDKs are often overexpressed in cancer, CDK inhibitors have been developed, targeting the phosphorylation of RB1 by CDKs. Palbociclib, formerly experimentally called PD0332991, is a bi-specific inhibitor of CDK4 and CDK6 (Fry et al., 2004). It binds to the catalytically active ATP pocket, which is highly conserved between CDK4 and CDK6, apart from an R/T switch at residue 88 and an E/Q switch at residue 131 (Martin et al., 2017). Palbociclib has been shown to be effective and safe in the treatment of HR⁺/HER2⁻ breast cancer, significantly prolonging the overall survival in combination with the aromatase inhibitor letrozole (Zhang et al., 2021). This CDK4/6 inhibitor is currently studied for various types of cancers, including T-cell acute lymphoblastic leukemia (T-ALL) and B-ALL, with yet to be determined efficacy (Richter et al., 2021). In a pre-clinical T-ALL model, the inhibition

of CDK4/6 in T-ALL did not only prove to efficiently induce apoptosis *in vitro* as well as *in vivo*, but it also elucidated a previously unknown role of CCND3-CDK6 in the regulation of glucose utilization (Wang et al., 2017). The authors were able to demonstrate that CCND3-CDK6 inhibition by palbociclib decreased the activity of the two rate-limiting enzymes in glycolysis, phosphofructokinase, and pyruvate kinase M2. This in turn decreased the amount of glucose metabolites shunted to the pentose phosphate and serin pathways, decreasing the production of reduction equivalents, thus inducing apoptosis by increased production of ROS. This result, amongst others, demonstrates that CDK inhibition is not just impacting cell cycle regulation but could further enable the targeting of metabolic vulnerabilities in cancer. Two other CDK4/6 inhibitors, ribociclib (LEE011) and abemaciclib (LY2835219) have been developed which preferentially inhibit CDK4 and not, like palbociclib, CDK4 and CDK6 equally (Zhang et al., 2021). Both are also currently undergoing clinical trials (Richter et al., 2021). Of note, pre-clinical studies have shown that different types of cancer seem to depend on CDK4/6 activity for cell cycle progression, but since many chemotherapeutics exploit cancer cells' rapid proliferation, CDK4/6 inhibition acts antagonistically to cytostatic agents (Richter et al., 2021). Apart from CDK4/6, inhibitors for various CDKs have been developed, like the pan-CDK inhibitor flavopiridol, which has first been clinically used in leukemia in the late 20th century but has not been employed much further because of severe side effects (Zhang et al., 2021). Other pan-CDK inhibitors have been developed since, like TG02, AT7519, and roniciclib, which in particular inhibit CDK1, CDK2, CDK4, CDK6, and CDK9 and show promising first results in clinical trials for different types of cancer, including hematologic malignancies (Zhang et al., 2021).

Non-canonical CDKs like CDK8 and CDK9 have recently been in the spotlight of cancer research. CDK8 and its activating binding partner CCNC are part of the catalytic subunit of the mediator complex of RNA-polymerase II (Uehara et al., 2020). Additionally, it has been shown to activate STAT1

at S727 and STAT5 at S726 via phosphorylation (Rzymiski et al., 2017). Although CDK8 has originally been deemed a non-cell cycle-related kinase, it has been found that CDK8 directly activates transcription of the cell cycle inhibitor p21, most likely as a part of p53-mediated transcription (Szilagyi and Gustafsson, 2013). Its inhibition has been shown to be effective in pre-clinical acute myeloid leukemia (AML) models by decreasing STAT-phosphorylation and is currently evaluated in a clinical trial (Borthakur et al., 2019). In B-ALL, not its enzymatic inhibition but its targeted degradation via a Proteolysis-Targeting Chimera (PROTAC) has been shown to be synthetically lethal with mechanistic Target of Rapamycin (mTOR) inhibition in a pre-clinical BCR-ABL1⁺ B-ALL mouse model (Menzl et al., 2019).

CDK9 in complex with Cyclin T1, T2a or T2b is a part of positive transcription elongation factor b, which phosphorylates the large subunit of the RNA-polymerase II (Morales and Giordano, 2016). Just like CDK8, CDK9 is an interesting target because of its implication in transcriptional processes. Hence, its inhibition could, similar to classic cytostatic agents, leverage the high proliferative and replicative activity of cancer cells. However, multiple inhibitors for CDK9 have been developed but none has proven to be efficient and without severe side-effects in clinical trials so far (Morales and Giordano, 2016).

CDK inhibition is a promising approach for cancer therapies, but the aforementioned examples show that not only do cancers vastly differ in dependence on different CDKs, their inhibition is also frequently connected to severe side effects.

1.5 Aim of the thesis

Our group has previously shown that the tight regulation of FOXO1 is essential in B-ALL (Wang et al., 2018). Genetic knockdown via shRNAs as well as inhibition of FOXO1 by the small molecular weight inhibitor AS1842856 were proven to efficiently induce cell cycle arrest and apoptosis in B-ALL models *in vitro* and *in vivo*. Mechanistically, FOXO1 genetic and pharmacological inhibition decreased mRNA and protein levels of CCND3. Furthermore, the shRNA-mediated knockdown of CCND3 induced apoptosis and, as expected, cell cycle arrest. Intriguingly, by overexpression of CCND3, the cytotoxic effects of FOXO1 inhibition could be ameliorated. In my thesis, I first focused on the investigation of the regulation of CCND3 by FOXO1. In order to achieve this, I employed different techniques including qRT-PCR, Luciferase-assay, electrophoretic mobility shift assay (EMSA), and Chromatin immunoprecipitation (ChIP). Furthermore, I used a BCR-ABL1⁺, *Foxo1*^{fl/fl} murine *ex vivo* model for further validation of the effects of FOXO1 depletion in B-ALL. Next, I performed an in-depth analysis of the mechanisms underlying the cytotoxic effects of CCND3 depletion in *in vitro*, murine *ex vivo*, and human patient-derived xenograft (PDX) *ex vivo* B-ALL models using RNA-interference, CRISPR/Cas9, and Cre-loxP gene editing. Furthermore, I aimed to compare the effects of CCND3 downregulation versus inhibition of its associated kinases CDK4/6 throughout different genetic subgroups of B-ALL. In order to understand the function of CCND3 in B-ALL, my goal was to distinguish the effects of CCND3 depletion from its function within the CCND3-CDK4/6 holoenzyme. To this end, I used shRNAs against CCND3 and palbociclib for CDK4/6 inhibition, respectively, and compared both effects via RNA-sequencing. Finally, I aimed to use the results of the RNA-sequencing to identify druggable genes that are regulated by CCND3.

Chapter 2

Materials and Methods

2.1 Materials

2.1.1 Reagents

All commonly used chemicals and reagents were supplied by AppliChem (Darmstadt, Germany), Roth (Karlsruhe, Germany), Merck (Darmstadt, Germany), or Sigma-Aldrich (St. Louis, MO, USA). Primers and oligonucleotides were ordered from Biomers (Ulm, Germany) and enzymes used for molecular cloning were supplied by New England Biolabs (Ipswich, MA, USA).

Buffers

Table 2: Buffers

Buffer	Ingredients
Annealing buffer (10X)	10 mM CH ₃ CO ₂ K 30 mM HEPES-KOH (pH=7.4) 2 mM Mg(CH ₃ COO) ₂
Annexin-V binding buffer (10X)	0.1 M HEPES (pH 7.4) 1.4 M NaCl 25 mM CaCl ₂
Apoptosis staining solution	1X Annexin-V binding buffer Annexin-V-FITC/APC 1:15 2 µg/ml PI
Cell Cycle (PI) staining solution	1X PBS 100µg/ml RNaseA 40 µg/ml PI
Elution buffer (ChIP)	1 % SDS 100 ml Ampuwa 840 mg NaHCO ₃

Table 2 – continued from previous page

Buffer	Ingredients
FACS surface staining buffer	1X PBS 0.5 % bovine serum albumin (BSA) 2 mM EDTA ₂
FACS intracellular staining buffer	1X PBS 1 % FCS 0.1 % Sodium Azide
Farnham lysis buffer	5 mM PIPES pH 8.0 85 mM KCl 0.5 % NP-40 1 protease inhibitor tab/10 ml
Immunoblot transfer buffer	0.02 M Tris 0.2 M Glycine 20 % Methanol
Laemmli Buffer (2X)	10 % Glycerol 6 M Urea 5 % β-Mercapto-ethanol 2 % SDS 62.25 mM Tris 0.00125 % Bromphenol-blue
LiCl Wash buffer (ChIP)	100 mM Tris (pH 8.0) 500 mM LiCl 1 % NP-40 1 % deoxycholic acid
Lysogeny broth (LB)	10 g/L Tryptone 10 g/L NaCl 5 g/L Yeast-extract
MTT-assay lysis buffer	20 % SDS 2 % Acetic acid 50 % Dimethylformamide 0.15 mM HCl (pH=4.7)
PBS (10X, pH=6.9)	1.5 M NaCl 0.03 M KCl 0.08 M Na ₂ HPO ₄ 0.02 M NaH ₂ PO ₄

Table 2 – continued from previous page

Buffer	Ingredients
RIPA lysis buffer	150 mM NaCl 50 mM Tris-HCl 1 % Sodium deoxycholate 1 % Triton-X 100 250 μ M EDTA
SDS lysis buffer	62.5 mM Tris-HCl (pH=6.8) 50 mM DTT 10 % Glycerol 2 % SDS 0.01 % Bromphenol blue 1 complete Mini Protease inhibitor cocktail tablet/10ml
SDS-PAGE 10X running buffer	0.2 M Tris 2 M Glycine 0.04 M SDS
TBS (10X, pH=7.6)	0.2 M Tris 1.5 M NaCl

Cell culture reagents

Table 3: Cell culture reagents

Reagent	Supplier
alpha-minimum essential medium (α -MEM)	PAN-Biotech, Aidenbach, Germany
CaCl ₂ -Phosphate transfection kit	Takara Bio Inc., Kusatsu, Shiga, Japan
Dulbecco's modified essential medium (DMEM)	Gibco, Waltham, MA, USA
FCS	Gibco, Waltham, MA, USA
GenomeLabHuman STR primer set	Beckman Coulter, Krefeld, Germany
Iscove's modified Dulbecco's medium (IMDM)	PAN-Biotech, Aidenbach, Germany
L-Glutamine	Gibco, Waltham, MA, USA
MTT	Sigma-Aldrich, St. Louis, MO, USA
MycAlert Mycoplasma Detection Kit	Lonza Group Ltd., Basel, Switzerland
Opti-MEM Reduced Serum Medium	Gibco, Waltham, MA, USA
Polyethylenimine (PEI)	Polysciences, Hirschberg a.d. Bergstraße, Germany
Penicillin/Streptomycin	Gibco, Waltham, MA, USA

Table 3 – continued from previous page

Reagent	Supplier
Propidium iodide (PI)	Sigma-Aldrich, St. Louis, MO, USA
Puromycin	Merck, Darmstadt, Germany
Retronectin	Takara Bio Inc., Kusatsu, Shiga, Japan
RPMI Medium 1640	Gibco, Waltham, MA, USA
Sodium Pyruvate	Gibco, Waltham, MA, USA
Trypan blue 0.4 %	Sigma-Aldrich, St. Louis, MO, USA
Trypsin (0.05/0.25 %)	Gibco, Waltham, MA, USA

Drugs

Table 4: Drugs

Reagent	Supplier
4-Hydroxy-Tamoxifen (4-OHT)	Calbiochem, San Diego, CA, USA
AS1842856	Merck, Darmstadt, Germany
Imatinib	SelleckChem, Houston, TX, USA
Palbociclib	SelleckChem, Houston, TX, USA
RNAasin Plus RNase inhibitor	Promega, Madison, WI, USA
SEL120	SelleckChem, Houston, TX, USA

Materials for molecular biology methods

Table 5: Materials for molecular biology methods

Reagent	Supplier
1 kb DNA ladder	Invitrogen, Waltham, MA, USA
Annexin V-APC, 1:15	BD Biosciences, Franklin Lakes, NJ, USA
Annexin V-FITC, 1:15	BD Biosciences, Franklin Lakes, NJ, USA
AMAXA cell line nucleofector kit T	Lonza Group Ltd., Basel, Switzerland
Ampicillin	AppliChem, Darmstadt, Germany
Cold water fish skin gelatine (FGEL)	Sigma-Aldrich, St. Louis, MO, USA
cOmplete Protease Inhibitor Cocktail	Roche, Penzberg, Germany
DCFDA / H2DCFDA - Cellular ROS Assay Kit	Abcam, Cambridge, UK
DNase I	Roche, Penzberg, Germany
DNeasy Blood and Tissue Kit	Qiagen, Hilden, Germany
Dual-Glo Luciferase Assay System	Promega, Madison, WI, USA
Protein G Dynabeads	Thermo Fisher, Waltham, MA, USA
Expand Long Template PCR Kit	Roche, Penzberg, Germany

Table 5 – continued from previous page

Reagent	Supplier
GeneRead FFPE DNA Kit	Qiagen, Hilden, Germany
GIBSON Assembly Master Mix (2X)	New England Biolabs, Ipswich, MA, USA
GoTaq DNA Polymerase	Promega, Madison, WI, USA
GreenMasterMix (2X) High ROX	Genaxxon, Ulm, Germany
Green GoTaq Buffer (2X)	Promega, Madison, WI, USA
HighPure RNA Isolation Kit	Roche, Penzberg, Germany
Kappa HiFi PCR Kit	Roche, Penzberg, Germany
LightShift EMSA kit	Thermo Fisher, Waltham, MA, USA
Magnisphere streptavidin paramagnetic particles	Promega, Madison, WI, USA
Medical X-ray Film	Fuji, Tokyo, Japan
M-MLV reverse transcriptase	Promega, Madison, WI, USA
Nitrocellulose blotting membrane 0.45 µM	Amersham Pharmacia, Piscataway, NJ, USA
NE-PER Nuclear and Cytoplasmic Extraction Reagents	Thermo Fisher, Waltham, MA, USA
PageRuler Prestained Protein Ladder	Thermo Fisher, Waltham, MA, USA
PureLink HiPure Plasmid Filter Maxiprep Kit	Invitrogen, Waltham, MA, USA
QIAprep Spin Miniprep Kit	Qiagen, Hilden, Germany
QIAquick Gel Extraction Kit	Qiagen, Hilden, Germany
QIAquick PCR Purification Kit	Qiagen, Hilden, Germany
QIASeq targeted DNA human comprehensive cancer panel DHS-3501Z	Qiagen, Hilden, Germany
QIASeq V3-chemistry	Qiagen, Hilden, Germany
QuantiTect SYBR Green PCR Kit	Qiagen, Hilden, Germany
Rapid DNA Ligation Kit	Roche, Penzberg, Germany
RNase A	Amersham Pharmacia, Piscataway, NJ, USA
RNeasy Mini Kit	Qiagen, Hilden, Germany
Sonicated salmon sperm DNA	Stratagene, San Diego, CA, US
Streptavidin-HRP	Cell Signaling, Danvers, MA, USA
West Dura Extended Duration Substrate	Thermo Fisher, Waltham, MA, USA

2.1.2 Plasticware

Table 6: Plastic ware

Product	Manufacturer
38.5 mL, Open-Top Thinwall Ultra-Clear Tube 25 x 89mm - 50Pk	Beckman Coulter, Brea, CA, USA
Cellstar Cell Culture Dishes	Greiner Bio-One, Kemsminster, Austria
Cellstar Cell Culture Flasks, 25 cm ² /75 cm ²	Greiner Bio-One, Kemsminster, Austria
Conical Centrifuge Tubes, 15 ml/50 ml	Falcon, San Diego, CA, USA
Eppendorf Tubes, Safe-Lock, 1.5 ml/2 ml	Eppendorf, Hamburg, Germany
6-/12-/24-/48-/96-well plates	Falcon, San Diego, CA, USA
PCR-Tubes	Sarstedt, Nümbrecht, Germany
Reagent Reservoir	Corning, New York, USA
Round bottom tube, 5 ml	Sarstedt, Nümbrecht, Germany
Round bottom tube with cell strainer lid	Falcon, San Diego, CA, USA
Syringe Filter, 0.2 µm/0.45 µm	Whatman, Maidstone, UK
Syringe, 10 ml/20 ml	Braun, Melsungen, Germany

2.1.3 Technical laboratory equipment

Table 7: Technical laboratory equipment

Product	Manufacturer
Bio-Analyzer	Agilent, Santa Clara, CA, USA
ChemiDoc MP	Bio-Rad, Hercules, CA, USA
EpiShear Probe Sonicator	Active Motif, Carlsbad, CA, USA
FACS Canto II	Becton Dickinson, Franklin Lakes, NJ, USA
GenoSmart	VWR, Ulm, Germany
LightCycler 480	Roche Applied Science, Penzberg, Germany
Lumat LB9507	Berthold Technologies, Bad Wildbach, Germany
Mi-Seq	Illumina, San Diego, CA, USA
Nanodrop 1000	Thermo Fisher Scientific, Waltham, MA, USA
Nucleofector IIb	Lonza Group Ltd., Basel, Switzerland
Optima L-90K Ultracentrifuge	Beckman Coulter, Brea, CA, USA
Primus 94 Plus Thermal Cycler	MWG Biotech, Ebersberg, Germany
S3e Cell Sorter	Bio-Rad Laboratories, Hercules, CA, USA
SpectraMax 250 Microplate Reader	Molecular Devices, San Jose, CA, USA
ViCell-XR Cell Viability Analyzer	Beckman Coulter, Brea, CA, USA

2.1.4 Websites and software

Table 8: Websites and software

Product	Manufacturer/URL	Version
BD FACSDiva	Beckton Dickinson	1.13
Cellosaurus	www.web.expasy.org/cellosaurus/	39
CLC Genomic Workbench	Broad Institute, MIT	20.0.3
FlowJo	Beckton Dickinson	10.0.8
Gene Set Enrichment Analysis	Broad Institute, MIT	4.1.0
Gene Palette	University of California	2.1.1
GENEVESTIGATOR	Nebion	9.0.0
Gene expression omnibus (GEO)	https://www.ncbi.nlm.nih.gov/geo/	N/A
ImageJ	NIH, USA	1.53k
Integrated genome viewer (IGV)	Broad Institute, MIT	2.10.3
LightCycler Software	Roche	1.5.0
Microsoft Office 2019	Microsoft	16.54
Omics Explorer	Qlucore	3.6
Primer-BLAST	www.ncbi.nlm.nih.gov/tools/primer-blast/	N/A
PRISM	GraphPad	9
ProSort Software	Bio-Rad	1.6
Snapgene	GSL Biotech LLC	5.3.2

2.1.5 Vectors

shRNA-knockdown

All shRNAs were cloned into the shRNA expression vector pRSI12-U6-sh-UbiC-TagRFP (Cellecta, Mountain View, California, USA). The scrambled control shRNA was derived from Cellecta (<https://www.cellecta.com>). The sequences cloned into the backbone were selected using the Broad Institute GPP Web Portal (<https://portals.broadinstitute.org/gpp/public/>), checked for on-/off-target effects using Primer-BLAST (<https://blast.ncbi.nlm.nih.gov/Blast.cgi>) and are listed in the table below.

Table 9: shRNA sequences

CCND3-shRNA1 (Wang et al., 2018)	5'-accggctagggttattgcatttggatgtaata tcatagcatccaaatgcaataaccctagtttttg -3'
	rev: 5'- aattcaaaaaactagggttattgcatttgg atgctatgaatattaacatccaaatgcaataaccctagc -3'
CCND3-shRNA2 (Radulovich et al., 2010)	fwd: 5'- accggcagaccagcactcctacagatgt taatattcatagcatctgtaggagtgcctgctgtttttg -3'
	rev:5'- aattcaaaaaacagaccagcactcctacagat gctatgaatattaacatctgtaggagtgcctgctgc-3'
Cend3-shRNA (mouse) cloneId=TRCN0000011978	fwd:5'- accgggcatgatggcagagaaatagt taatattcatagctatttctctgacctcatggctttttg -3'
	rev: 5'- aattcaaaaaagccatgatggcagaga aatagctatgaatattaactatttctctgacctcatggcc -3'
CDK8-shRNA1 cloneId=TRCN000019998	fwd: 5'- accggcagaccagcactcctacagatgt taatattcatagcatctgtaggagtgcctgctgtttttg -3'
	rev: 5'- aattcaaaaaagtccatgactgttgcgaat ggctatgaatattaaccattcgcaacagtgcattggacc -3'
CDK8-shRNA3 cloneId=TRCN0000382350	fwd: 5'- accggcagaccagcactcctacagatgtt aatattcatagcatctgtaggagtgcctgctgtttttg -3'
	rev: 5'- aattcaaaaaatggtgaagtcaattattata tgctatgaatattaacatataatagtgacttcaccatc -3'

CRISPR/Cas9

The gRNA targeting CCND3 in exon 2 was designed using the Broad Institute GPP Web Portal (<https://portals.broadinstitute.org/gpp/public/>) and cloned into lentiCRISPRv2-GFP, which was a gift from Feng Zhang (Addgene plasmid 52961).

Table 10: gRNA sequence

gRNA	Sequence
gCCND3-1	fwd: 5'- caccgacacacgcacccgcaactgg -3' rev: 5'- aaaccagttgcgggtgcgtgtgtc -3'

Overexpression constructs For ectopic expression of CCND3, I used the SFFV-CCND3-eGFP vector that was previously described (Wang et al., 2018).

For overexpression of CCND2, I first amplified the CCND2 open reading frame from the genome of NALM-6 cells, using the following primers:

Fwd: 5'-taattaactcgagttaacgcaccatggagctgctgtgc-3'

Rev: 5'-gggggggaggaggagggggctcacaggtcgatatcccgc-3'

The amplicon was cloned into the NotI cutting site of SFFV-eGFP using GIBSON assembly ligation according to the manufacturer's instructions.

2.1.6 Antibodies

Primary unconjugated antibodies

Table 11: Primary unconjugated antibodies used for immunoblot and flow cytometry

Target	Host species	Dilution	Manufacturer	Product ID
ACTB-HRP	Rabbit	1:2000	Santa Cruz	#sc-47778
CBFB	Rabbit	1:1000	Cell Signaling	D4N2N, #62184
CCND1	Rabbit	1:1000	Cell Signaling	29G2, #2978
CCND2	Rabbit	1:2000	Cell Signaling	D52F9, #3741
CCND3	Mouse	1:500	Cell Signaling	DCS22, #2936
CDK8	Rabbit	1:1000	Cell Signaling	P455, #4106
FLAG M2	Mouse	1:1000	Sigma-Aldrich	F1804
FOXO1	Rabbit	1:250	Cell Signaling	C29H4, #2880
FOXO1-pS254	Rabbit	1:1000	Cell Signaling	E1F7T, #84192
ICMT	Rabbit	1:1000	St John Laboratory	STJ112331
LAMIN A/C	Goat	1:1000	Santa Cruz	#sc-6215
Mouse IgG2a	Mouse	1:2000	Cell Signaling	E5Y6Q, #61656
MYC	Rabbit	1:500	Santa Cruz	#sc-788
RB1	Mouse	1:1000	Cell Signaling	4H1, #9309
TUBB	Rabbit	1:400000	Abcam	#ab6046

Secondary antibodies

Table 12: HRP- and fluorophore-coupled secondary antibodies used for immunoblot and flow cytometry

Species	Dilution	Manufacturer	Product ID
Donkey anti-goat-HRP	1:5000	Santa Cruz	#sc-2020
Donkey anti-mouse Alexa Flour 488	1:2000	Invitrogen	A11029
Goat anti-rabbit-HRP	1:10,000	Thermo Fisher Scientific	#31460
Goat anti-mouse-HRP	1:5000	Santa Cruz	#2005

2.2 Methods

2.2.1 Bioinformatical methods

RNA-expression data mining

RNA-expression data were mined using GENEVESTIGATOR (Nebion AG,

Zurich, Switzerland) (Hruz et al., 2008). Experimental data sets used for analysis are listed in Table 13. Data were analyzed and visualized using Microsoft Excel (Microsoft, Redmond, Washington, USA) and Graphpad PRISM 9 (Graphpad, San Diego, CA, USA).

Table 13: Experiment IDs of the data sets mined with GENEVESTIGATOR.

Cell type	Experiment ID
Double positive thymocyte	HS-01453
Splenic CD8 activated T-cell	HS-03092
Peripheral blood CD8 T-cell	HS-02178
	HS-01060
	HS-01905
	HS-01403
	HS-00803
	HS-00060
Bone marrow	HS-00217
	HS-00587
	HS-00730
	HS-01525
	HS-00017
CD4 single-positive thymocyte	HS-01453
Peripheral blood CD8 cytotoxic T-cell	HS-03111
Peripheral blood CD4 naive T-cell	HS-02934
	HS-03472
	HS-00520
	HS-01443
	HS-01467
	HS-01454
	HS-01451
Tonsillar centroblast	HS-01901
	HS-01906
	HS-01904
CD4 regulatory T-cell	HS01310
	HS-00812

Table 13 – continued from previous page

Cell type	Experiment ID
Peripheral blood lymphocyte	HS-00914
	HS-00927
	HS-01365
	HS-00472
	HS-02303
	HS-00801
Peripheral blood CD4 resting T-cell	HS-00631
	HS-00415
	HS-00944
Peripheral blood CD4 T-cell	HS-02178
	HS-01060
	HS-02810
	HS-01487
	HS-01905
	HS-00529
	HS-01299
	HS-01403
	HS-00940
	HS-00803
HS-00060	
Peripheral blood CD8 naive T-cell	HS-02934
	HS-03558
	HS-03472
	HS-01441
Tonsillar CD8 T-cell	HS-01470
Peripheral blood CD8 activated T-cell	HS-03558
	HS-03092
	HS-00631
Lymphocyte	HS-00776
	HS-00261
Peripheral blood NK cell	HS-02934
	HS-01403
Peripheral blood NK T-cell	HS-02934
	HS-00639
Peripheral blood CD4 naive regulatory T-cell	HS-01467

Table 13 – continued from previous page

Cell type	Experiment ID
Peripheral blood CD4 activated T-cell	HS-00944
	HS-00504
	HS-00415
	HS-00631
	HS-00400
Peripheral blood CD8 memory T-cell	HS-02934
	HS-01468
	HS-03472
Peripheral blood CD4 central memory T-cell	HS-02934
	HS-01454
	HS-01451
	HS-03472
CD4 activated T-cell	HS-00217
Peripheral blood CD4 effector memory T-cell	HS-02934
	HS-01443
	HS-03472
	HS-01451
	HS-01454
Tonsillar CD4 T-cell	HS-01470
Monocyte	HS-00989
B-cell	HS-02501
Breast stroma cell	HS-01330
Osteoblast	HS-00509
Neuron	HS-00396
Skeletal muscle myoblast	HS-02732
Pancreatic islet cell	HS-02062
Renal tubulointerstitium	HS-02631
Bronchiolar epithelium cell	HS-01926
Adipose tissue	HS-00217
Hepatocyte	HS-01472
Colonocyte	HS-00899
Epidermal keratinocyte	HS-02490
Progenitor B-ALL	HS-00636

Table 13 – continued from previous page

Cell type	Experiment ID
Precursor B-ALL	HS-01387
	HS-01385
	HS-00730
	HS-00719
	HS-00636
	HS-00635
	HS-00430
	HS-00240
ETV-RUNX1 B-ALL	HS-01387 HS-01385
MLL-rearranged B-ALL	HS-01387 HS-01385
BCR-ABL1 ⁺ B-ALL	HS-01387 HS-01385
TCF3-PBX1 B-ALL	HS-01387 HS-01385
Hyperdiploid	HS-01387 HS-01385
Acinar cell carcinoma	HS-01196
Pancreas, neoplasm	HS-00620
Osteosarcoma	HS-00694
Astrocytoma	HS-01935
Colon, neoplasm	HS-00608
Multiple myeloma	HS-02108
Breast, neoplasm	HS-00756
Malignant melanoma	HS-01114
Hepatocellular carcinoma	HS-01472
Brain, neuroblastoma	HS-00906
Renal cell carcinoma	HS-01301

ChIP-sequencing analysis

Publicly available ChIP-sequencing data for FOXO1 from CD34⁺ pre-leukemic stem cells (GSM2136846) and mature B-lymphocytes (GSM1668935) were mined from the GEO repository database. Data were visualized and analyzed using IGV and GenePalette.

2.2.2 Cell culture

Human B-ALL cell lines

All human B-ALL cell lines (Table 14) were cultivated in RPMI1640

supplemented with 20 % fetal bovine serum (FBS), 2 mM L-glutamine, 100 U/mL penicillin and 100 µg/mL streptomycin at 37 °C and 5 % CO₂. The identity of all cell lines was regularly authenticated by short tandem-repeat (STR) analysis using the GenomeLab GeXP Genetic Analysis System (Sciex, Darmstadt, Germany) and the GenomeLabHuman STR primer set (Beckman Coulter, Brea, CA, USA). STR profiles were analyzed using the Cellosaurus database (<https://web.expasy.org/cellosaurus>). All cells were regularly tested for contamination with mycoplasma using the luciferase-based MycoAlert Mycoplasma Detection Kit (Lonza Group Ltd., Basel, Switzerland).

Table 14: Human B-ALL cell lines

Cell line	Genetic Alteration
BV-173	t(9;22) (q34;q11) BCR-ABL1
EU-3/697	t(1;19)(q23;p13) E2A-PBX1
KOPN-8	t(11;19)(q23;p13.3) MLL-ENL
NALM-6	t(5;12) (q31q33;p12) ETV6-PDGFRB
NALM-20	t(9;22) (q34;q11) BCR-ABL1
O18Z	del(9)(p13) deletion CDKN2A/B
REH	t(12;21)(p13;q22) ETV6-AML1
RS4;11	t(4;11) (q21;q23) MLL-AF4
SUP-B15	t(9;22) (q34;q11) BCR-ABL1
TOM-1	t(9;22) (q34;q11) BCR-ABL1

Adherent cells

HEK293T and LentiX cells were grown in DMEM which was supplemented with 10 % FCS, 2 mM L-glutamine and 100 U/mL penicillin and 100 µg/mL streptomycin. Both cell lines were passaged or split before reaching over 90 % confluency.

OP9 mouse fibroblasts were cultivated in α -MEM, supplemented with 20 % FBS, 2 mM L-glutamine, 100 U/mL penicillin, 100 µg/mL streptomycin and 1 mM sodium pyruvate at 37 °C and 5 % CO₂.

Mouse *Foxo1^{fl/fl}* BCR-ABL1⁺ B-ALL cells

Murine pre-B-cells isolated from mice with homozygously *loxP*-flanked

Foxo1 loci, transformed with BCR-ABL1 and expressing either Cre^{ERT2} or a control vector (ERT2) were a kind gift from H. Jumaa (Ulm University, Germany). The cells were cultivated in IMDM containing 10% FBS, 2 mM L-glutamine, 100 U/mL penicillin, 100 µg/mL streptomycin 50 µM β-mercaptoethanol at 37 °C and 7.5 % CO₂. Selection for Cre^{ERT2} was done with 2 µg/ml puromycin. Deletion of *Foxo1* was induced with 200 nM 4-OHT and confirmed by PCR (Figure 8).

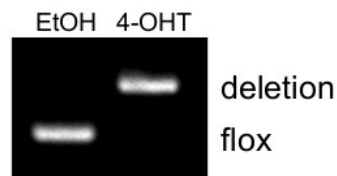


Figure 8: Confirmation of *Foxo1* deletion by PCR

Foxo1 deletion in Cre-^{ERT2} expressing BCR-ABL1-transformed murine pre-B-cells was induced with 200 nM 4-OHT 24 h before genomic DNA was extracted for PCR. Primers used: Primer 1: CAAGTCCATTAATTCAGCACATTGA Primer 2: CCAGACTCTTTGTATCAGCAAATAA Primer 3: GCTTAGAGCAGAGATGTTCTCACATT

Primers 1 and 2 result in the flox band, primers 1 and 3 result in the deletion band.

Patient-derived xenograft *ex vivo* culture

The B-ALL PDXs JFK125R, PDX2 and BLQ5 were a kind gift from M. Müschen (Yale School of Medicine, USA) For the culture of PDX cells, OP9 murine stroma cells were irradiated with 25 Gray, and seeded at 0.35 x 10⁶ cells per well in a six-well plate coated with 0.2 % gelatine. The next day, PDX cells were thawed and transferred to the six-well plate containing the irradiated OP9 cells. OP9 and all PDXs were grown in alpha-MEM with 20 % FBS, 2 mM L-glutamine, 100 U/mL penicillin, 100 µg/mL streptomycin and 1 mM sodium pyruvate at 37 °C and 5 % CO₂.

Lentiviral transduction

Lentivirus production

All lentivirus was produced with the envelope VSV-G and the packaging vector pCMV-dR8.91. For human B-ALL cell lines, virus was produced in

HEK293T cells with 2.8 µg VSV-G, 4.3 µg pCMV-dR8.91 and 4.3 µg plasmid of interest per dish. Transfection was performed by mixing the plasmids with 500 µl OptiMEM and 45.6 µg polyethylenimine. After incubation of 15 minutes, the mix was added dropwise onto HEK293T cells that were split to 9×10^6 cells per 10 cm dish the day prior and which medium was changed to 7.5 ml pre-warmed OptiMEM while the transfection mix was incubating. 8 hours after transfection, the medium was replaced with 8 ml fresh OptiMEM. Virus was harvested 48 h and 72 h after transfection and filtered with a 0.45 µm syringe filter. If not used directly, virus was stored at -80 °C until further use.

For both murine BCR-ABL1 transformed pre-B-cells and human PDX cells, virus was produced in LentiX cells that were split the day prior in the same way as the HEK293T cells were. Per transfected plate, 5 µg VSV-G, 10 µg pCMV-dR8.91 and 12 µg plasmid of interest were transfected using the TAKARA CaCl₂-Phosphate transfection method according to the manufacturer's instructions. The next day, the medium was changed to the culture medium of either murine or human PDX cells, 5 ml per plate. For PDX virus, harvesting was done as described for B-ALL cell lines. For murine B-ALL cells, virus from 5 plates containing 5 ml of the same transfection each was pooled after three days, amounting to approximately 50 ml total. Virus was then transferred to round bottom, 38 ml ultracentrifuge tubes, together with 5 ml 70 % sucrose which was placed at the bottom of the tube. Ultracentrifugation was carried out at 25,000 rpm at 4 °C for 2 hours. Medium and sucrose were aspirated and virus pellet was resuspended in 500 µl IMDM mouse B-ALL culture medium. If not used directly, virus was stored at -80 °C until further use.

Lentiviral transduction

For human B-ALL cell line transduction, 1 ml of virus stock was mixed with 2×10^6 B-ALL cells and inoculated while spinning at 2000 rpm for 2 hours at 4 °C. Supernatant was removed and cells were resuspended in 4 ml culture

medium and put back in the incubator for culture until further analysis.

For the transduction of human PDX cells, the day before the transduction, 0.35×10^6 OP9 stroma cells were irradiated at 25 Gy and split on a 6-well plate that has been coated with 0.2 % gelatine. On the day of transduction, 3 ml of virus stock was spun onto wells of a 6-well plate coated with 50 $\mu\text{g/ml}$ Retronectin at 2000 x g for 2 hours at 32 °C. Next, 2×10^6 PDX in 1 ml fresh culture medium were added to each well and centrifuged at 600 x g for 30 minutes at 35 °C. The plate was incubated at 37 °C overnight. The next day, transduced cells were collected, the supernatant was removed and cells were transferred to the well plate with prepared OP9 cells and left in the incubator at 37 °C until further analysis.

For transduction of murine B-ALL cells, the protocol was the same as for the PDX cells with a few alterations. Instead of 3 ml pure virus in a 6-well plate, 50 μl of concentrated virus stock in 500 μl culture medium was spun onto the Retronectin-coated 12-well plate. Furthermore, 0.5×10^6 murine B-ALL cells were added to each well before further centrifugation and incubation as described for PDXs.

2.2.3 Molecular biological methods

Molecular cloning procedures

After the design of the target sequences, the vectors for shRNA mediated knockdown and CRISPR/Cas9 gene editing (Tables 9 & 10) were cloned using the following procedure:

1. Annealing of oligonucleotides

Two complementary oligonucleotides (either containing the shRNA target site or the gRNA target site, flanked with recognition sequences for the enzyme restriction sites in their respective target backbones) were annealed by incubating 3 μg of each oligonucleotide with 48 μl annealing buffer at 95 °C, for 3 minutes. Subsequently, the mix was incubated for 10 minutes at 70 °C and very slowly cooled to 10 °C.

2. *Restriction digest*

The target vector for shRNA expression was cut with BbsI and EcoRI, pLentiV2-Cas9 was restriction digested with BsmBI. The resulting products were applied on an agarose gel and subsequently purified for downstream ligation.

3. *Ligation*

For ligation of the annealed oligonucleotides into the backbones, ligation was performed with the Roche Rapid DNA Ligation kit according to the manufacturer's instructions.

4. *Heat-shock transformation and plasmid purification*

After ligation, 2 μ l of ligation mix were incubated with 50 μ l XLBlue E.Coli bacteria and spread on LB_{AMP} agarose plates and incubated at 37 °C overnight. The next day, clones were picked and inoculated shaking in 1.5 ml LB_{AMP} medium for 6-10 h. Plasmids were extracted using the QIAprep Spin Miniprep Kit according to the manufacturer's instructions, then sent for Sanger sequencing at Eurofins Genomics with a sequencing primer binding in the shRNA/gRNA U6 promoter. After verification of successful cloning, 100 μ l of miniprep bacteria was inoculated in 200 ml LB_{AMP} overnight, shaking at 37 °C. The next day, plasmid DNA was purified using the PureLink HiPure Plasmid Filter Maxiprep Kit according to the manufacturer's instructions.

Growth dynamics measurement

In order to assess the consequences of acute loss of *CCND3* and *CDK8* in B-ALL cell lines, murine B-ALL and PDXs, the amount of successfully transduced, living RFP⁺ were analyzed by flow cytometry in a competitive growth assay. The first measurement was conducted four days after transduction and set as baseline (100%, day 0) for all targeting shRNAs and the scrambled control. The transduced cells were then measured every three days, three times until day 13 after transduction (day 9 after first measurement). RFP⁺ cells of each transduction were calculated relative to

day 0. Flow cytometry analysis was performed with the FACSCanto II (BD) or S3e cell sorter (Bio-Rad). Further analysis of data was done using FlowJo software.

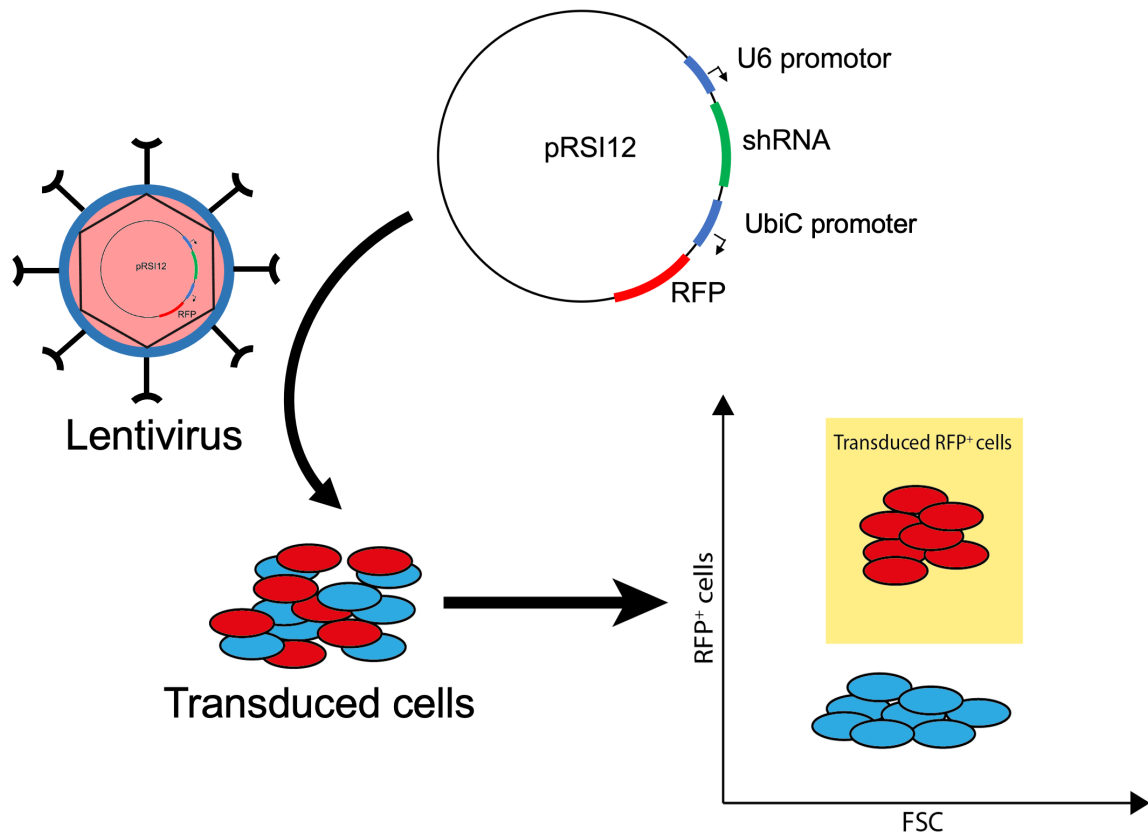


Figure 9: Schematic principle of growth dynamic measurement by flow cytometry

B-ALL cells were lentivirally transduced with plasmids co-expressing RFP and either a scrambled control or an shRNA. Cells were measured by flow cytometry on days 4, 7, 10 and 13 after transduction. The number of RFP⁺ cells was calculated relative to day 0

For relative growth measurements, NALM-6 cells were lentivirally transduced with SFFV-EV or SFFV-CCND2-eGFP or SFFV-CCND3-GFP, then treated with 40 nM or 80 nM AS1842856 or 0.1 μ M, 0.5 μ M or 1 μ M palbociclib, starting 6 days post-transduction. Percentages of GFP⁺ cells (by flow cytometry) and the total number of live cells (by cell counting with trypan blue exclusion) were measured at indicated time points. Data are shown as fold changes normalized to the initial number of live GFP⁺ cells. The number of live GFP⁺ cells was calculated as $N \times \% \text{ GFP}^+ \text{ cells}/100$,

where N is the number of live cells per well and % GFP⁺ is the percentage of GFP⁺ cells. Analysis was done with the FACSCantoII and FlowJo software.

Apoptosis measurement

For transduction experiments, cells were sorted four days post-transduction for 100 % transduced cells and kept in culture for two more days before apoptosis assay was performed. For palbociclib experiments, cells were treated three days with 1 μM palbociclib before staining and analysis. 0.5-1x10⁶ cells were washed once in Annexin V binding buffer and then incubated in 76.5 μl staining solution for 15 minutes at room temperature in the dark. Cells were analyzed using the FACSCanto II flow cytometer. Unstained cells were defined as living, the remaining cells were defined as dead or dying. Further analysis and quantification were done with FlowJo.

Formula for specific apoptosis:

$$100 \times \frac{Apoptosis_{Experiment} - Apoptosis_{Control}}{100 - Apoptosis_{Control}}$$

Cell cycle analysis

For transduction experiments, cells were sorted four days post-transduction for 100 % transduced cells and kept in culture for two more days before cell cycle analysis was performed. For palbociclib experiments, cells were treated three days with 1 μM palbociclib before staining and analysis. 0.5-1x10⁶ cells were washed once in 10 ml 1X PBS. 1 ml ice-cold PBS and 3 ml ice-cold 70 % Ethanol were added dropwise during vortexing and cells were incubated on ice for one hour to fix. Next, the fixing solution was removed and cells were resuspended in 400 μl PI staining solution. Samples were incubated for 30 minutes at 37 °C in the dark before analysis with the FACSCanto II. Analysis of cell cycle distribution was done using FlowJo.

Immunoblotting

Whole-cell protein lysates for immunoblotting were prepared by first washing the cells once in 1X PBS and lysis in 100 μ l SDS sample buffer per 1×10^6 cells. Samples were boiled for 5 minutes at 95 °C.

Nuclear extracts were prepared using the Thermo Fisher NE-PER Nuclear and Cytoplasmic Extraction Reagents according to the manufacturer's instructions. 1 volume of 2X Laemmli buffer was added to the extracts and boiled for 10 minutes at 95 °C.

For gel electrophoresis, 10 % polyacrylamide gels were prepared and 10 μ l protein lysates were loaded per pocket. Electrophoresis was performed at 80 V until samples passed the collection gel and was then set to 120 V until the running front reached the bottom of the gel. Blotting was done in a wet blotting chamber filled with immunoblot transfer buffer, the cassette was stacked, from the red (+) to the black (-) side, in the following order:

Sponge - Two Whatman papers - 0.45 μ M nitrocellulose membrane - Two Whatman papers - Sponge.

Wet blotting was conducted at 80 V for 80 minutes in a 4 °C cold room. Membrane was blocked with 5 % skim milk in 0.1 % TBS-T for 15 minutes at 37 °C. Primary antibodies were applied slowly shaking at 4 °C overnight, HRP-coupled secondary antibodies for 1 hour at room temperature. Washing in between antibodies was done twice with 0.05 % TBS-T and once with TBS. For the detection of the chemiluminescent signal, West Dura Extended Duration Substrate was added on the membrane, incubated for 5 minutes and then detected using the ChemiDoc MP.

Luciferase assay

For the construction of the CCND3 promoter constructs, the promoter region of CCND3 (NC_000006.12, www.ncbi.nlm.nih.gov, 22.05.2020) -1389 bp to +259 bp (long) or only the core promoter (short) from the transcriptional start site (TSS) was cloned from genomic DNA isolated from RS4;11 cells. This was cloned into the XhoI restriction site of the pGL4.22

luciferase reporter vector using GIBSON assembly with the cloning primers listed below. Verification of the cloned fragments was verified by Sanger sequencing (Eurofins Genomics, Ebersberg, Germany).

Cloning primers:

Fwd: 5'- ggtacctgagctcgctagccttacaggcgtgagctaccgc -3'

Rev: 5'- gaggccagatcttgatatccaccagcaccgatcccca -3'

For measurement of luciferase reporter activity, 5×10^6 NALM-6 and RS4;11 cells were nucleofected with help of the AMAXA cell line kit T using the program C-005 on the Lonza Amaxa nucleofector IIb. As the internal control, the ubi-*Renilla* expression plasmid was co-transfected in 100-fold fewer amounts (50 ng), as described previously by our group (Vogel et al., 2014). Immediately after transfection, cells were transferred to 6 well plates containing 2 ml medium with 80 nM of the FOXO inhibitor AS1842856 or the equivalent amount of DMSO as control. Using the Dual-Luciferase Reporter Assay System (Promega, Madison, Wisconsin, USA) and the Lumat LB 9507 tube luminometer (Berthold Technologies, Bad Wildbad, Germany), luciferase reporter activity was measured 24 hours later. Firefly luciferase activity was normalized to ubi-*Renilla* luciferase activity.

Electrophoretic mobility shift assay (EMSA)

9×10^6 HEK293T cells were transfected with either 11.4 μ g pFLAG-CMV2 (D19) or pFLAG-CMV2-FhBox (D22) and 45.6 μ l PEI in OptiMEM. Nuclear extracts were taken after 48 h with the Thermo Fisher NE-PER Nuclear and Cytoplasmic Extraction Reagents according to the manufacturer's instructions.

Two pairs of 25 bp complementary, 5' biotinylated oligonucleotides were designed, derived from the FOXO1 binding motif located in the CCND3 (NC_000006.12, <https://www.ncbi.nlm.nih.gov>, 22.05.2020) promoter region, 126 bp upstream of the CCND3 TSS. One pair of probes contains the FOXO binding motif "GTAAACA" in the genomic context. In the other

oligo, the binding motif was scrambled to "CGTGCAG" as described previously (Vogel et al., 2014), context stayed the same. Annealing of oligos was performed as described for shRNAs.

EMSA was performed with the LightShift EMSA kit according to the manufacturer's instructions. Final amounts for each reaction were:

Table 15: EMSA Setup

All amounts given in μl .

EMSA	Final amount	Oligo only	EV/FhBox		
			Shift	Super Shift	Mutant
H2O		12	9	7	9
10X Binding Buffer	1X	2	2	2	2
1 $\mu\text{g}/\mu\text{l}$ Poli (dI-dC)	50 ng/ μl	1	1	1	1
Unlabeled target DNA	4 pmol				
Protein extract			3	3	3
Biotin End-Labeled Target DNA	20 fmol	5	5	5	5
Antibody (α -FLAG)				2	

Chromatin immunoprecipitation (ChIP)

2×10^7 NALM-6 cells were transfected with humanized biotin ligase BirA and either a constitutively active variant of FOXO1 containing an N-terminal biotinylation signal (bFOXO1) or the empty vector control (EV) pcDNA3.1. Transfection was performed using the AMAXA cell line nucleofactor kit T and the Lonza nucleofactor IIb with program C-005.

The next day, each 2×10^7 transfected cells were split into two 50 ml falcon tubes and filled up to 20 ml with pre-warmed culture medium. For crosslinking, 540 μl 37 % formaldehyde (stabilized with Methanol) was added to each 20 ml sample and inverted repeatedly for 10 minutes. Reaction was stopped by adding 2.5 ml ice-cold 1 M Glycin to each tube, inverted repeatedly for 5 minutes. Samples were centrifuged at 1200 rpm for 5 minutes in a pre-cooled centrifuge (4 $^{\circ}\text{C}$), then washed twice in 10 ml ice-cold 1X PBS. Nuclei were isolated by lysis with 600 μl Farnham lysis buffer, transferred to a 1.5 ml Eppendorf tube, 15 minutes rotating at 4 $^{\circ}\text{C}$, 15 minutes standing on ice. Lysate was centrifuged 5 minutes, 5000 rpm at 4

°C. 450 µl Farnham lysis buffer was removed. Homogenization was performed with a pestle 12 times half rotations and centrifuged for 5 minutes at 6000 rpm at 4 °C. Supernatant was completely removed and the pellet was thoroughly resuspended in 350 µl RIPA. Fragmentation was performed by sonication with the EpiShear sonicator in a cooling rack for 30 cycles, 20 seconds on, 30 seconds off at 40 % amplitude. After sonication, samples were centrifuged at 4 °C for 10 minutes at 13000 rpm.

25 µl of each sample was used for input and fragmentation control. Both were reverse crosslinked by adding 175 µl Elution buffer (freshly prepared each day) and 8 µl 5 M NaCl, boiled for 15 minutes at 95 °C. Samples were left to cool, 1 µl 20 mg/ml proteinase K was added and incubated for at least 2 hours at 62 °C, then boiled for 10 minutes at 95 °C. Samples were purified using the QIAGEN PCR purification kit according to the manufacturer's instructions. Fragmentation was confirmed by 1.8 % agarose gel electrophoresis, mean fragment size at approximately 500 bp. For this, 8 µl 10X DNA loading buffer supplemented with 20 µl glycerol per 100 µl buffer was added to 50 µl elution from the PCR purification kit. 40 µl were applied per pocket (Figure 10).

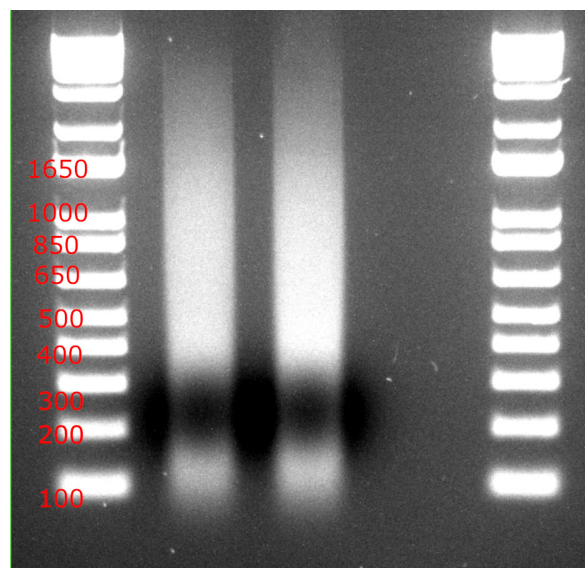


Figure 10: Confirmation of chromatin shearing

Shearing of chromatin to a mean fragment size of 500 bp was confirmed by 1.8 % agarose gel electrophoresis.

The remaining 300 μ l of sheared chromatin was pre-cleared rotating at 4 °C for 1 hour with 40 μ l Protein G Dynabeads (blocked for 1 h at 4 °C with 2 % FGEL + 100 μ g sonicated salmon sperm DNA in 1 ml RIPA). Supernatant was transferred to new tubes and 40 μ l blocked magnisphere streptavidin beads were added, rotating 3 hours at 4 °C. Next, supernatant was discarded and beads (pooled from both tubes of the same transfection) were washed three times in 2 % SDS (in Ampuwa) and three times in LiCl wash buffer. A 10 % Chelex/water solution was freshly prepared and 100 μ l added to the beads, vortexed 10 seconds and boiled at 95 °C for 10 minutes to extract the DNA. 1 μ l RNase A was added and incubated for 15 minutes at 37 °C. 1 μ l 20 mg/ml proteinase K was added and incubated at 55 °C for 30 minutes shaking at 1000 rpm. Samples were boiled again for 10 minutes at 95 °C and DNA was purified using the QIAGEN PCR purification kit according to the manufacturer's instructions.

qRT-PCR was performed with 2 μ l ChIP DNA and 2 μ l Input (1:10 dilution) per well and 8 μ l QIAGEN Quantitect SYBR Green master mix (+ primers and water for 1X concentration). For the gene desert Ch12 control, Human Negative Control Primer Set 1, Active Motif (Carlsbad, CA, USA) was used. For CCND3, primers flanking the FOXO binding motif in the CCND3 promoter with the following sequences were used:

Fwd: 5'-CTGTCACAGTGCCTGACGTG-3'

Rev: 5'-GCAACTCCTCCACGTGCTA-3'

Calculation of fold enrichment was done as follows: the regions of interest (ROI) over the control Chromosome 12 (Ch12) region (R) was calculated. ChIP DNA was first normalized to input (i) DNA by using the following formula: $R_i = 2^{(ct^{Input} - ct^{ChIP})}$. Then, fold enrichment was calculated of ROI in samples transfected with bFOXO1 compared to EV: $R_{bFOXO1/EV} = R_{i(bFOXO1)} / R_{i(EV)}$. R (Fold change relative to Ch12) was calculated using the formula $R = R_{bFOXO1/EV ROI} / R_{bFOXO1/EV CH12}$.

ROS measurement

For detection of ROS accumulation in B-ALL cells after knockdown of CCND3, the Abcam DCFDA / H2DCFDA - Cellular ROS Assay Kit was used according to the manufacturer's instructions. All oxidizable components were handled under argon gas atmosphere. As a control for ROS induction, the provided tert-Butyl hydroperoxide (tBHP) control was used. Measurement of 488 spectrum emission by DCFDA conversion as a consequence of ROS accumulation was measured with the S3e cell sorter (Bio-Rad) and further analyzed using FlowJo software.

RB1 staining

Intracellular staining was performed by fixing and permeabilizing the cells in 10 % formalin for 10 minutes at 37 °C and in methanol for 30 minutes on ice. Staining was done with 1:50 diluted RB1 primary and 1:100 diluted secondary FITC-conjugated antibody, each for 1 hour on ice in intracellular staining buffer. Cells were analyzed by flow cytometry with the FACSCanto II and FlowJo software.

2.2.4 Gene expression analysis

Quantitative reverse transcriptase polymerase chain reaction (qRT-PCR)

RNA was isolated with the Roche HighPure RNA isolation kit (Roche, Basel, Switzerland) according to the manufacturer's instructions. cDNA synthesis was started by incubating 2 µg RNA with 0.5 µg oligo-dT primer, incubating 5 minutes at 70 °C. Next, reverse transcription was performed using the M-MLV reverse transcriptase (Promega, Madison, Wisconsin, USA) according to the manufacturer's instructions. Primers were designed using Primer-BLAST (<http://www.ncbi.nlm.nih.gov/tools/primer-blast>) and synthesized by biomers.net (Ulm, Germany). Annealing of primers was

performed at 60 °C and qRT-PCR was performed in technical duplicates with the Roche LighCycler 480 (Roche, Basel, Switzerland), program listed in Table 17. Relative gene expression was analyzed and calculated using the $2^{-\Delta\Delta ct}$ method. The housekeeping gene used for both human and murine samples was RPL13a/*Rpl13a*. Primer sequences are listed in Table 16.

Table 16: Primers used for qRT-PCR

Primer	Sequence
human CCND1	fwd: 5'- aagctgtgcatctacaccga -3'
	rev: 5'- cttgagcttggtcaccagga -3'
human CCND2	fwd: 5'- gttagagtgcgcgaaggagt -3'
	rev: 5'- gtggggcacaacagctagaga -3'
human CCND3	fwd: 5'- gtggcactaagcagaggag -3'
	rev: 5'- cccttcaggcttagatgtgg -3'
human c-MYC	fwd: 5'- tcgattctctgctctctc -3'
	rev: 5'- tgttctctctcagatcgct -3'
human RPL13A	fwd: 5'- cggaccgtgcgaggtat-3'
	rev: 5'- caccatccgctttttctgtc -3'
mouse Ccnd1	fwd: 5'- cgaagtggagaccatccgcc -3'
	rev: 5'- agggctccagggacaggaag -3'
mouse Ccnd2	fwd: 5'- ccgtacatgcgcaggatggt -3'
	rev: 5'- gcagtcagcgggatggtctc -3'
mouse Ccnd3	fwd: 5'- ggctctccttccccctcaca -3'
	rev: 5'- ttggagccccggacagaaga -3'
mouse c-Myc	fwd: 5'- tcctaccgctcaacgaca -3'
	rev: 5'- cagcagcagatccgaggaag -3'
mouse Rpl13a	fwd: 5'- cctgctgctctcaagttgt -3'
	rev: 5'- ggtacttcacccgacctc -3'

Table 17: qRT-PCR program

Step	Cycles	Temperature	Time
Melting	1	95 °C	15 min
Denaturation	40	94 °C	15 sec
Annealing		60 °C	30 sec
Extension		72 °C	30 sec
Melting	1	95 °C	1 sec
		65 °C	15 sec
		95 °C	0 sec
Cooling	1	40 °C	30 sec

RNA-sequencing

RNA isolation was performed from 1×10^6 cells of each biological triplicate of each sample using the RNeasy kit (Qiagen, Hilden, Germany) according to the manufacturer's instructions. RNA integrity was analyzed with the Agilent 2100 bioanalyzer (Agilent, Santa Clara, USA) and purity was confirmed with Nanodrop (ThermoFisher, Waltham, USA).

For CCND3-knockdown vs. palbociclib RNA-sequencing, construction of the cDNA library and sequencing were performed by the Beijing Genomics Institute (BGI, Shenzhen, China) using the BGISEQ-500. Filtering of raw data was performed with SOAPnuke (version 1.5.2), mapping to hg38 was done with Bowtie2 (version 2.2.5).

For murine *Foxo1* deletion, library construction and RNA-sequencing were conducted by Novogene (London, UK). Base-calling was done with CASAVA base recognition. Mapping to the murine reference genome mm10 was performed by STAR.

Analysis of differentially expressed genes and all other analyses of RNA-sequencing data were performed using Qlucore Omics Explorer (version 3.6) and GSEA (Subramanian et al., 2005).

Sequencing of *RB1* mutations

For targeted sequencing of *RB1*, QIASeq V3-chemistry (Qiagen) was used with the QIAseq targeted DNA human comprehensive cancer panel (Qiagen). DNA isolation was performed with the GeneRead FFPE DNA Kit

(Qiagen) according to the manufacturer's instructions. Target enrichment, amplicon processing and library preparation was done according to the manufacturer's instructions. For target enrichment, 40 ng genomic DNA was used. Successful enrichment and library preparation was checked with a high-sensitivity DNA kit on a Bio-Analyzer (Agilent). Libraries were diluted to 10 pM and sequencing was performed using the Illumina Mi-Seq with a V2 flow cell. medium read-depth was 3000 X and approximately 95 % of sequences reached a unique molecular identifier depth of 100 X. The resulting .fastq files were analyzed using CLC Genomic Workbench and variants were verified using Integrated Genome Viewer (Broad Institute).

Chapter 3

Results

3.1 CCND3 is the highest expressed D-type Cyclin in B-ALL

In lymphoid malignancies, particularly in lymphomas, concurrent expression of Cyclin D2 (CCND2) and CCND3 has been reported (Teramoto et al., 1999). CCND2 is directly transcriptionally activated by MYC (Buchner and Müschen, 2014). Additionally, in MYC-driven Ph⁺ B-ALL, CCND2 is highly expressed (Geng et al., 2015). Because of this and the generally assumed redundancy of D-Cyclins in cell proliferation, CCND2 has typically been used as a stand-in for all three D-Cyclins in studies of B-cell malignancies. Here I set to investigate the expression of Cyclins D1, D2, and D3 in healthy and malignant tissue and most importantly in different genetic subgroups of B-ALL.

3.1.1 CCND3 is distinctly highly expressed in lymphoid cells

By data mining of publicly available gene expression profiling data using the GENEVESTIGATOR database (Hruz et al., 2008), I first compared the RNA expression levels of *Cyclin D1* (CCND1), CCND2, and CCND3 in all tissues and cell types available. Of note, progenitor and precursor B-cells are not indexed in this database and are therefore not shown. Compared to all other anatomical compartments listed in the database, it became apparent that CCND3 was expressed at the highest level in hematopoietic cell types, particularly in T-cells, natural killer cells, monocytes, and B-cells, while CCND1 expression was low in all of these cells (Figure 11). CCND1 was highest expressed in breast stromal tissue, osteoblasts, neurons, and skeletal

muscle cells. In hematopoietic cells, the expression of *CCND2* was higher than *CCND1* but typically lower than *CCND3*.

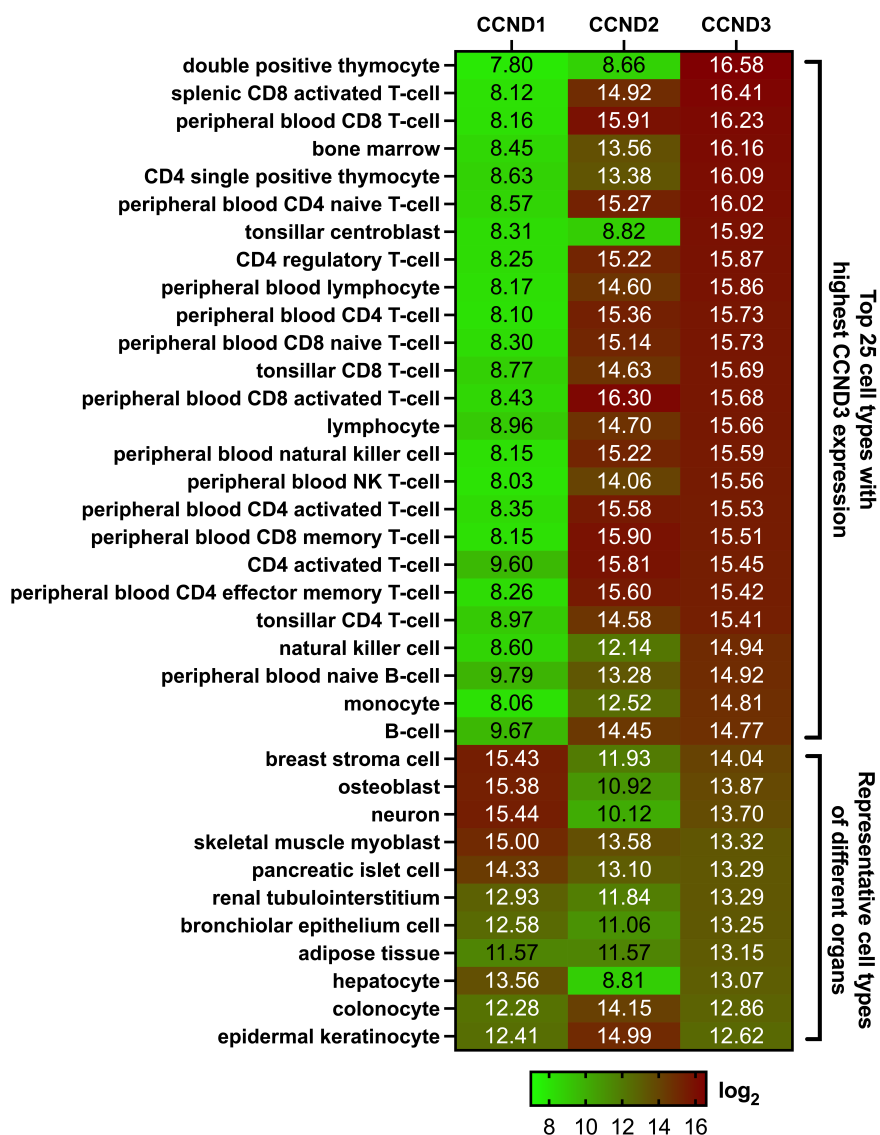


Figure 11: Expression of *CCND3* is most abundant in hematopoietic tissue

Tissue RNA expression data were mined using the GENEVESTIGATOR database. Shown are the top 25 *CCND3* expressing cell types and representative cell types of different organs. For experiment IDs, refer to the materials and methods section. Data are shown as $\log_2(\text{mean})$, $n \geq 3$ for each cell type.

Comparing the expression of D-Cyclins in all 339 types of cancer indexed in the database, *CCND3* was again preferentially expressed in lymphoid tissue. However, instead of T-cells, the highest levels of *CCND3* were found in malignant B-cells, most importantly in B-ALL (Figure 12).

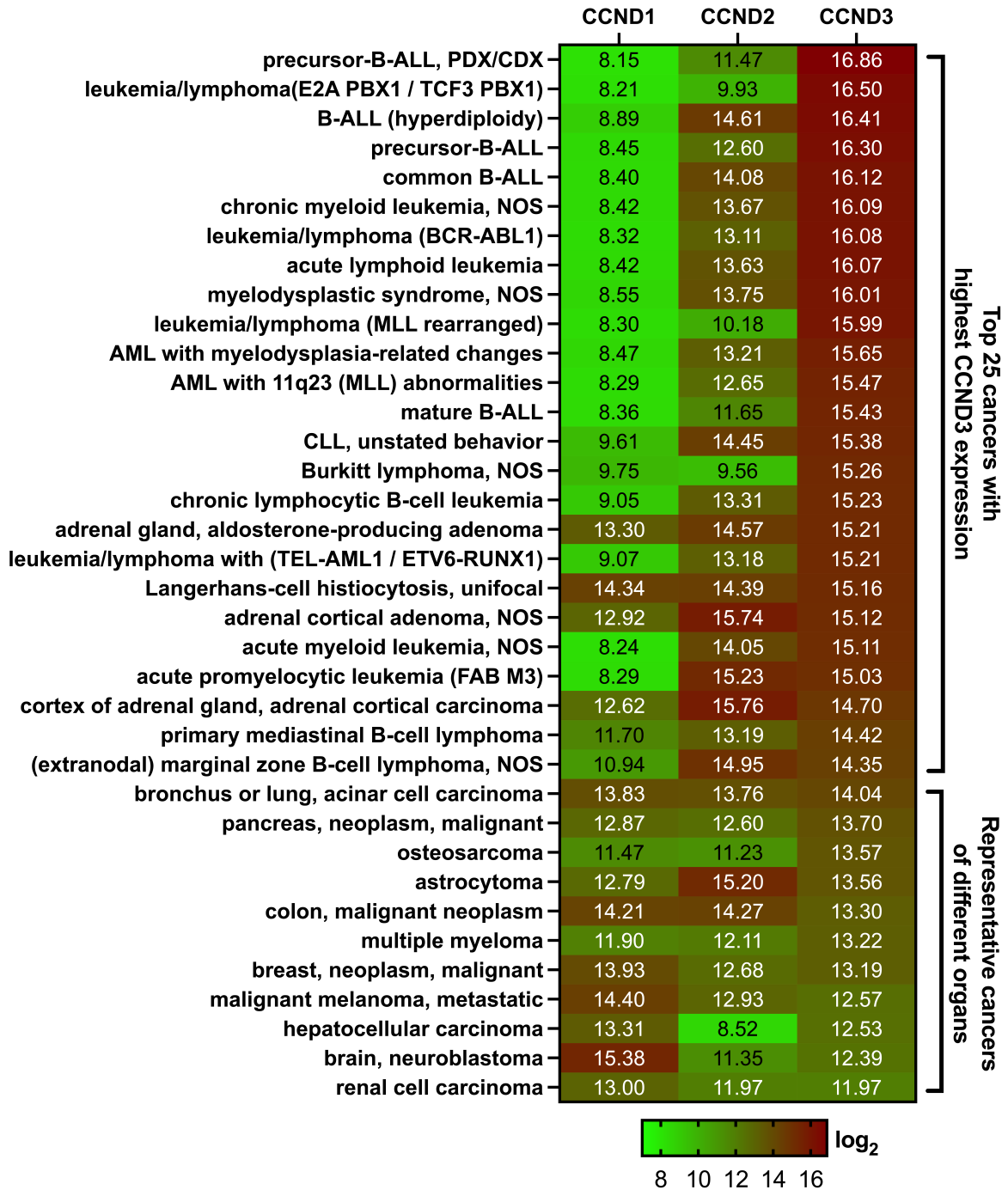


Figure 12: B-lymphoid malignancies show the highest *CCND3* expression

Patient-derived RNA expression data were mined using the GENEVESTIGATOR database. Shown are the top 25 *CCND3* expressing types of cancer and representative cancers of different organs. For experiment IDs, refer to the materials and methods section. Data are shown as $\log_2(\text{mean})$, $n \geq 3$ for each cell type.

Furthermore, as observed in healthy lymphoid tissue, *CCND1* was still expressed at low levels in *CCND3*^{high} lymphoid malignancies like B-ALL. RNA expression levels of *CCND2* were always lower than *CCND3* in all

B-cell-derived malignancies shown and in some cases like MLLr B-ALL and TCF3-PBX1 leukemia almost as low as *CCND1*.

3.1.2 Expression of *CCND3* in cell lines resembles that of primary patient samples

Given that *CCND2* is generally accepted as the primary D-Cyclin in B-ALL (Buchner and Müschen, 2014; Geng et al., 2015) but no further analysis of D-Cyclin expression in B-ALL has been done so far, I performed data mining of the RNA expression of the three D-type Cyclins in patient-derived samples from different genetic backgrounds of B-ALL (Ketzer et al., 2022). First, I stratified B-ALL into pre-BCR⁻ ("Progenitor B-ALL") and pre-BCR⁺ ("Precursor B-ALL"). Next, I analyzed the most common genetic subgroups of B-ALL, namely *ETV6-RUNX1*, *MLL*-rearranged, *BCR-ABL1*, *TCF3-PBX1*, and hyperdiploid B-ALL (Zhang et al., 2017). In these primary samples, *CCND3* was the highest expressed D-Cyclin, while *CCND1* was only expressed at minimal levels (Figure 13). *CCND2*, however, varied in expression, with low levels, comparable to *CCND1* in *MLL*-rearranged and *TCF3-PBX1*⁺ B-ALL and high levels, yet still lower than *CCND3*, in *ETV6-RUNX1*, hyperdiploid and *BCR-ABL1*⁺ B-ALL.

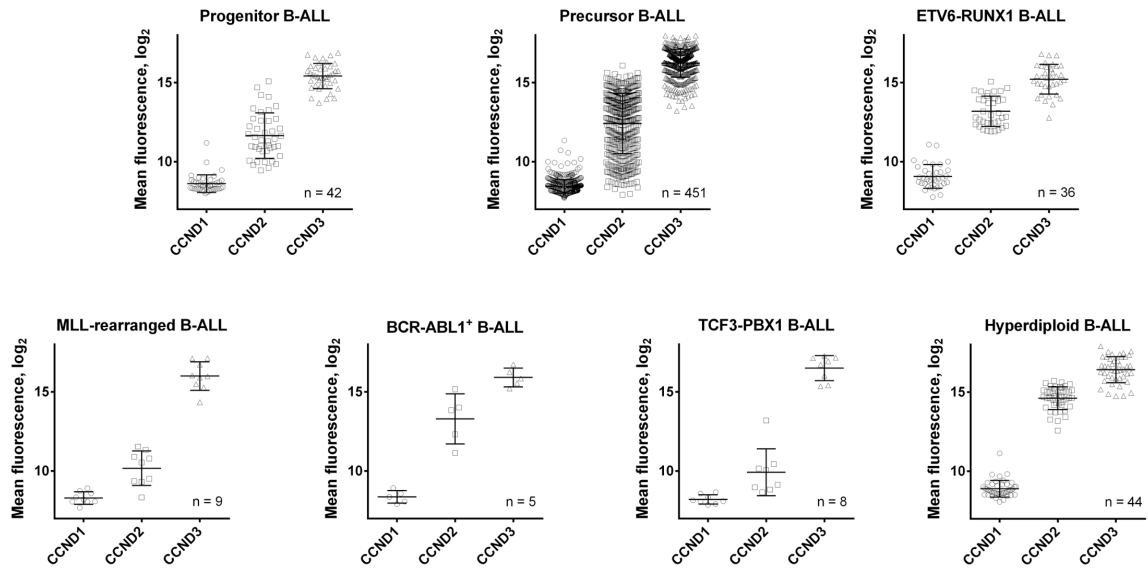


Figure 13: RNA expression of D-type cyclins in B-ALL patient samples

The gene expression profiling data of *CCND1*, *CCND2*, and *CCND3* obtained from B-ALL patients were mined using the GENEVESTIGATOR database. Ketzner et al. (2022)

In B-ALL cell lines of different genotypes, including EU3/697 (TCF3-PBX1), NALM-6 (ETV6-PDGFRB), RS4;11 and KOPN-8 (MLLr), REH (ETV6-RUNX1), 018Z (47, XY, +8, del(9)(p13), CNS invasive) and multiple BCR-ABL1⁺ cell lines, D-Cyclin expression resembled closely that of primary B-ALL samples on mRNA as well as on protein levels (Ketzner et al., 2022) (Figure 14A & C). *CCND3* was always the highest expressed D-Cyclin, while *CCND2* was mostly expressed in BCR-ABL1⁺ cell lines. By calculating the ratio of *CCND3/CCND2* mRNA expression of B-ALL cells lines, it became apparent that *CCND2* expression was always lower than that of *CCND3*, even in BCR-ABL1⁺ cases (Figure 14B). *CCND1* was not detectable on protein level for any of the cell lines analyzed, although being expressed in comparable amounts to *CCND2* on mRNA level in most cell lines.

These data demonstrate that *CCND3* but not *CCND2*, as previously assumed, is the highest expressed D-type Cyclin in B-ALL cell lines as well as in patient samples, indicating a previously unnoticed importance of *CCND3* in B-ALL. Additionally, my data validate the conservation of D-Cyclin expression of primary B-ALL in B-ALL cell lines.

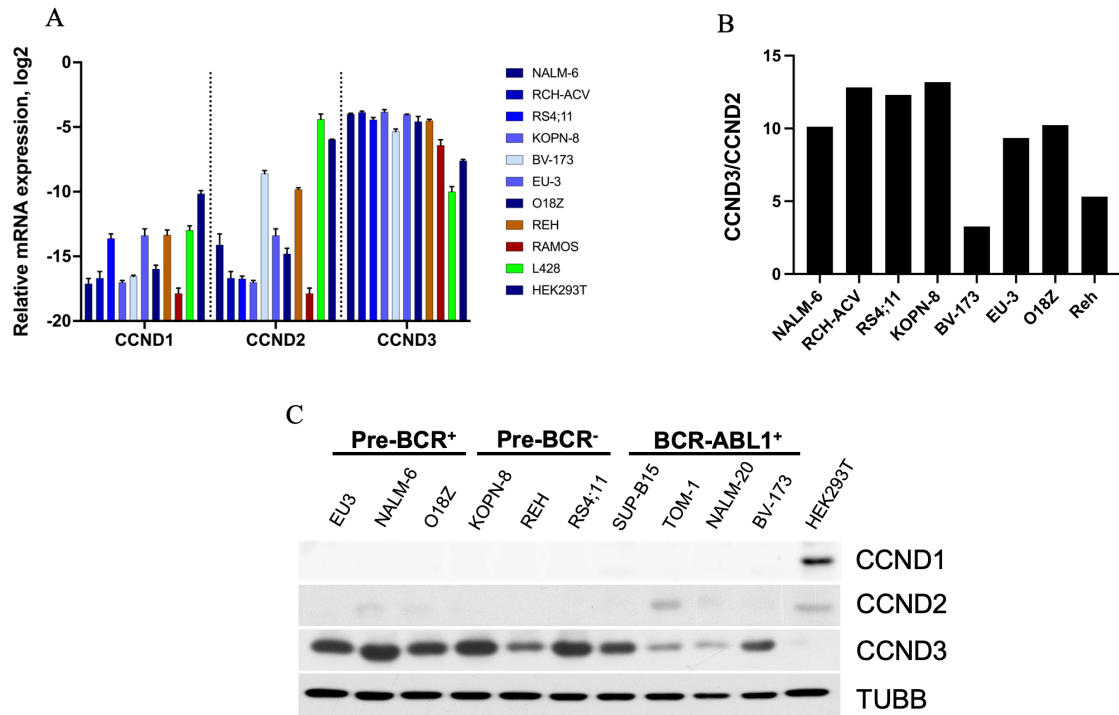


Figure 14: Expression of D-type cyclins in B-ALL cell lines

(A) qRT-PCR of B-ALL cell lines was performed to measure the mRNA expression levels of *CCND1*, *CCND2*, and *CCND3*. The control cell lines included Burkitt Lymphoma (Ramos), Hodgkin Lymphoma (L428) and HEK293T. Data shown as $n = 3 \pm SD$. (B) Ratio of mRNA levels *CCND3/CCND2* measured by qRT-PCR in B-ALL cell lines. (C) Expression of *CCND1*, *CCND2*, and *CCND3* proteins in B-ALL cell lines was measured by immunoblot and corroborated the mRNA expression levels of D-type Cyclins. TUBB was used as the loading control. Image is representative of $n = 3$. Ketzner et al. (2022)

3.2 *CCND3* expression is directly regulated by FOXO1

Previous work of our group has demonstrated a strong decrease of *CCND3* expression on mRNA and protein level after shRNA-mediated FOXO1 knockdown as well as after pharmacological FOXO1 inhibition (Wang et al., 2018). Furthermore, the cytotoxic effects of FOXO1 depletion could be rescued by ectopic expression of *CCND3*. Additionally, it has been shown that FOXO1 directly binds to the *Ccnd3* promoter in murine pancreatic cells (Zhang et al., 2016) and is an inhibitor of *Ccnd1* and *Ccnd2* expression (Kode et al., 2012). Taken together, this suggested a mechanistic basis for the regulation of *CCND3* by FOXO1, which I set to investigate by using a BCR-ABL1 transformed *Foxo1^{fl/fl}* Cre-ER^{T2} mouse pre-B-cells, human B-ALL cell lines, luciferase assay, EMSA, and ChIP.

3.2.1 Assessment of comparability between *FOXO1* knockdown in human cells and conditional *Foxo1* deletion in a murine B-ALL model

In order to achieve quick and reliable depletion of FOXO1 as well as control for potential methodological errors, I employed a BCR-ABL1 transformed *Foxo1^{fl/fl}* B-ALL mouse model, transduced with either Cre-ER^{T2} or empty vector control (ER^{T2}) (Abdelrasoul et al., 2020). Since our group has demonstrated a panel of genes downregulated in human cell lines by shRNA knockdown and pharmacological inhibition of FOXO1 in the past (Wang et al., 2018), I performed deletion of *Foxo1* in the murine B-ALL model *ex vivo* by induction with 200 nM 4-OHT and checked for some of the same genes in order to assess the comparability of both models.

First, I confirmed the efficiency of the *Foxo1* deletion via immunoblot at 24 hours and 48 hours after induction with 4-OHT (Ketzer et al., 2022) (Figure 15A). Next, I performed RNA-sequencing of these cells at the same time points after induction of *Foxo1* deletion. I analyzed the differentially expressed genes after induction of *Foxo1* deletion compared to controls

treated with equivalent amounts of ethanol by volcano plot (Figure 15B). As expected, *Foxo1* mRNA expression was strongly decreased. mRNA expression of *Myc*, *Id3*, and *Ccnd3*, three important genes identified after FOXO1 shRNA knockdown and pharmacological inhibition in human cell lines (Wang et al., 2018) were also significantly downregulated (Figure 15B). The decreased expression of these three genes was additionally corroborated via qRT-PCR 24 hours and 48 hours after induction of *Foxo1* deletion (Figure 15C).

Thus, I concluded that the *Foxo1*^{fl/fl} B-ALL mouse model resembles the human B-ALL cell line shRNA knockdown model close enough in order to be used as an additional model for my investigations of the FOXO1-CCND3 axis.

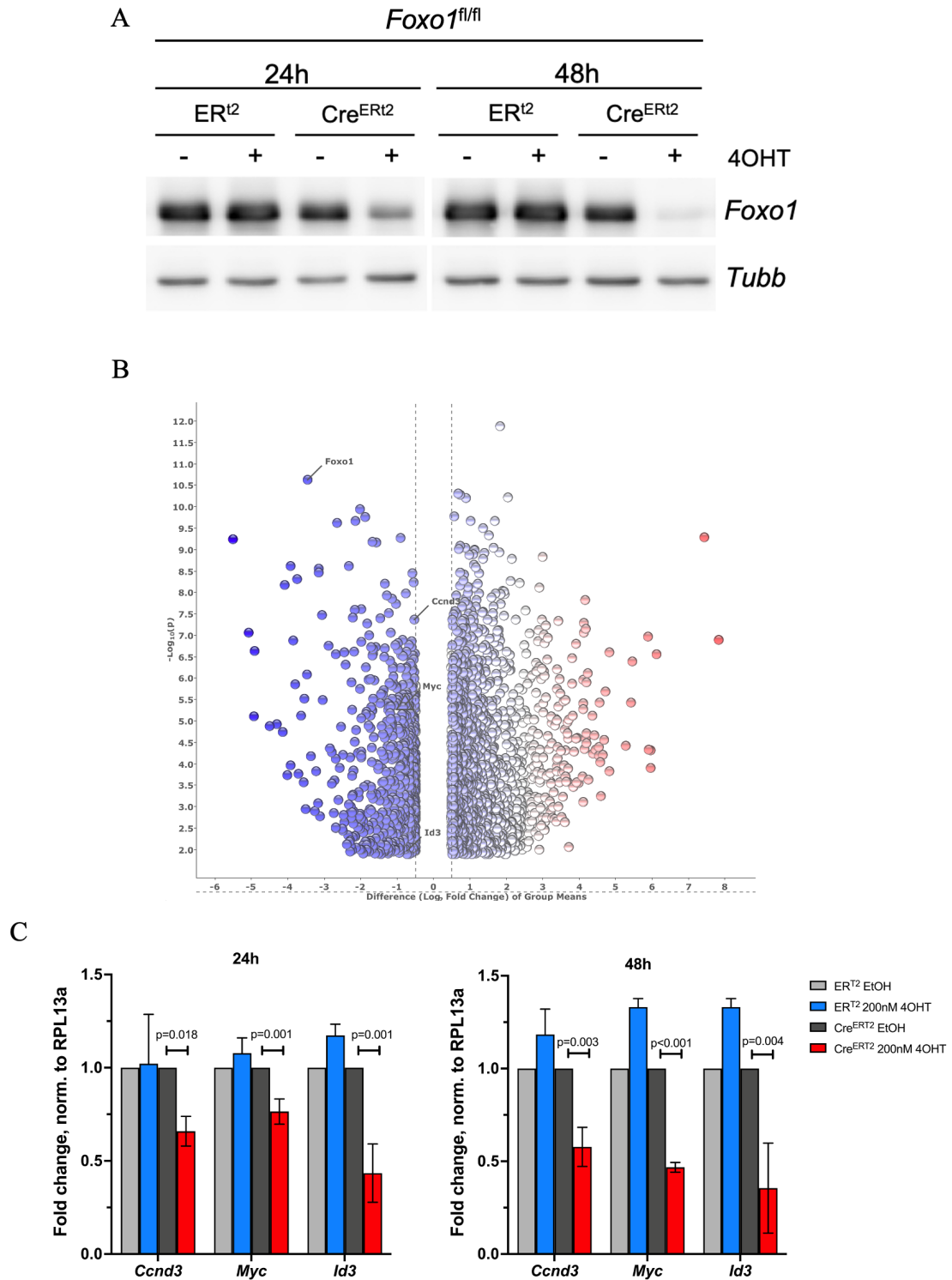


Figure 15: Alterations in gene expression by depletion of *Foxo1* in a murine B-ALL model resemble the human shRNA model

(A) Deletion of *Foxo1* in BCR-ABL1⁺ murine B-ALL cells with 200 nM 4-OHT is efficient on protein level after 24 h and 48 h. Image is representative of n = 3. Ketzer et al. (2022) (B) Differentially expressed genes combined after 24 h and 48 h after induction of *Foxo1* deletion with 200 nM 4-OHT were identified via volcano plot. Fold change > 1.4, p < 0.05. (C) qRT-PCR confirms the downregulation of genes seen in the RNA-sequencing. Data shown as mean ± SD, n = 3. Statistical analysis was performed with Students t-test.

3.2.2 Genetic *Foxo1* depletion exclusively reduces expression of *Ccnd3* but no other D-Cyclin

First, I analyzed the consequences of loss of *Foxo1* in a *Foxo1^{fl/fl}* BCR-ABL1 transformed mouse model either expressing Cre-ER^{T2} or only ER^{T2}. *Foxo1* deletion was induced *ex vivo* and mRNA and protein expression of all three D-type Cyclins was measured (Ketzer et al., 2022). In line with what we previously reported in human B-ALL cell lines (Wang et al., 2018), loss of *Foxo1* induced concurrent and significant decrease of CCND3 protein and mRNA expression (Figure 16). Additionally, a significant increase in mRNA expression of both FOXO1 repression targets, *CCND1* and *CCND2* became apparent on mRNA level. *CCND2* was also upregulated on protein level 24 hours after induction of *Foxo1* deletion, *CCND1*, however, was not detectable on immunoblot. The control cells only expressing ER^{T2} did not show a reduction of *Ccnd3*, neither on mRNA nor on protein level.

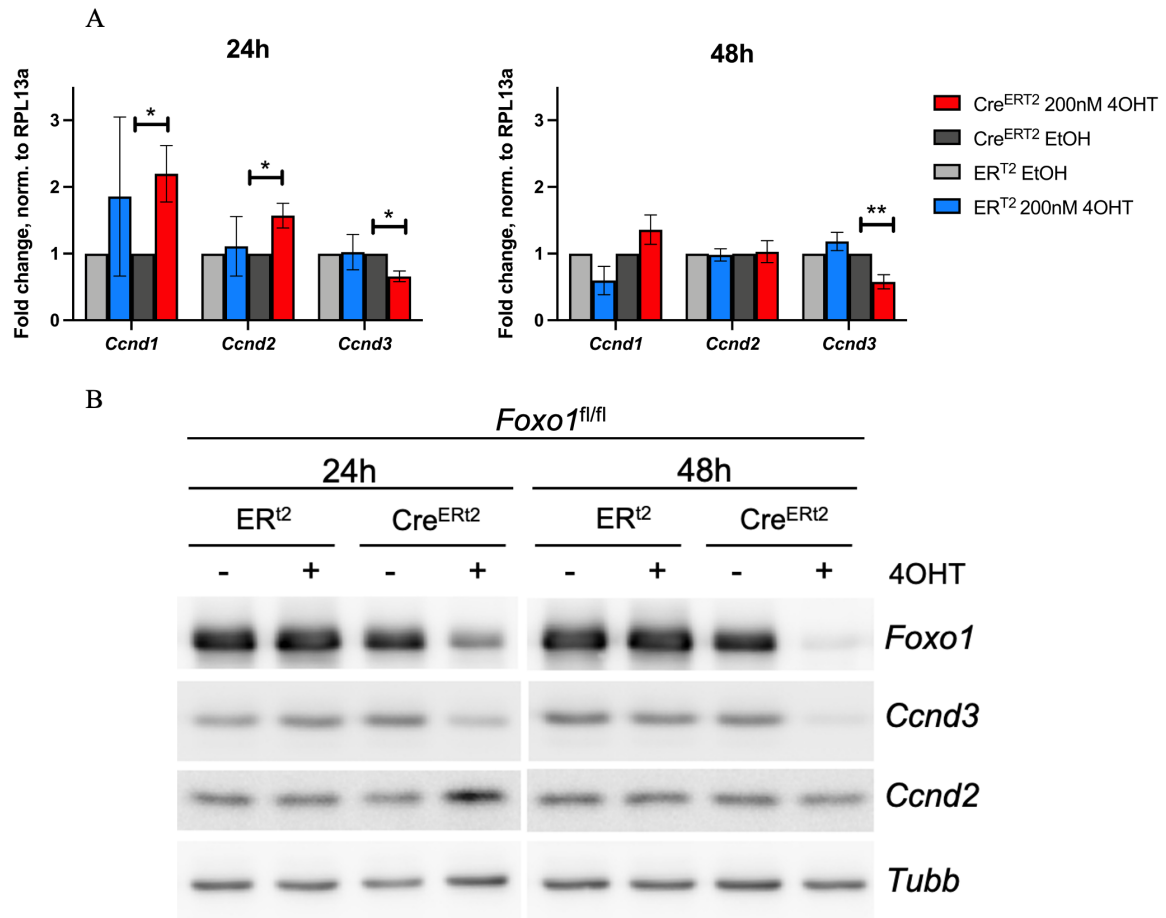


Figure 16: *Ccnd3* is the only D-Cyclin decreasing after *Foxo1* deletion in B-ALL

(A) Deletion of *Foxo1* in BCR-ABL1⁺ murine B-ALL cells decreases mRNA and (B) protein expression of *Ccnd3* but not of *Ccnd1* or *Ccnd2*. CCND1 was not detectable on protein level. Data shown as mean ± SD, n = 3. Statistical analysis was performed with Students t-test. * = p < 0.05 ** = p < 0.01. Ketzner et al. (2022)

Of note, similar to human B-ALL cell lines after FOXO1 shRNA knockdown, *Foxo1* deletion in mouse BCR-ABL1⁺ cells induced apoptosis and cell cycle arrest (Ketzner et al., 2022) (Figure 17). Taken together, this provides evidence of reliable comparability of the human and murine model, not only in molecular but also functional aspects.

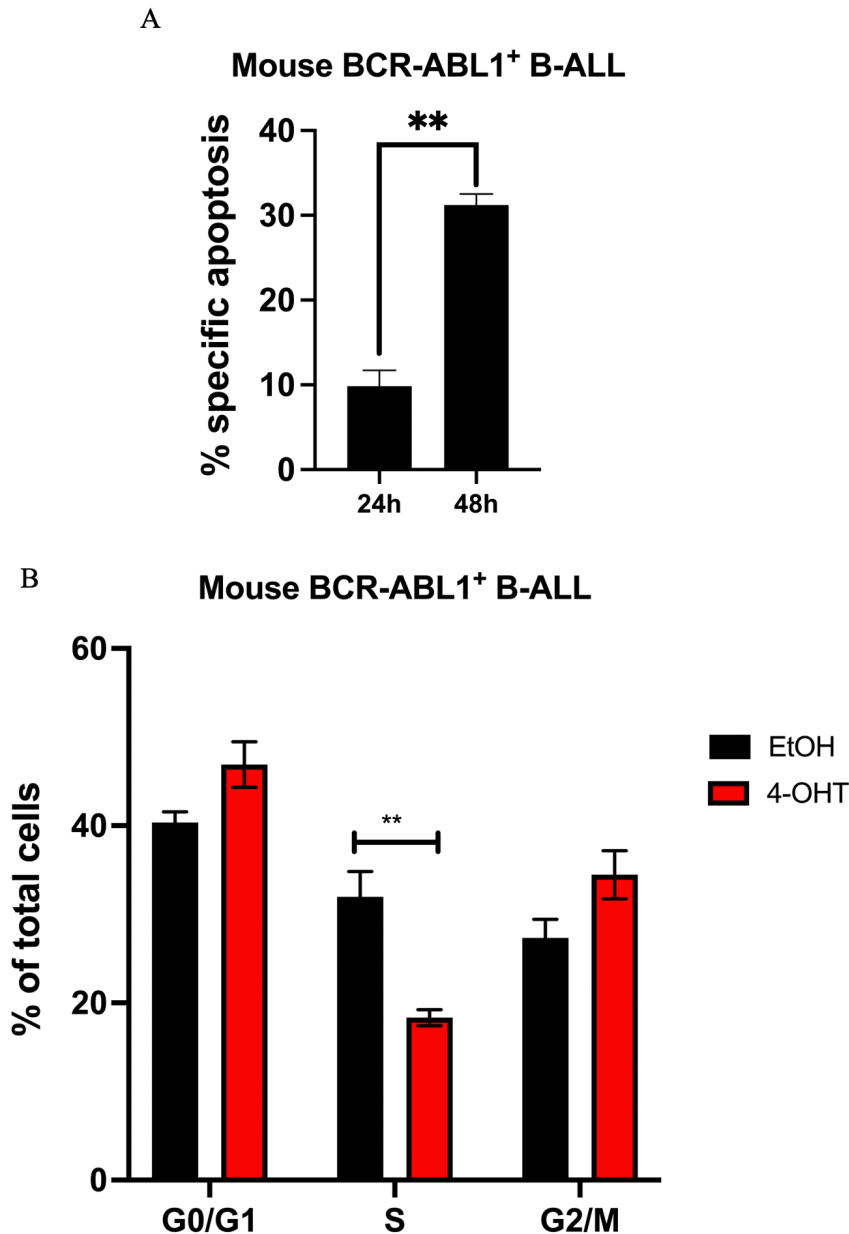


Figure 17: *Foxo1* deletion induces apoptosis and cell cycle arrest

(A) Deletion of *Foxo1* in BCR-ABL1⁺ murine B-ALL cells induces apoptosis, significantly more after 48 h than after 24 h after induction of deletion with 200 nM 4-OHT. Cells were fixed and stained with PI 24 h and 48 h after induction of *Foxo1* deletion. For analysis of cells, flow cytometry was used. Data was processed using FlowJo. Data shown as mean \pm SD, n = 3. Statistical analysis was performed with Students t-test. ** = p < 0.01 (B) Deletion of *Foxo1* in BCR-ABL1⁺ murine B-ALL cells induces significant cell cycle arrest 48 h after induction of deletion with 200 nM 4-OHT. Cells were stained with Annexin-V-APC and PI 24 h and 48 h after induction of *Foxo1* deletion. For analysis of cells, flow cytometry was used. Data was processed using FlowJo. Data shown as mean \pm SD, n = 3. Statistical analysis was performed with Students t-test. ** = p < 0.01. Ketzner et al. (2022)

3.2.3 Pharmacological *Foxo1* inhibition reduces expression of *Ccnd3*

Previously, our group has shown that human B-ALL cell lines and *in vivo* B-ALL xenografts are highly sensitive to the FOXO1 inhibitor AS1842856 (Wang et al., 2018). Furthermore, it was shown that pharmacological FOXO1 inhibition reduced *CCND3* expression and induced cell cycle arrest as well as apoptosis. In order to assess the comparability of these findings not only to the genetic but also of pharmacological *Foxo1* inhibition in the BCR-ABL B-ALL mouse model, I first analyzed the sensitivity of the mouse cells to the FOXO1 inhibitor AS1842856 by MTT assay. The murine B-ALL cells were as sensitive to FOXO1 inhibition as most human B-ALL cell lines (Wang et al., 2018), with an IC_{50} of 34 nM (Figure 18A). Importantly, qRT-PCR analysis of the mRNA expression levels of the three D-Cyclins after 24 h and 48 h treatment with 70 nM AS1842856 showed a significant decrease only of *Ccnd3* expression (Figure 18B).

These results demonstrate a similar sensitivity of the murine BCR-ABL1⁺ B-ALL model and human B-ALL cell lines to FOXO1 inhibition. Furthermore, I was able to show a clear effect of FOXO1 depletion and inhibition only on *Ccnd3* but not the other two D-type Cyclins.

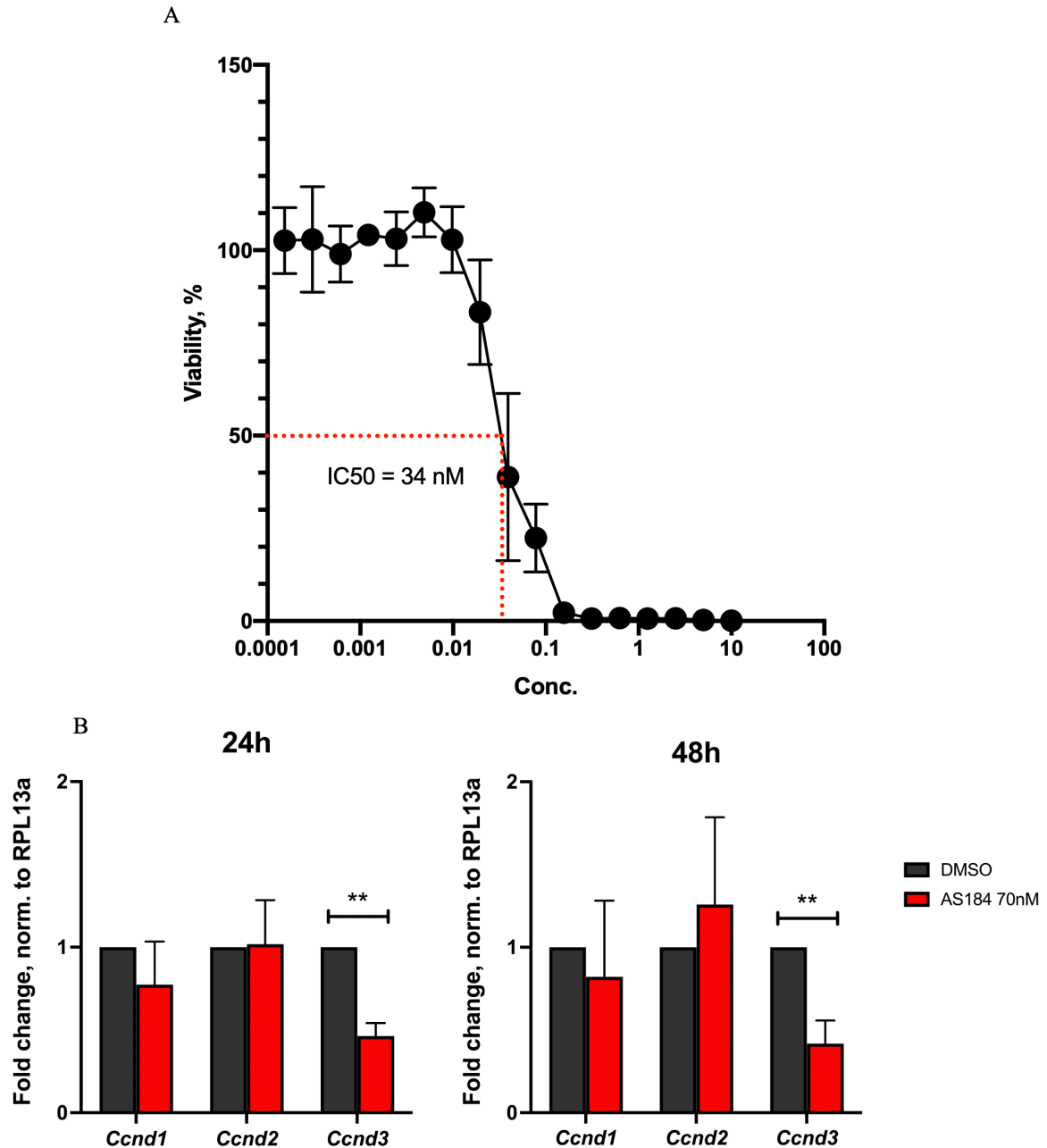


Figure 18: *Ccnd3* is the only D-Cyclin decreasing after pharmacological *Foxo1* inhibition in a murine B-ALL model

(A) IC_{50} of murine BCR-ABL1 transformed B-ALL cells for the FOXO1 inhibitor AS1842856 was determined by MTT assay and non-linear regression curve fit with GraphPad Prism 9. Data shown as mean \pm SD, $n = 3$. (B) Inhibition of *Foxo1* by 70 nM AS1842856 in BCR-ABL1⁺ murine B-ALL cells for 24 h and 48 h significantly decreases mRNA of *Ccnd3* but not of *Ccnd1* or *Ccnd2*. Data shown as mean \pm SD, $n = 3$. Statistical analysis was performed with Students t-test. ** = $p < 0.01$

3.2.4 The cytotoxic effects of FOXO1 inhibition cannot be ameliorated by ectopic CCND2 expression

Our group has shown that the overexpression of CCND3 could salvage B-ALL cells from the cytotoxic consequences of pharmacological FOXO1 inhibition (Wang et al., 2018). In order to assess if this effect is exclusive to CCND3 and not redundant with CCND2, I lentivirally transduced NALM-6 cells with either a CCND2 overexpression vector or an empty vector control. I hypothesized that if present in high amounts, CCND2 might be sufficient to substitute for CCND3 in the context of FOXO1 depletion-induced cytotoxicity. Hence, I treated CCND2 overexpressing NALM-6 cells with either 40 nM or 80 nM of the FOXO inhibitor AS1842856 (50% or 100% of IC_{50} , (Wang et al., 2018)) for 9 days and calculated the relative growth.

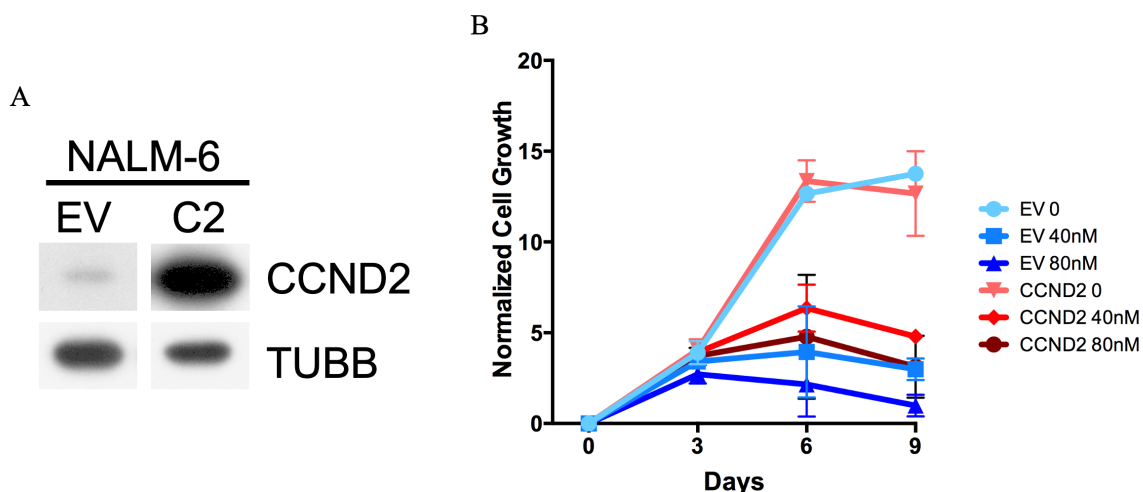


Figure 19: The cytotoxic effects of FOXO1 inhibition cannot be ameliorated by overexpression of CCND2

(A) Immunoblot of NALM-6 that were lentivirally transduced with SFFV-EV-eGFP (EV) or SFFV-CCND2-eGFP (C2). Image is representative of $n = 3$. (B) NALM-6 cells were lentivirally transduced with SFFV-EV or SFFV-CCND2-eGFP, then treated with 40 nM or 80 nM AS1842856, starting 6 days post-transduction. Percentages of GFP^+ cells (by flow cytometry) and the total number of live cells (by cell counting with trypan blue exclusion) were measured at indicated time points. Data are shown as fold changes normalized to the initial number of live GFP^+ cells. The number of live GFP^+ cells was calculated as $N \times \% GFP^+ \text{ cells}/100$, where N is the number of live cells per well and $\% GFP^+$ is the percentage of GFP^+ cells. Data are shown as mean \pm SD, $n = 3$.

Interestingly, as opposed to CCND3, CCND2 overexpression did not salvage the cells from the growth-inhibitory effect of treatment with

AS1842856, compared to the EV control cells. Of note, ectopic expression of CCND2 did not induce increased proliferation in the transduced NALM-6 cells compared to EV controls.

3.2.5 *Ccnd3* expression is neither regulated by MYC nor by E2F

It has been shown that MYC and E2F are both involved in the regulation of *Ccnd3* expression (Coller et al., 2007; Ma et al., 2003). Additionally, we have previously demonstrated a downregulation of MYC after FOXO1 depletion (Wang et al., 2018). Hence, I aimed to reveal the role of MYC and E2F in the regulation of *CCND3* (Ketzer et al., 2022).

After *Foxo1* deletion in murine BCR-ABL transformed precursor B-cells by induction with 200 nM 4-OHT, I observed that *Myc* RNA and protein expression is significantly reduced, simultaneously with *Ccnd3* mRNA expression (Figure 20A & B). This provided an incentive to further investigate a possible regulation of *Ccnd3* by MYC. In order to assess the influence of MYC on *Ccnd3* expression, I inhibited MYC activity and expression in murine BCR-ABL1 transformed precursor B-cells by incubation with 1 μ M imatinib *ex vivo* for 24 hours. Imatinib is an efficient inhibitor of the BCR-ABL1 kinase, which directly activates *Myc* transcription (Klein et al., 2005). After 24 hours, *Myc* RNA expression was completely abolished and protein expression strongly diminished (Figure 20C & D). In line with what has been previously reported (Abdelrasoul et al., 2020), FOXO1 protein expression was increased while its degradation- and nuclear export-inducing phosphorylation at T-254 was decreased. However, at the same time, *Ccnd3* RNA expression remained stable. This indicates no involvement of *Myc* in the regulation of *Ccnd3* expression.

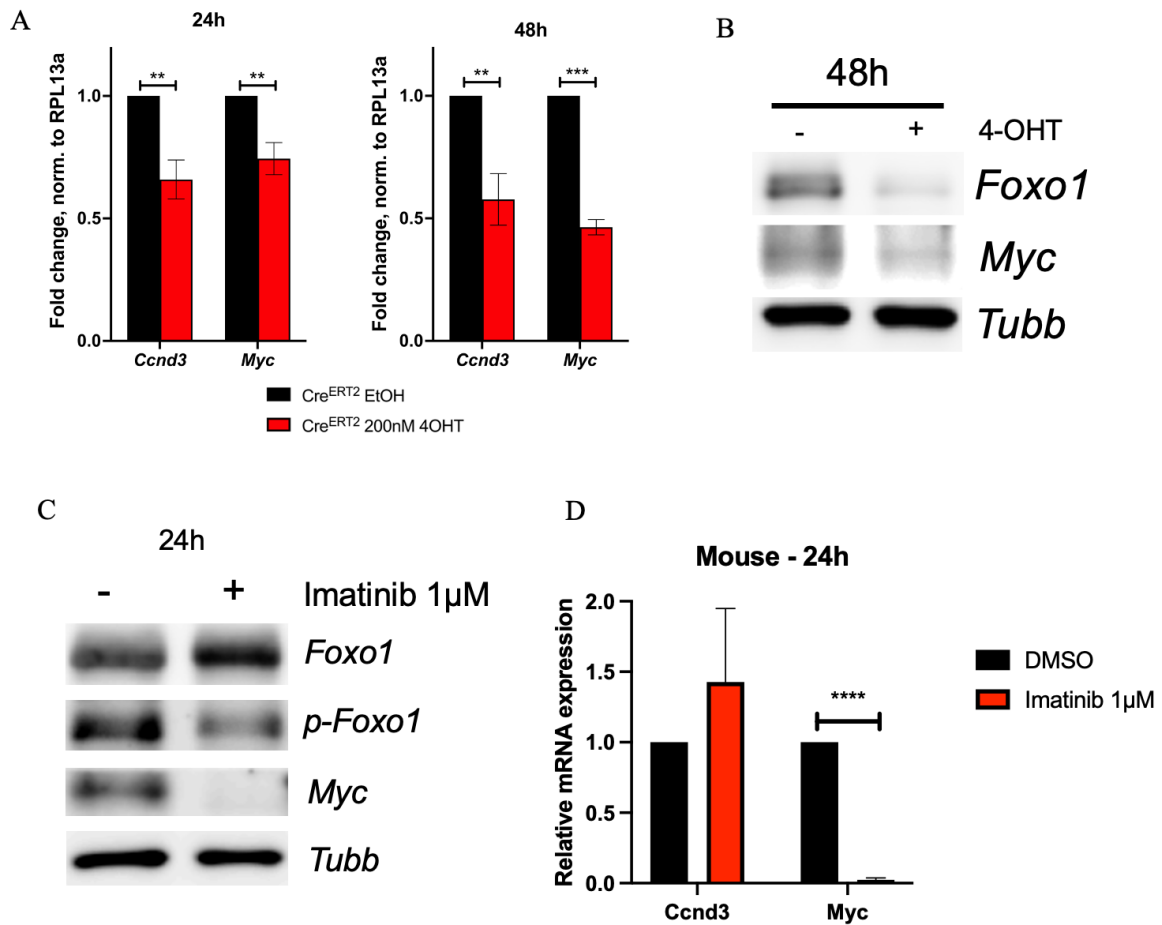


Figure 20: *Ccnd3* transcription is independent of MYC

(A) Deletion of Foxo1 in BCR-ABL1-transformed murine pre-B-cells decreases both *Ccnd3* and *Myc* mRNA and (B) protein levels. Data shown as mean \pm SD, n = 3. Image representative of n = 3 (C) Treatment of BCR-ABL1-transformed murine pre-B-cells with 1 μ M imatinib increases FOXO1 levels and efficiently abolishes MYC protein expression. Image representative of n = 3. (D) *Ccnd3* mRNA expression remains stable while *Myc* expression is significantly reduced. Data shown as mean \pm SD, n = 3. Ketzer et al. (2022)

Next, I treated human B-ALL cells with 1 μ M palbociclib, a clinically used inhibitor of CDK4/6, which stops dephosphorylation of RB1 by CDK4/6, keeping E2F in an inactive state, and thereby halting cell cycle progression (Roskoski, 2016). Upon treatment with palbociclib for three days, human B-ALL cells displayed a simultaneous upregulation of FOXO1 and CCND3 protein expression (Ketzer et al., 2022) (Figure 21A). Next, I treated murine B-ALL cells with the same amount of palbociclib and observed an increase not only of CCND3 protein expression but also of *Ccnd3* mRNA expression (Figure 21B & C). This indicates an E2F-independent control of *Ccnd3* transcription.

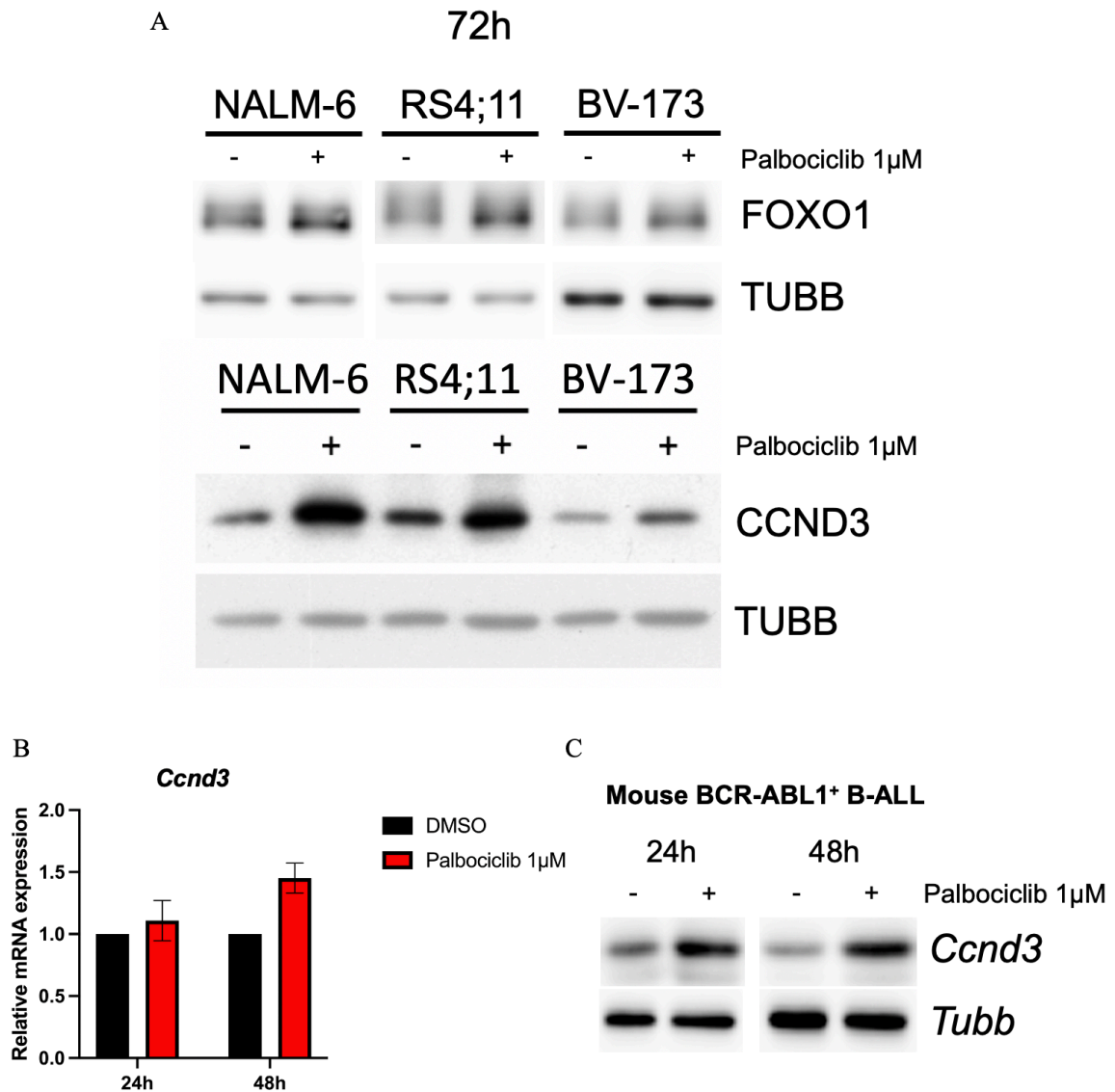


Figure 21: *Ccnd3* transcription is independent of E2F activity

(A) Treatment of B-ALL cell lines with 1 μ M palbociclib for 72h increases FOXO1 and CCND3 protein levels. Image representative of n = 3. (B) Treatment of BCR-ABL1-transformed murine pre-B-cells with palbociclib increases *Ccnd3* transcription. Data shown as mean \pm SD, n = 2-3. (C) CCND3 protein expression increases after 24h and 48h of treatment with palbociclib in BCR-ABL1-transformed murine pre-B-cells. Image representative of n = 3. Ketzer et al. (2022)

3.2.6 FOXO1 directly binds to and activates the *CCND3* promoter

Having excluded a role of MYC and E2F in the transcriptional regulation of *CCND3* in B-ALL, I aimed to investigate the role of FOXO1-dependent regulation of *CCND3* expression (Ketzer et al., 2022). Hence, I analyzed the *CCND3* promoter for FOXO1 binding motifs. Indeed, 126 bp upstream of

the core promoter, the FOXO1 binding motif GTAAACA is located (Shin et al., 2012) (Figure 22A). Hence, I cloned the *CCND3* promoter region spanning 1708 bp including the FOXO1 binding motif and exceeding the transcriptional start site by 259 bp into a luciferase reporter vector. As a control, I cloned the core promoter not containing the FOXO1 binding motif in the same vector. NALM-6 and RS4;11 B-ALL cells were nucleofected with either of these constructs and luciferase reporter activity was measured 24 hours after treatment with 80 nM (two-times IC_{50} , (Wang et al., 2018)) of the FOXO inhibitor AS1842856. The cells containing the *CCND3* luciferase-reporter significantly decreased in relative luminescence compared to the control (Figure 22B). Since the luciferase reporter assay indicated a negative effect of FOXO1 inhibition on *CCND3* promoter activity, I set to investigate direct FOXO1 DNA binding to the *CCND3* promoter. Therefore, HEK293T cells were transfected with either a FLAG-tagged Forkhead Box (FhBox) expressing plasmid or empty vector (EV) and nuclear proteins were extracted. These extracts were co-incubated with either a 25 bp DNA oligo probe containing the FOXO1 binding motif cloned from the *CCND3* promoter (FOXO1-wt) or a scrambled FOXO1 binding motif (FOXO1-mut). Equal protein loading and expression of FLAG-tagged FhBox were controlled for by immunoblot (Figure 22C). EMSA was performed and a shift was observed only for the sample containing the FOXO1-binding motif containing oligo and the nuclear extracts containing FLAG-FhBox (Figure 22D). Additionally, a supershift occurred for this sample when co-incubated with an anti-FLAG antibody, confirming specific binding of the FhBox to the FOXO binding motif in the *CCND3* promoter.

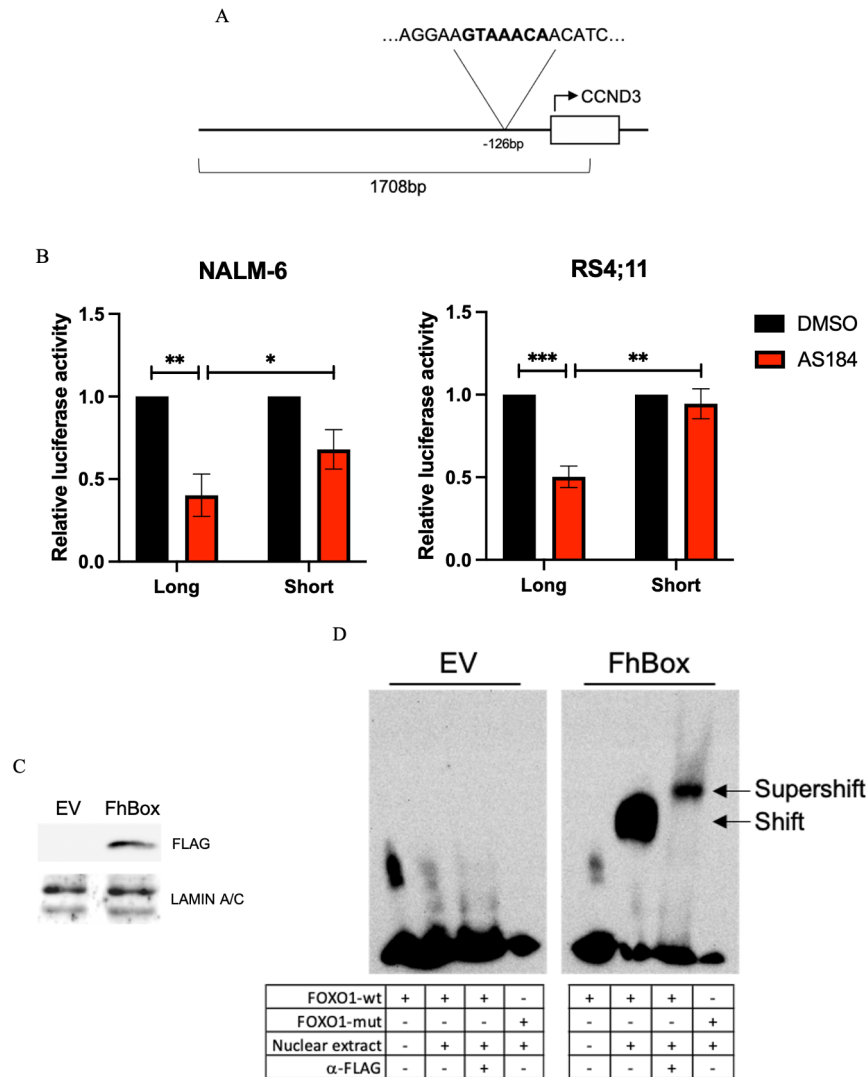


Figure 22: FOXO1 directly activates CCND3 transcription

(A) *CCND3* promoter region -1389bp to +259bp from the *CCND3* core promoter used for luciferase assay containing the FOXO1 binding motif GTAAACA -126bp from the transcriptional start site. (B) NALM-6 and RS4;11 cells were co-transfected with either pGL4.22- *CCND3*-promoter (long) or a truncated version only containing the core promoter without the FOXO1 binding motif (short), together with Ubi-Renilla luciferase reporter vectors and treated for 24h with the FOXO1 inhibitor AS1842856. *CCND3* reporter activity was normalized to Ubi-Renilla RLU. Data shown as mean \pm SD, n = 3. Statistical analysis was performed with student's t-test. * = p < 0.05; ** = p < 0.01; *** = p < 0.005 (C) HEK293T cells were transfected with either pFLAG-CMV2-Empty Vector (EV) or pFLAG-CMV2-FhBox (FhBox). Equal protein loading and expression of FhBox was analyzed by immunoblot. Image representative of n = 2. (D) Binding of FOXO1 to the *CCND3* promoter shown by EMSA. Nuclear extracts were harvested from HEK293T cells transfected with either pFLAG-CMV2-Empty Vector (EV) or pFLAG-CMV2-FhBox (FhBox), co-incubated with DNA probes containing FOXO1 binding motif from the *CCND3* promoter (FOXO1-wt) or scrambled FOXO1 binding motif (FOXO1-mut). For supershift assay, samples were co-incubated with 5 μ g of a FLAG antibody. Image representative of n = 2. Ketzer et al. (2022)

Next, I analyzed publicly available ChIP-sequencing data for FOXO1 of two

experiments that were closest to B-ALL: Pre-leukemic stem cells and mature B-cells (Ketzer et al., 2022) (Figure 23A). Both samples showed significant peaks at the promoter region of *CCND3*, at the position from which I derived the oligonucleotide probe containing the FOXO binding motif for EMSA.

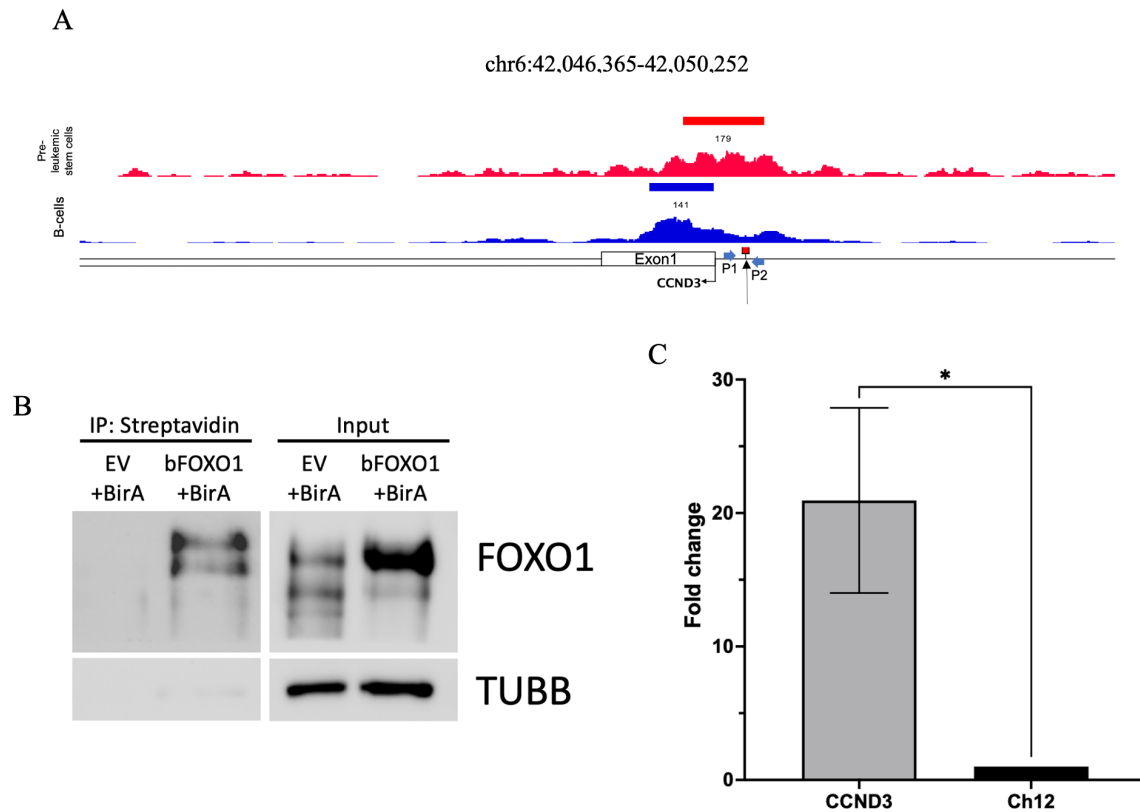


Figure 23: FOXO1 directly binds the *CCND3* promoter

(A) The data used for analysis were downloaded from the GEO database (<https://www.ncbi.nlm.nih.gov/geo/>, accessed on November 4th, 2022). Pre-leukemic stem cells: GSM2136846; Mature B-lymphocytes: GSM1668935. ChIP-peaks were called with $q < 0.05$. Analysis and visualization was performed with Integrated Genome Viewer and GenePalette. P1 and P2 represent the primers used for qRT-PCR analysis of ChIP. (B) Transfection with bFOXO1 and efficiency of pulldown with streptavidin was controlled by immunoblot following immunoprecipitation. Image is representative of $n=2$. (C) qRT-PCR analysis of ChIP for bFOXO1 and EV shows significant enrichment of the chromatin fragment containing the FOXO binding motif in the *CCND3* promoter. Ch12 gene desert was used as a negative control and for normalization. Data shown as \pm SD, $n = 3$. Statistical analysis was performed with student's t-test. * = $p < 0.05$. Ketzer et al. (2022)

In order to confirm this finding *in vivo*, I performed ChIP for FOXO1 in B-ALL cells. For this, I transfected NALM-6 cells with humanized BirA biotin ligase and either a constitutively active FOXO1 variant with N-terminal biotinylation signal (bFOXO1) or empty vector control (EV)

(Figure 23B). Chromatin was pulled down with streptavidin paramagnetic particles and qRT-PCR analysis was performed. For qRT-PCR, I used primers which amplify a 240 bp fragment from the *CCND3* promoter containing the FOXO binding motif which was also used for EMSA (Figure 22D). showed significant enrichment of the DNA segment of the *CCND3* promoter containing the FOXO binding motif (Figure 23C). This confirms my prior results as well as the *in silico* ChIP-sequencing analysis. Taken together, I have shown direct binding and transcriptional activation of *CCND3* by FOXO1.

3.3 Depletion of CCND3 is toxic for B-ALL cells

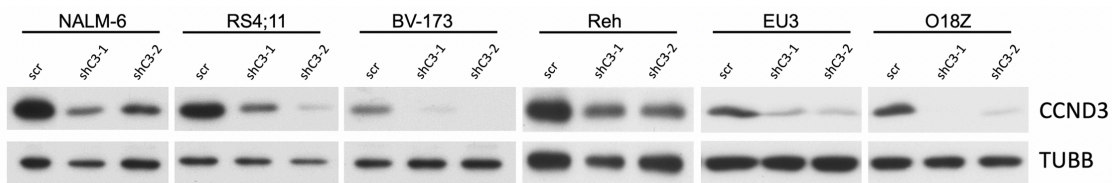
As demonstrated by our group in the past, small-hairpin RNA (shRNA)-mediated knockdown of CCND3 induces growth arrest and apoptosis in the cell lines NALM-6 (ETV6-PDGFRB) and RS4;11 (MLL-AF4) (Wang et al., 2018). Here I set to investigate the effects of two shRNAs as well as CRISPR/Cas9 against CCND3 in more cell lines of other genotypes, including BV-173 (BCR-ABL1⁺), REH (ETV6-AML1), EU-3 (TCF3-PBX1), and 018Z (47, XY, +8, del(9)(p13), CNS invasive). Additionally, I employed human PDXs and a murine *ex vivo* model of different genotypes in order to confirm the observed effects.

3.3.1 CCND3 knockdown in B-ALL cell lines

First, I designed a new shRNA, targeting a different part of the *CCND3* mRNA than the one used by our group before (Wang et al., 2018). I lentivirally transduced different B-ALL cell lines with either one of the shRNAs targeting *CCND3* or a scrambled control, all co-expressing RFP (Ketzer et al., 2022). Knockdown efficiency was controlled by immunoblot (Figure 24A). Both shRNAs were effective in decreasing CCND3 protein levels in all cell lines.

The shRNAs decreased all cell lines' performance in the competitive growth assay (Figure 24B). Interestingly, the same shRNA did not yield the same protein depletion in all cell lines. However, the efficiency of protein depletion was mostly proportional to the effect observed in the growth dynamic.

A



B

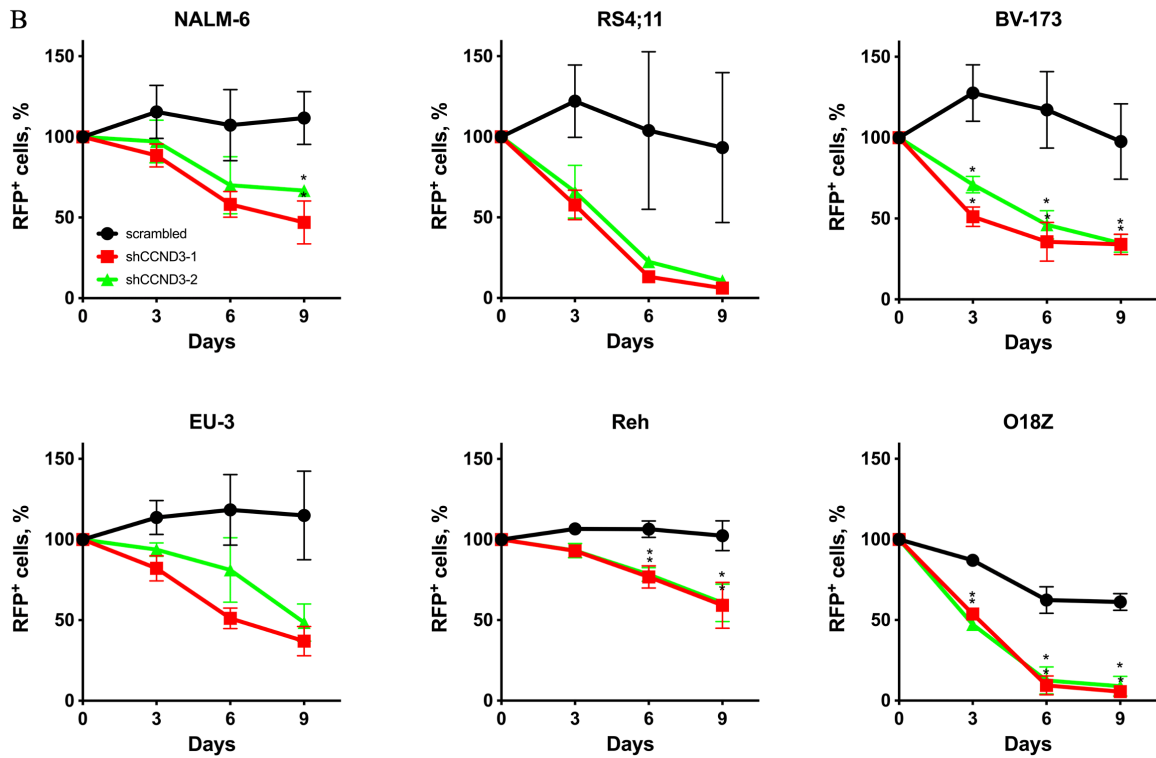


Figure 24: CCND3 is essential for the growth of B-ALL cell lines

(A) B-ALL cell lines of different genotypes were lentivirally transduced with plasmids expressing RFP and either a scrambled control or one of two shRNAs targeting CCND3. Immunoblot was performed as confirmation of knockdown efficiency of the shRNAs against CCND3. Image is representative of $n = 3$. (B) The shRNA knockdown of CCND3 in human B-ALL cell lines inhibits growth in a competitive growth assay. RFP⁺ Cells were first measured by flow cytometry four days after transduction, then every three days until 13 days post-transduction. Cell growth was calculated relative to the first measurement. Data shown as mean \pm SD, $n=3$. Statistical analysis was performed with student's t-test. * = $p < 0.05$. Ketzer et al. (2022)

Next, I used a lentivirally transduced CRISPR/Cas9 vector for targeting Exon 2 of the *CCND3* gene in NALM-6 B-ALL cells (Ketzer et al., 2022). The knockout efficiency on protein level was approximately 40%, proportional to the decrease in performance observed in the growth dynamic (Figure 25).

These data demonstrate that the method of *CCND3* depletion does not influence the cytotoxic effect in B-ALL cells.

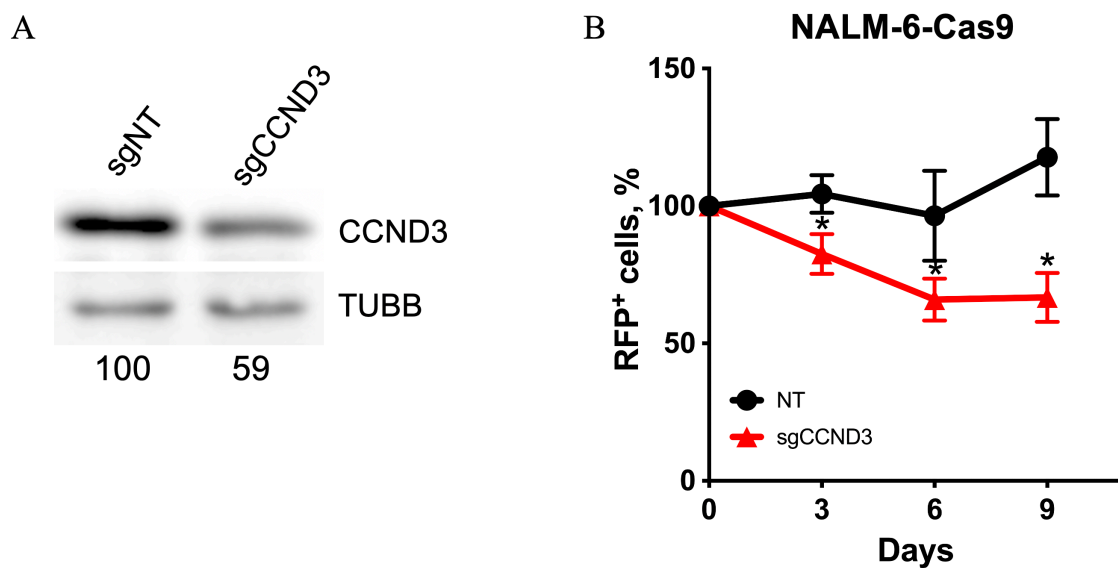


Figure 25: CRISPR/Cas9 knockout of *CCND3* resembles the effects of the shRNA knockdown (A) CRISPR/Cas9 knockout of *CCND3* in NALM-6 cells verified by immunoblot, knockout efficiency approx. 40%. Image representative of n=2. (B) CRISPR/Cas9 knockout displays a growth inhibitory effect that correlates to the amount of protein lost after knockout. Data shown as mean \pm SD, n=3. Statistical analysis was performed with student's t-test. *=p<0.05. Ketzer et al. (2022)

3.3.2 Targeting *CCND3* in different *ex vivo* models

Since BCR-ABL1⁺ B-ALL represents a particularly aggressive subtype of B-ALL (Leoni and Biondi, 2015) and expresses high levels of *CCND2*, I chose a BCR-ABL1⁺ transformed primary *ex vivo* murine B-ALL model in order to investigate the effects of *Ccnd3* knockdown in a *Ccnd2*^{high} subtype of B-ALL (Ketzer et al., 2022). This could answer the question of the possible redundancy of *CCND2* and *CCND3* for the survival of B-ALL cells. I designed a new shRNA targeting murine *Ccnd3* and lentivirally

transduced the murine BCR-ABL1⁺ B-ALL cells with either the targeting shRNA or a scrambled control, both co-expressing RFP. The knockdown was very efficient, shown by immunoblot (Figure 26A). Although the transduced mouse cells expressed high levels of CCND2 (Figure 16B), this could not salvage cell growth after depletion of *Ccnd3* (Figure 26B).

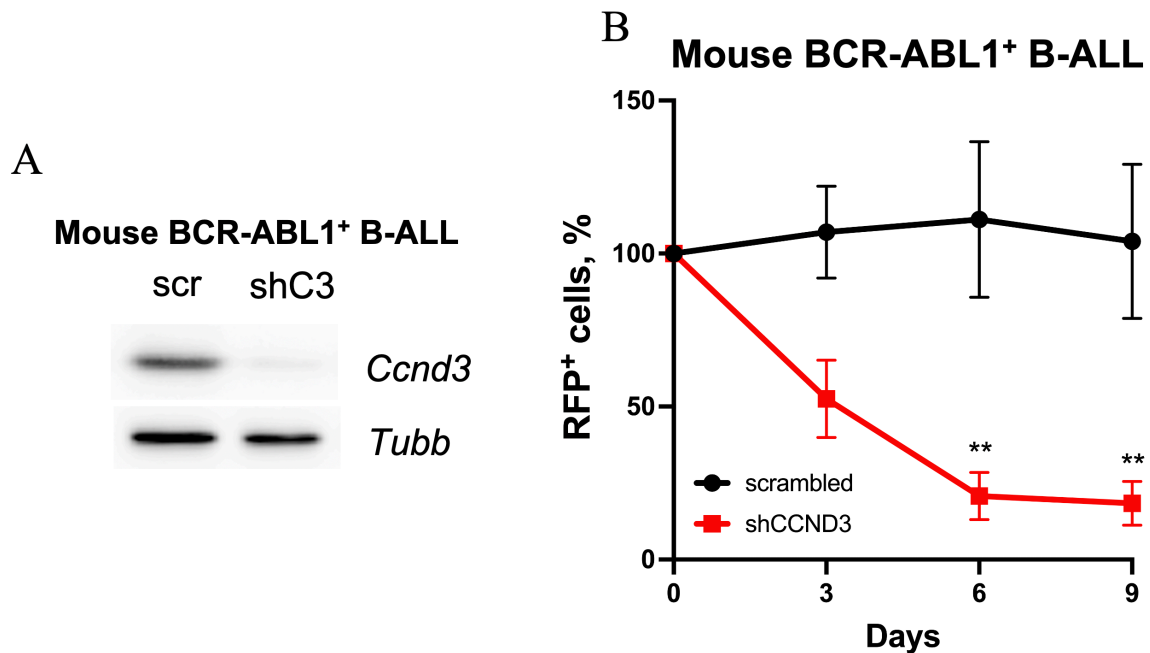


Figure 26: Growth inhibition after shRNA knockdown of *Ccnd3* in murine BCR-ABL1⁺ B-ALL cells

(A) Immunoblot as confirmation of lentivirally transduced shRNA efficiency against *Ccnd3* in murine BCR-ABL1 transformed pre-B-cells. Image representative of n = 3. (B) shRNA knockdown of *Ccnd3* in BCR-ABL1 transformed murine pre-B-cells significantly inhibits cellular growth. Data shown as mean \pm SD, n=3. Statistical analysis was performed by student's t-test. **=p<0.01. Ketzner et al. (2022)

In order to assess the need for CCND3 expression in primary B-ALL cells, I used three different PDXs. The refractory, *KRAS*^{G12D} PDX JFK125R, the BCR-ABL1⁺ PDX2 with additional IKZF1 deletion, and the BCR-ABL1⁺ PDX BLQ5, relapsed after treatment with imatinib (Chan et al., 2020). The cells were *ex vivo* lentivirally transduced with either a *CCND3*-targeting shRNA or a scrambled control, both co-expressing RFP (Ketzner et al., 2022). The knockdown of *CCND3* was efficient on protein-level and *CCND3*-depletion led to significantly decreased cellular growth (Figure 27).

These results demonstrate an essential role of CCND3 in B-ALL, not only in human cell lines but also in a murine BCR-ABL1⁺ model as well as in *ex vivo* PDX models of different mutational backgrounds and treatment history.

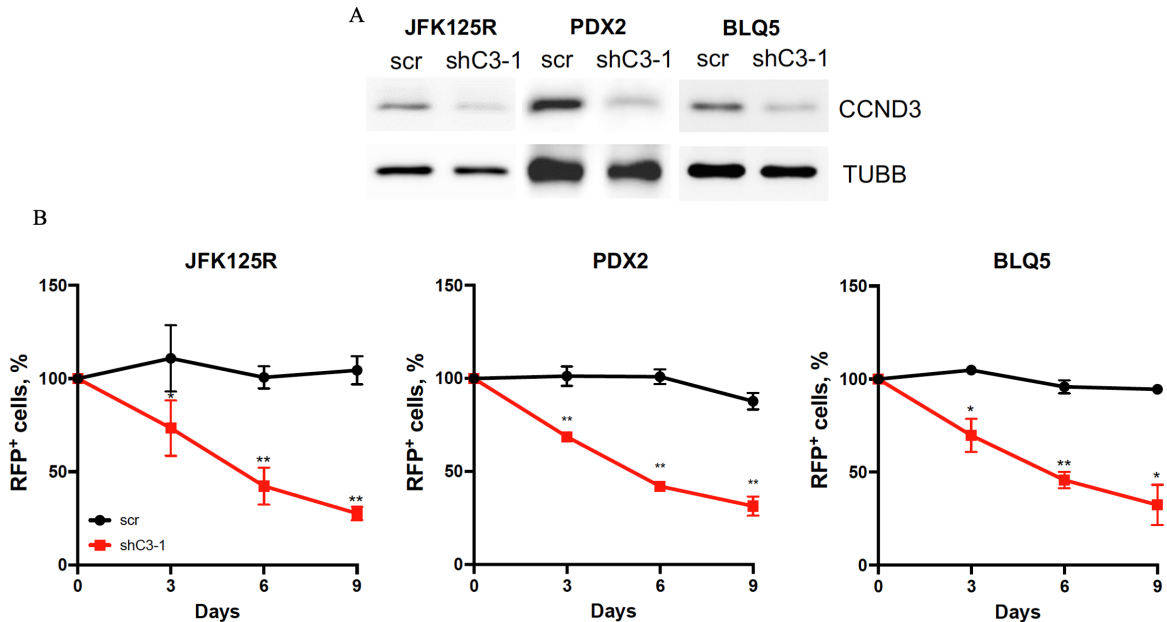


Figure 27: Growth inhibition after genetic *ex vivo* downregulation of CCND3 in PDX B-ALL cells

(A) Immunoblot as confirmation of lentivirally transduced shRNA efficiency against *CCND3* in patient-derived xenograft B-ALL cells. JFK125R was derived from a relapsed B-ALL patient with *KRAS^{G12D}* mutation. PDX2 was derived from a BCR-ABL1⁺ patient with additional IKZF1 deletion. BLQ5 was derived from a relapsed BCR-ABL1⁺ patient after treatment with imatinib. Image representative of n = 2. (B) shRNA knockdown of *CCND3* in patient-derived xenografts inhibits cellular growth. Data shown as mean ± SD, n=3. Statistical analysis was performed with student's t-test. * = p < 0.05, ** = p < 0.01. Ketzer et al. (2022)

3.3.3 Depletion of CCND3 but not inhibition of the enzymatic activity of its associated kinases CDK4/6 induces apoptosis in B-ALL cells

The efficacy of palbociclib, a CDK4/6 inhibitor that is successfully used for the treatment of breast cancer (Roskoski, 2016) has previously been evaluated in T-ALL and B-ALL (Wang et al., 2017; De Dominici et al., 2020). In T-ALL, inhibition of CDK4/6 by palbociclib induced apoptosis *in vitro* and *in vivo*. In BCR-ABL1⁺ B-ALL however, it was shown that CDK4/6 inhibition is inefficient in inducing apoptosis when compared to CDK6 knockdown or targeted protein degradation. However, it remains unclear which role CDK4/6

and *CCND3* play in the survival program of B-ALL.

First, I treated the B-ALL cell lines NALM-6, RS4;11, and BV-173 with 1 μ M palbociclib which was two-fold higher than the maximally achievable plasma concentration in patients (Fry et al., 2004; Tamura et al., 2016) (Ketzer et al., 2022). This concentration was previously used to analyze the sensitivity of B-cell malignancies to CDK4/6 inhibition (Schmitz et al., 2012). I compared this treatment to the knockdown of *CCND3* by lentiviral transduction of an shRNA against *CCND3*. As controls, incubation with equivalent amounts of DMSO or transduction of a scrambled shRNA was done, respectively. The effects of palbociclib and *CCND3* shRNA knockdown on the cell cycle were comparable throughout all cell lines, both inducing G0/G1 cell cycle arrest after three and four days, respectively (Figure 28).

Interestingly, induction of specific apoptosis was significantly greater after *CCND3* knockdown than after treatment with palbociclib, which induced almost no apoptosis (Ketzer et al., 2022) (Figure 29A). The apoptotic effect of *Ccnd3* knockdown but not treatment with palbociclib was also observed in murine BCR-ABL1-transformed pre-B-cells (Figure 29B).

These findings suggest an anti-apoptotic function of *CCND3* in B-ALL independently of its function within the CDK4/6 complex.

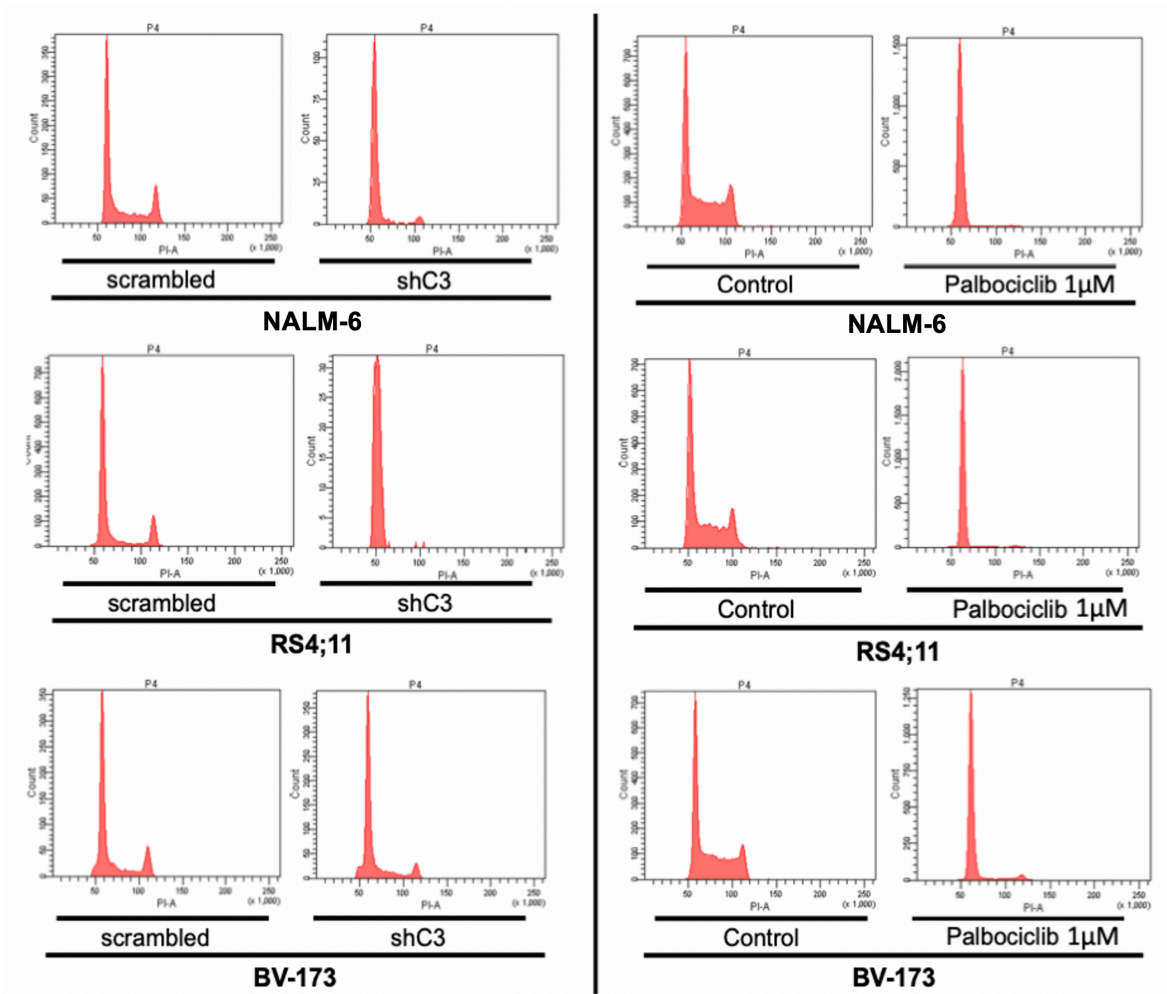


Figure 28: Cell cycle arrest after CDK4/6 inhibition and *CCND3* knockdown

NALM-6, RS4;11, and BV-173 B-ALL cell lines were either treated with 1µM palbociclib for 72h or lentivirally transduced with *CCND3* targeting shRNA, sorted after four days and fixed and stained with propidium iodide after three more days. DNA content of the cells was analyzed by flow cytometry. G0/G1 cell cycle arrest was observed for both treatments. Image representative of n=3. Ketzner et al. (2022)

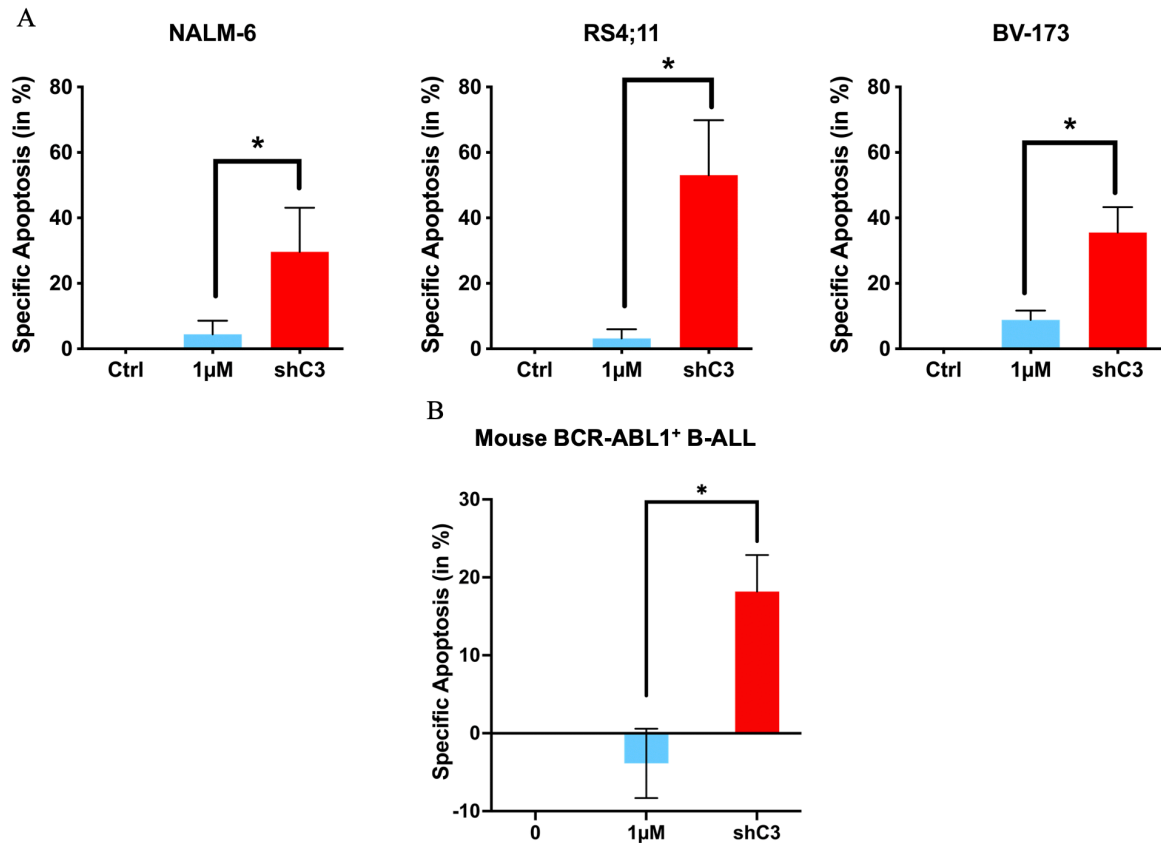


Figure 29: Depletion of *CCND3* but not treatment with palbociclib induces apoptosis in B-ALL cell lines

(A) B-ALL cell lines were treated with 1µM palbociclib for 3 days or transduced with either a scrambled (control) or a *CCND3*-shRNA containing vector, harboring a fluorescent marker (RFP). The RFP⁺ cells were sorted by a FACS 4 days post-transduction and cultured for 3 more days. Apoptosis was analyzed by PI/annexin V staining, with help of flow cytometry. Data shown as mean ± SD, n=3. Statistical analysis was performed by student's t-test. * = p < 0.05. (B) Murine BCR-ABL1⁺ B-ALL cells were either *ex vivo* lentivirally transduced with a shRNA against *Ccnd3* (shC3) or a scrambled control (scr), both co-expressing RFP, or treated with 1 µM palbociclib for 3 days. The RFP⁺ cells were sorted by a FACS 4 days post-transduction and cultured for 3 more days. Apoptosis was analyzed by PI/annexin V staining, with help of flow cytometry. Data shown as mean ± SD, n=3. Statistical analysis was performed by student's t-test. * = p < 0.05. Ketzer et al. (2022)

3.3.4 Cytotoxicity of *CCND3* knockdown is not caused by the accumulation of reactive oxygen species

In T-ALL, induction of apoptosis after either knockdown of *CCND3* or inhibition of CDK4/6 by palbociclib through the accumulation of ROS has been reported (Wang et al., 2017). Since my data indicate no significant induction of specific apoptosis after palbociclib but after knockdown of *CCND3*, I analyzed ROS levels after genetic knockdown of *CCND3* in two

B-ALL cell lines, NALM-6 and RS4;11 (Figure 30). None of the two cell lines showed an increase in ROS seven days after lentiviral transduction of either an shRNA against *CCND3* or a scrambled control. Cells treated with tert-butyl hydroperoxide (tBHP) were used as a positive control.

These results suggest a different mechanism of cytotoxicity after *CCND3* knockdown in B-ALL compared to T-ALL.

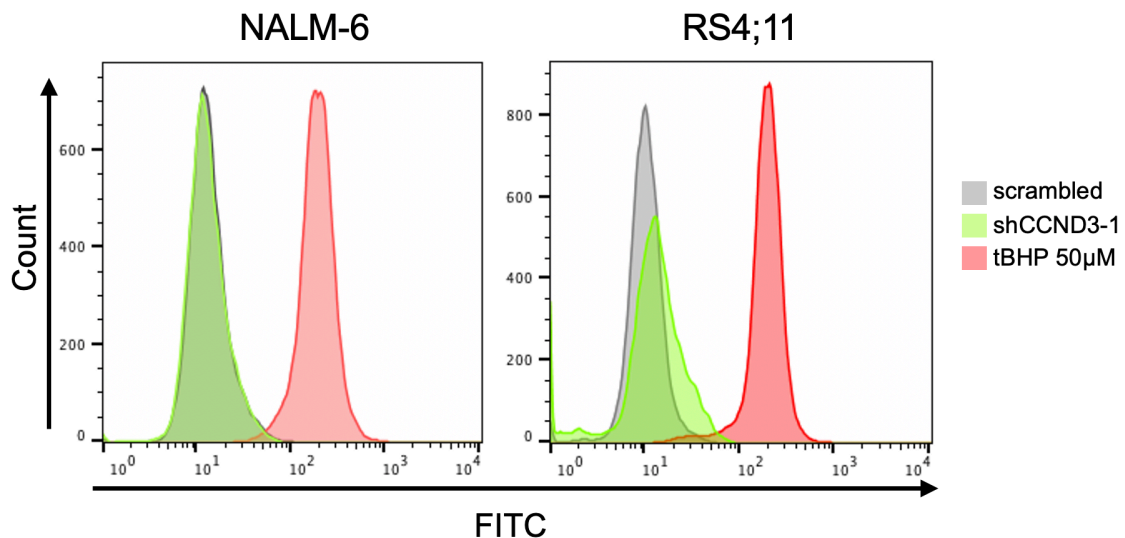


Figure 30: *CCND3* knockdown does not induce accumulation of ROS in B-ALL cell lines

NALM-6 and RS4;11 cells were lentivirally transduced with either an shRNA targeting *CCND3* or a scrambled control co-expressing RFP. Cells were sorted for 100% RFP⁺ cells four days after transduction and cultured for another three days before ROS analysis was performed. For ROS measurement, cells were either incubated with 20 µM 2',7' – dichlorofluorescein diacetate (DCFDA) or 20 µM DCFDA + 50 µM tBHP as a positive control. Accumulation of 2',7' –dichlorofluorescein (DCF) by ROS induction was measured by flow cytometry. Images are representative of n = 2.

3.4 CCND3 upregulation protects B-ALL cells from the cytotoxic effects of CDK4/6 inhibition

3.4.1 Upregulation of CCND3 ameliorates growth arrest induced by palbociclib

Having shown that depletion of CCND3 but not inhibition of its associated kinases CDK4/6 induces apoptosis in B-ALL cells, I wanted to investigate the underlying mechanism. Immunoblot of the three cell lines NALM-6, RS4;11, and BV-173 either treated with 1 μ M palbociclib or a *CCND3*-targeting shRNA for three or four days, respectively, revealed a strong increase in protein expression of CCND3 after treatment with palbociclib (Ketzer et al., 2022) (Figure 31A). CCND1 protein remains undetectable in these cell lines and CCND2 is only strongly upregulated in BV-173, a BCR-ABL1⁺ cell line with higher baseline CCND2 protein expression than others (Figure 31B). Of note, treatment of BCR-ABL1⁺ mouse B-ALL cells with 1 μ M palbociclib induces upregulation of CCND3 protein expression as well (Figure 31C).

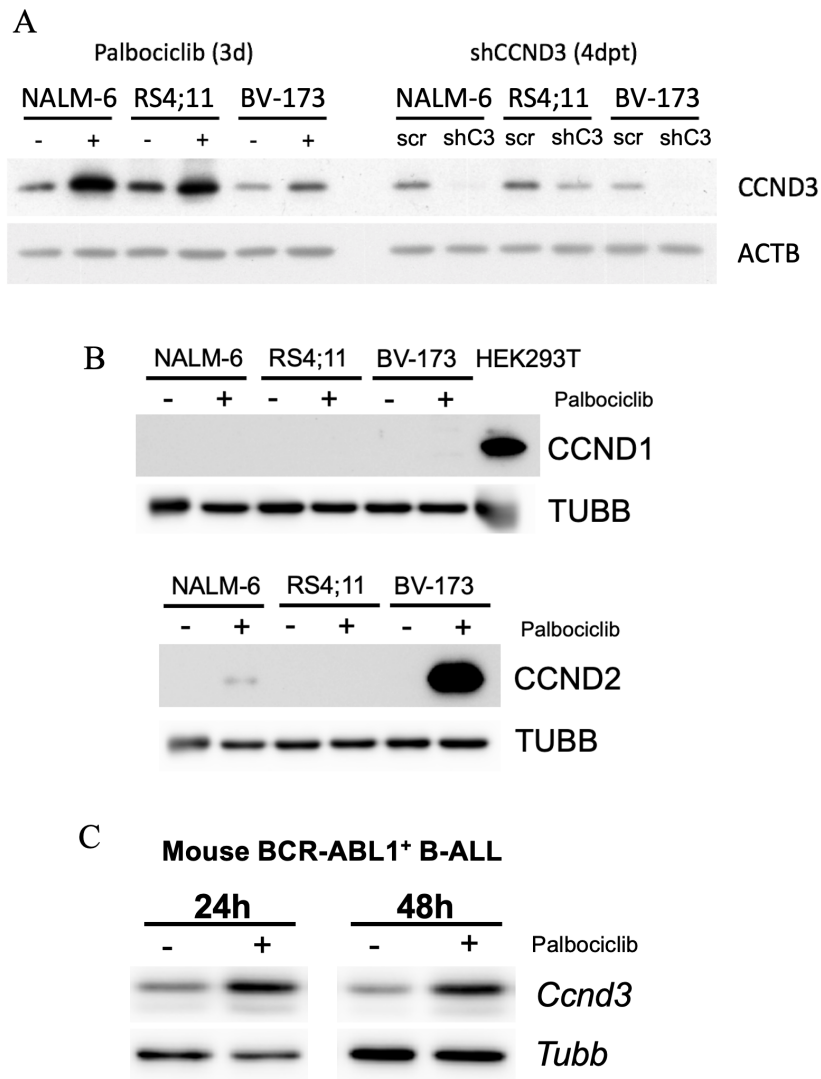


Figure 31: Treatment of B-ALL cells with palbociclib increases CCND3 protein expression

(A) CCND3 protein expression level as analyzed by immunoblot 3 days after treatment with 1 μ M palbociclib and 4 days after transduction with either scrambled control or CCND3 targeting shRNA. Image is representative of n = 3. (B) CCND1 and CCND2 protein expression after 3 days of treatment with 1 μ M palbociclib, analyzed by immunoblot. Image is representative of n=2. (C) BCR-ABL1 transformed murine pre-B-cells were treated for 24 h and 48 h with 1 μ M palbociclib which induced an increase in CCND3 protein expression. Image is representative of n = 3. Ketzer et al. (2022)

In order to assess if the upregulation of CCND3 protein is a salvaging mechanism for B-ALL cells in order to escape the cytotoxic consequences of treatment with palbociclib, I lentivirally transduced NALM-6 cells with either a CCND3-expressing vector or an EV control (Ketzer et al., 2022). The cells were treated with different sub- to supraclinical concentrations of palbociclib from 0.1 μ M to 1 μ M. Ectopic expression of CCND3 was shown

by immunoblot (Figure 32A). CCND3 overexpression partially rescued NALM-6 cells from the growth-inhibitory effects of treatment with palbociclib, even when treated with a supraclinical concentration of 1 μM (Figure 32B). Of note, untreated NALM-6 cells overexpressing CCND3 did not have a growth advantage compared to the EV control cells.

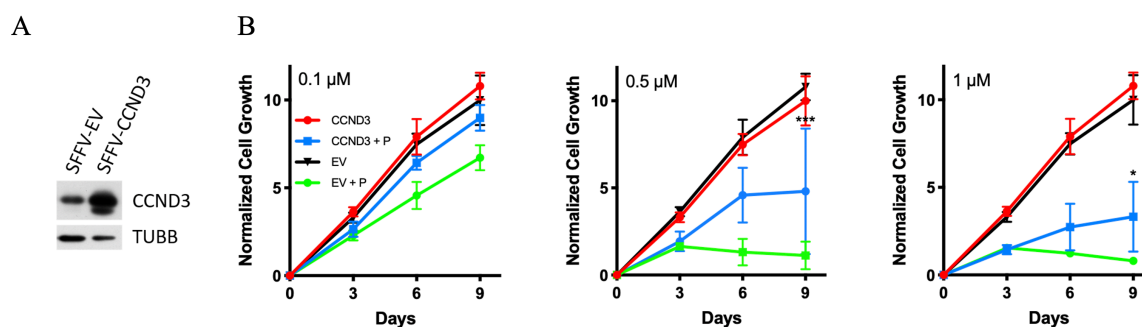


Figure 32: Overexpression of CCND3 protects B-ALL cells from growth arrest induced by palbociclib

(A) NALM-6 cells were lentivirally transduced with either SFFV-wtCCND3-GFP (CCND3) or SFFV-EV-GFP (EV). Cells were sorted to 100% GFP⁺ cells. CCND3 expression was analyzed by immunoblot. Image representative of $n = 2$. (B) CCND3 and EV NALM-6 cells were treated with either 0.1 μM , 0.5 μM , or 1 μM palbociclib or an equivalent amount of DMSO as a control for 9 days. Cell growth of CCND3 overexpressing NALM-6 cells and EV control expressing NALM-6 cells was determined by calculating GFP⁺ cells relative to the absolute cell number of living cells. Data shown as mean \pm SD, $n=3$. Statistical analysis was performed by student's t-test. * = $p < 0.05$, *** = $p < 0.005$. Ketzner et al. (2022)

3.4.2 B-ALL cells acquire resistance to palbociclib by increasing CCND3 expression

Having demonstrated that the increase of CCND3 expression represents an adaptive mechanism to evade the cytotoxic effects of acute treatment with palbociclib, I continued by investigating if long-term treatment with palbociclib would elicit the same resistance mechanism (Ketzner et al., 2022). First, I treated the two B-ALL cell lines NALM-6 and RS4;11 with increasing amounts of palbociclib, from 0.01 μM to 1.7 μM , until the proliferation rate was comparable to the control cells. The increase of the IC₅₀ was determined by MTT assay (Figure 33A). Both cell lines became significantly resistant to palbociclib, increasing the IC₅₀ from 0.5 μM to 4.9 μM in NALM-6 and 0.5 μM to 6.5 μM in RS4;11. The IC₅₀ of BV-173 cells

was already at 2.663 μM before treatment and increased to 6.733 μM . Thus, BV-173 was deemed not sensitive to palbociclib and was therefore excluded from further analysis.

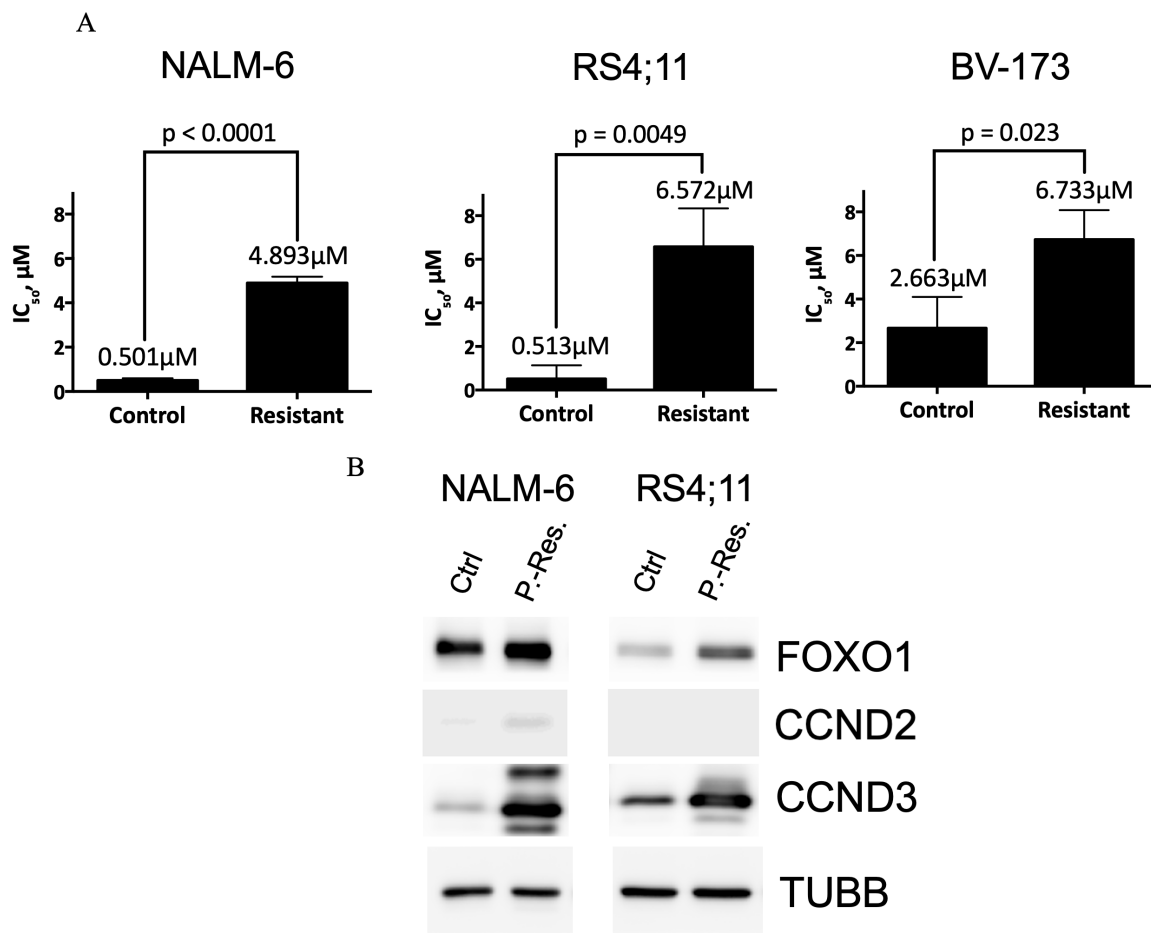


Figure 33: B-ALL cells resistant to palbociclib increase expression of CCND3

(A, B) Cells were cultured in the presence of increasing (from 0.01 μM to 1.7 μM) concentrations of palbociclib for 3 months. After reaching 1.7 μM concentration with cells growing at a speed comparable to the DMSO control cells, the sensitivity of control and resistant cells to palbociclib was measured using MTT Assay (A), FOXO1, CCND2, and CCND3 expression were measured by immunoblot (B). Data shown as mean \pm SD, n = 3. Image is representative of n = 3. Statistical analysis was performed by student's t-test. * = p < 0.05. Ketzner et al. (2022)

Of note, in one experiment, RS4;11 cells resistant to palbociclib stopped expressing RB1 protein. This was shown by immunoblot as well as via FACS staining (Figure 34). Next-generation sequencing for *RB1* in these cells revealed a deletion of an adenosine on exon 9, leading to a frameshift at asparagine 290 of RB1 (p.Asn290fs) and therefore stopping RB1 protein expression. Importantly, this mutation was not found in the control cells.

The mutation was first observed when cells were in the presence of 0.7 μ M palbociclib. However, this could not be replicated in another MLLr cell line (KOPN-8) nor a second replicate of RS4;11 cells and could therefore be considered an arbitrary event. Hence, for the following experiments, only RS4;11 cells with intact RB1 expression were chosen.

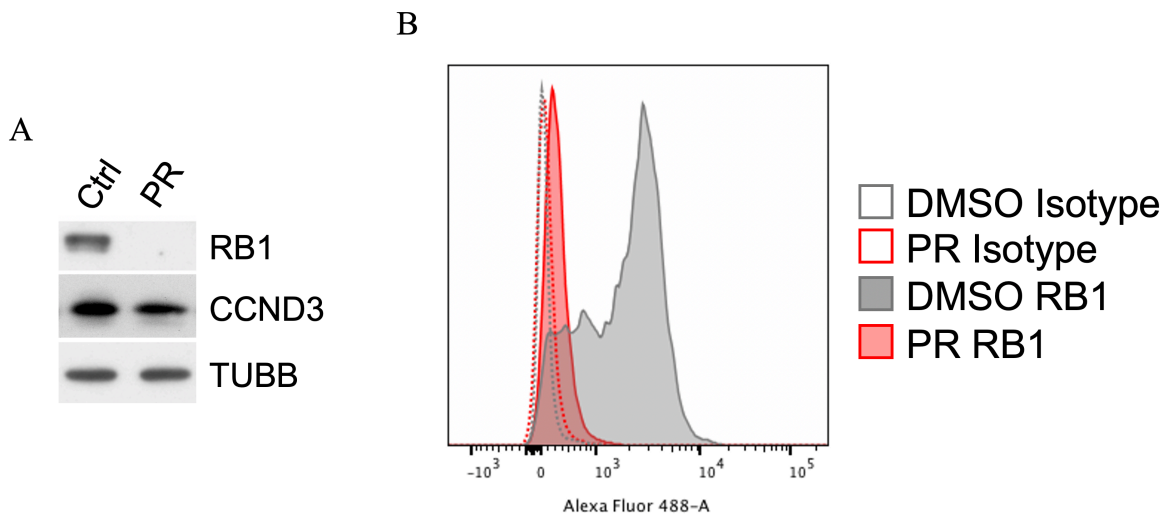


Figure 34: RS4;11 with acquired palbociclib resistance display loss of RB1 expression

(A) Immunoblot of palbociclib resistant (PR) RS4;11 with loss of RB1 expression. (B) Control (DMSO) and palbociclib-resistant (PR) RS4;11 cells were intracellularly stained for RB1 expression and analyzed by flow cytometry. Image representative of n = 2

Protein analysis by immunoblot revealed a strong increase of CCND3 in both cell lines which acquired resistance to palbociclib, higher than observed after acute treatment with palbociclib (Figure 33B). CCND2 was upregulated in NALM-6 but not detectable in RS4;11. Interestingly, the RS4;11 cells with mutated *RB1* displayed no increased CCND3 expression, indicating that RB1 phosphorylation by CCND3-CDK4/6 is not obligatory for proliferation in these cells. Interestingly, in line with my earlier findings of direct CCND3 transcriptional activation by FOXO1, its protein is concomitantly increased in palbociclib-resistant cells.

Next, the B-ALL cells resistant to palbociclib as well as control cells were transduced with either an shRNA targeting *CCND3* or a non-targeting control, both co-expressing RFP (Ketzner et al., 2022). Both resistant cell

lines were sensitive to knockdown of *CCND3*, showing decreased performance in a competitive growth assay (Figure 35A & B). Although the levels of *CCND3* protein after knockdown in the palbociclib resistant cells were much less diminished than in untreated cells after knockdown (Figure 35A, 31), even this reduction in protein expression was enough in order to decrease cellular growth and exploit the addition of palbociclib resistant cells to *CCND3*.

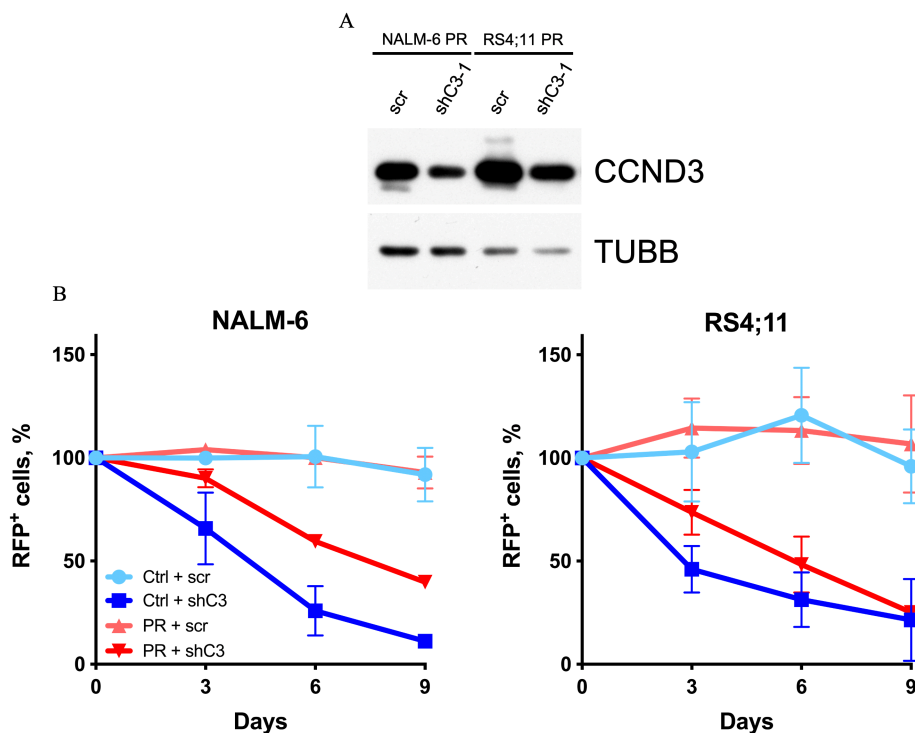


Figure 35: B-ALL resistance to palbociclib depends on *CCND3*

(A) Immunoblot of palbociclib resistant (PR) NALM-6 and RS4;11 that were lentivirally transduced with either an shRNA targeting *CCND3* (shC3) or a scrambled (scr) control vector. Cells were sorted four days post-transduction. The image is representative of $n = 2$. (B) Control (Ctrl) and palbociclib-resistant (PR) NALM-6 and RS4;11 cells were transduced with either a scrambled shRNA (scr) or shRNA against *CCND3* (shC3), co-expressing RFP. The proportion of RFP⁺ cells was monitored throughout 9 days, starting 4 days post-transduction. Data shown as mean \pm SD, $n = 3$. Ketzer et al. (2022)

This indicates a role of upregulated *CCND3* expression in acquired palbociclib resistance in B-ALL cells, independently of CDK4/6 enzymatic activity and regardless of the underlying driver mutation.

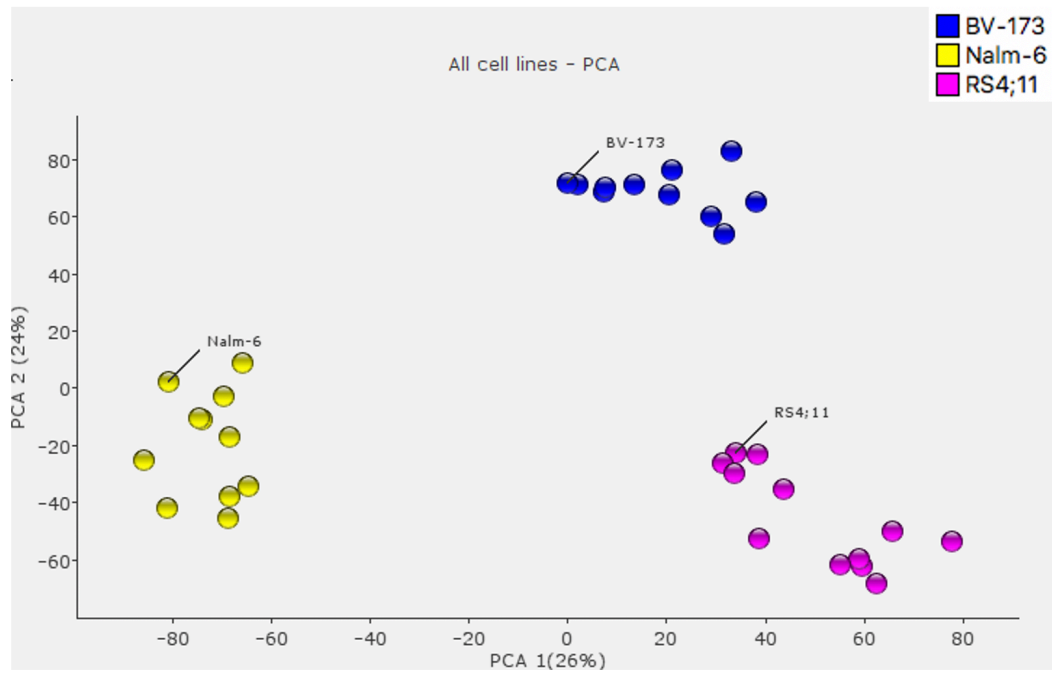
3.5 CCND3 regulates the transcription of a distinct subset of genes independently of CDK4/6 kinase activity

Although the D-Cyclins are well-known regulators of the cell cycle, it has been shown that they can also act independently of their role as activators of CDK4/6 kinase activity (Hydbring et al., 2016). Since my data show a strong apoptosis-inducing effect of CCND3 depletion but not of CDK4/6-inhibition, I aimed to isolate the effects of CCND3 knockdown in three B-ALL cell lines of different genotypes on transcriptome level by conducting RNA-sequencing after each treatment for the three B-ALL cell lines NALM-6, RS4;11, and BV-173. Each cell line represents different mutational backgrounds (ETV6-PDGFRB, MLLr, BCR-ABL1⁺) but all of them undergo apoptosis upon loss of CCND3 expression. Hence, my goal was to find common mechanisms exclusively after CCND3 depletion between all three cell lines as a potential point of intervention for the most common types of B-ALL.

3.5.1 Palbociclib and CCND3 knockdown induce distinct gene expression dependent on genotype and treatment

First, in order to analyze the accuracy and variance between the three cell lines and all four treatments (DMSO - palbociclib; scrambled - shCCND3), I performed principal component analysis (PCA) for all samples. On a two-dimensional scale, the three cell lines clustered in three distinct groups, demonstrating great variance in gene expression depending on their respective genotypes (Figure 36A). Furthermore, both controls (0/scrambled) clustered together within each cell line as well as the two treatments (palbociclib/shCCND3) (Figure 36B). This indicates mostly similar effects of CCND3 knockdown to treatment with palbociclib, which, concluding from my previous experiments showing G0/G1 arrest after both treatments (Figure 28), was expected.

A



B

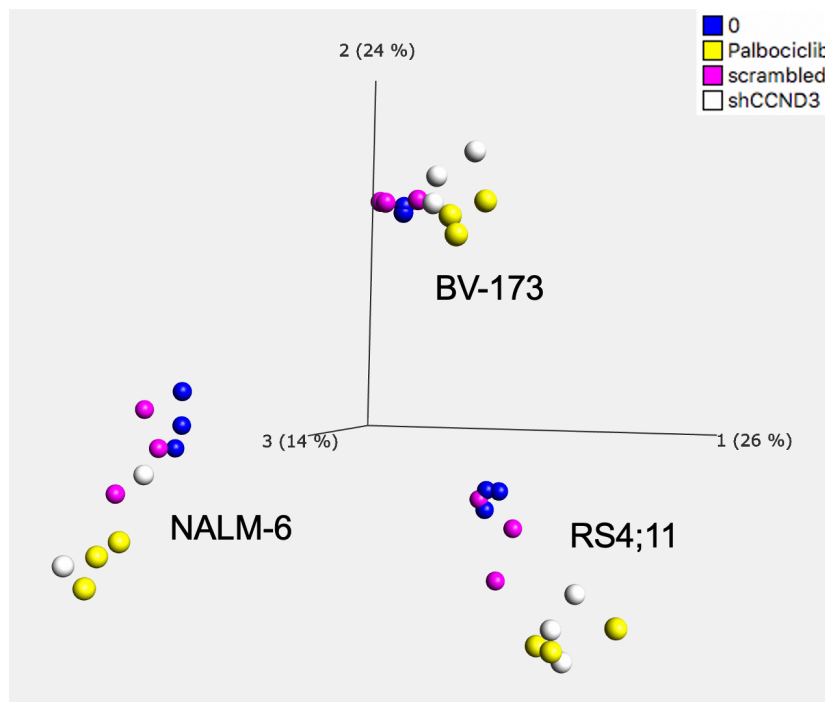


Figure 36: PCA of NALM-6, RS4;11, and BV-173 after *CCND3* knockdown or treatment with palbociclib

PCA for (A) the three cell lines and (B) the different treatments were performed with Qlucore Omics Explorer. Genes were filtered by $p < 0.05$. Data representative of $n = 2-3$.

In order to further analyze the transcriptome changes in all cell lines after each treatment in detail, I performed unsupervised hierarchical clustering for

all samples (Ketzer et al., 2022) (Figure 37). Palbociclib treatment significantly modulated gene expression of 632 genes while knockdown of CCND3 significantly affected the expression of 262 genes across all three cell lines. Hence, distinct effects of CCND3 knockdown and CDK4/6 inhibition were becoming apparent.

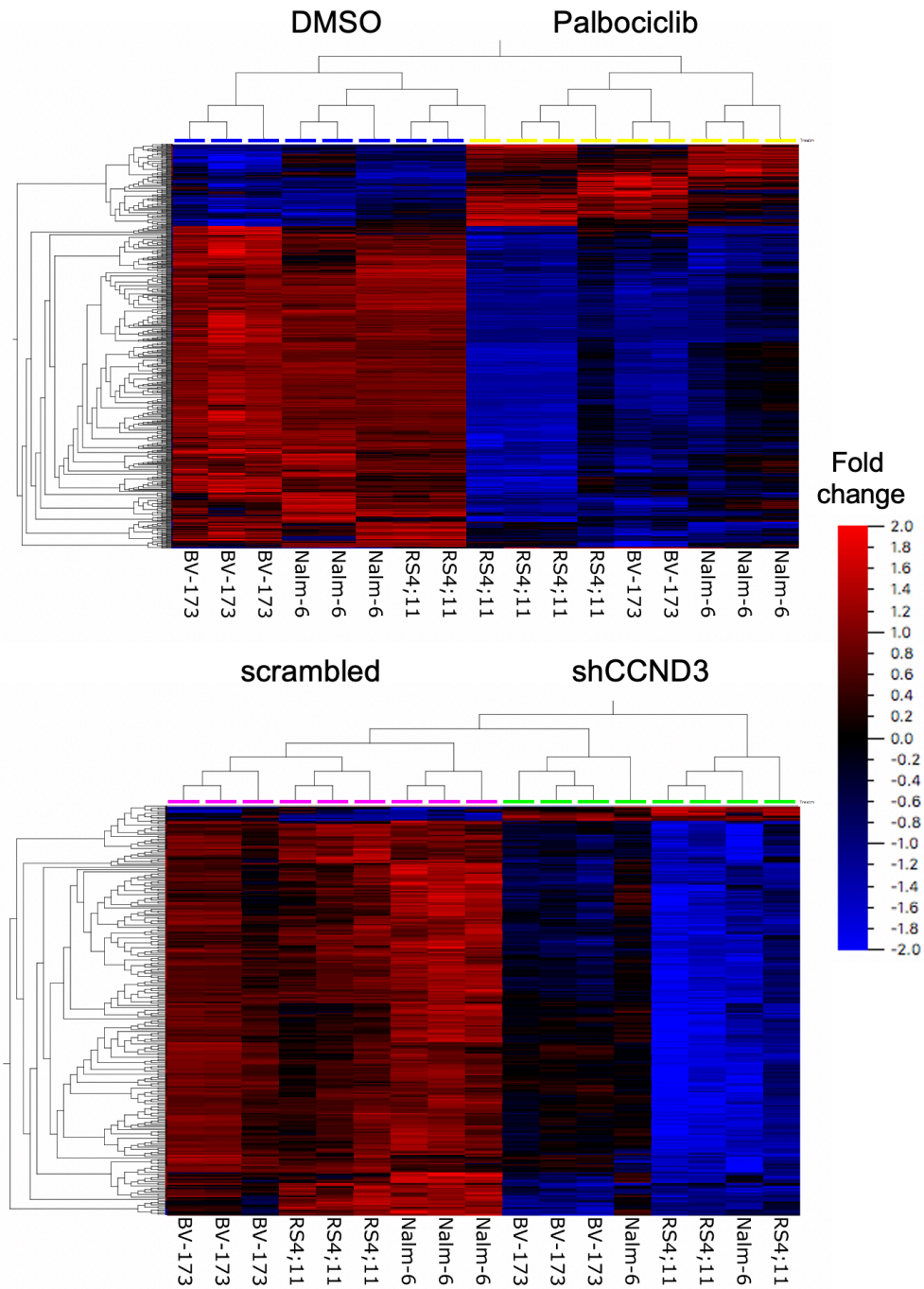


Figure 37: Hierarchical clustering of NALM-6, RS4;11, and BV-173 after *CCND3* knockdown or treatment with palbociclib

Unsupervised hierarchical clustering was performed with Qlucore Omics Explorer. Genes were filtered by fold change >1.5 , $q < 0.1$, $p < 0.05$. Data representative of $n = 2-3$.

3.5.2 CCND3 modulates the transcription of genes independently of CDK4/6

As expected, gene set enrichment analysis (GSEA) of cell cycle-related gene sets reveals comparable effects of CCND3 knockdown and CDK4/6 inhibition on RB1 mediated cell cycle progression (Figure 38). Both treatments led to significantly negatively enriched gene signatures for gene sets related to G1-S phase progression.

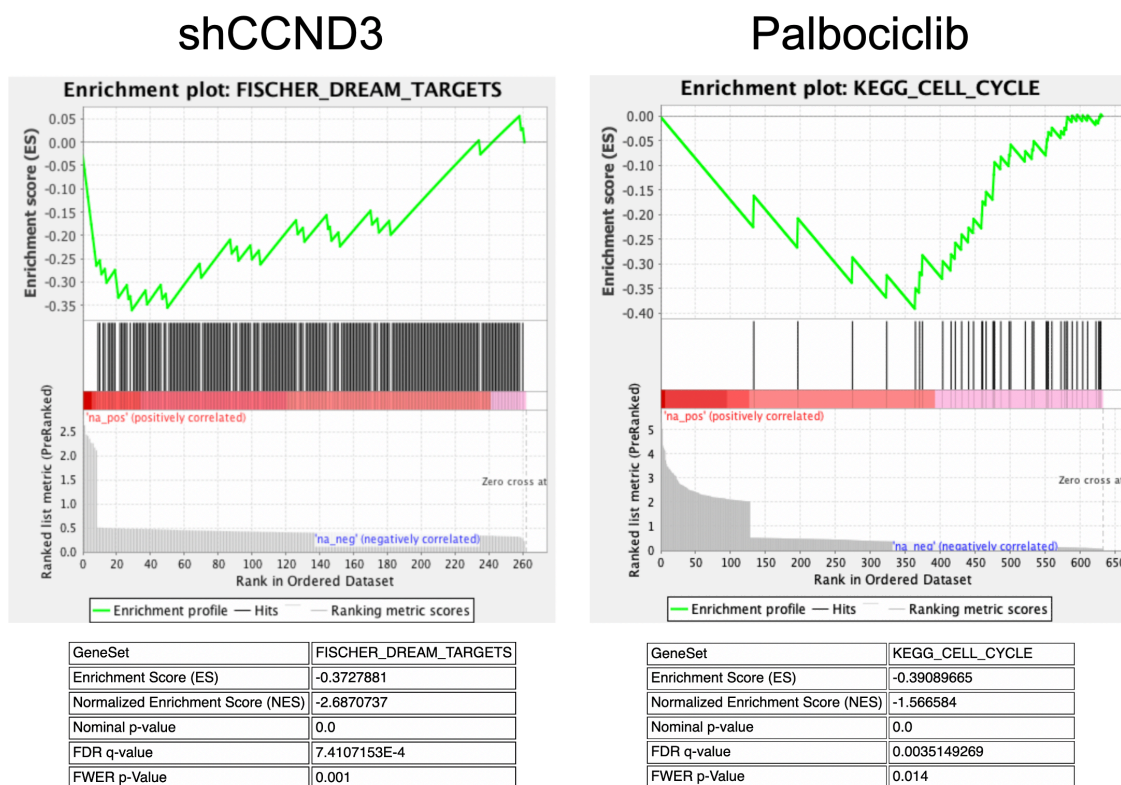


Figure 38: GSEA of cell cycle gene sets after CCND3 knockdown and palbociclib treatment
Significantly modulated genes after CCND3 knockdown or palbociclib treatment were tested against gene sets containing cell cycle progression related genes via GSEA.

Neither treatment showed significant enrichment of apoptosis-related gene sets. Since *CCND3* knockdown but not treatment with palbociclib induced apoptosis in all three B-ALL cell lines, I subtracted the differentially expressed genes identified after each treatment to isolate the genes exclusively regulated after *CCND3* knockdown but not CDK4/6 inhibition (Ketzner et al., 2022) (Figure 39). Three genes were exclusively upregulated

after *CCND3* knockdown and nine genes were exclusively downregulated. Among the downregulated genes was *CCND3*, serving as an internal control for the quality of the shRNA knockdown as well as the quality of the RNA-sequencing and confirming my earlier findings of *CCND3* not being repressed by treatment with palbociclib. The three upregulated genes were *Renin binding protein (RENBP)*, *Hydroxysteroid 17-Beta Dehydrogenase 10 (HSD17B10)*, and *Dynein Light Chain Roadblock-Type 1 (DYNLRB1)*. *RENBP* is involved in blood pressure regulation by binding and modifying the activity of renin (Kelly et al., 2017). *HSD17B10* catalyzes different steps in steroidogenesis and is involved in steroid metabolism. It is a putative target in hormone-responsive cancers like prostate and testicular cancer as well as osteosarcoma (Salas et al., 2009; Meier et al., 2009). The last upregulated gene by *CCND3* knockdown is *DYNLRB1*, which is essential for the activation of MEK and RAS-mediated production of Transforming Growth Factor beta (TGF- β) in colorectal carcinoma cells (Raza et al., 2020). The downregulated genes were *Acyl-CoA binding domain-containing 7 (ACBD7)*, *Cyclin-dependent kinase 8 (CDK8)*, *Protein-S-isoprenylcysteine O-methyltransferase (ICMT)*, *Peroxiredoxin 3 (PRDX3)*, *SEPTIN7*, *CBFB*, *CCND3*, *Glutamine-Fructose-6-Phosphate Transaminase 1 (GFPT1)* and *Never In Mitosis A-Related Kinase 7 (NEK7)*. *ACBD7* has so far only been investigated in neurons, in which it is implicated in the hypothalamic leptin signaling pathway (Lanfray et al., 2016; Lanfray and Richard, 2017). *PRDX3* participates in the detoxification of ROS. However, my prior experiments have shown that ROS accumulation is not a mechanism of *CCND3* knockdown-induced cytotoxicity in B-ALL cell lines (Figure 30). *SEPTIN7* is a member of the Guanosine-5'-triphosphate (GTP)-binding cytoskeletal SEPTIN proteins, implicated in metastasis and migration of breast cancer cells (Zhang et al., 2016). However, its up- but not downregulation has previously been described to induce cell death (Cui et al., 2020). *CBFB* has been known to compete with *CCND3* for the binding to *RUNX1*, modulating its transcriptional program (Peterson et al.,

2005). *GFPT1* expression has been linked to esophageal cancer progression (Zhang et al., 2020). The expression of *ICMT* is controlled by p53 and is needed for the final steps of prenylation of RAS and has been implicated in cancer cell survival, proliferation, regulation of mitochondrial respiration and cancer cell metabolism (Xu et al., 2019; Etichetti et al., 2019; Teh et al., 2015). Lastly, *CDK8* is a non-canonical Cyclin-dependent kinase and forms the CCNC-CDK8 holoenzyme together with Cyclin C (CCNC), phosphorylating the mediator complex of the RNA polymerase II and thereby regulating its activity (Osman et al., 2021). Additionally, CDK8 is a co-regulator of p53 target genes and is involved in phosphorylation of Signal transducer and activator of transcription (STAT)1/5 (Donner et al., 2007; Rzymiski et al., 2017). An inhibitor of CDK8 enzymatic activity, SEL120 has been developed and is currently clinically tested in AML (Borthakur et al., 2019).

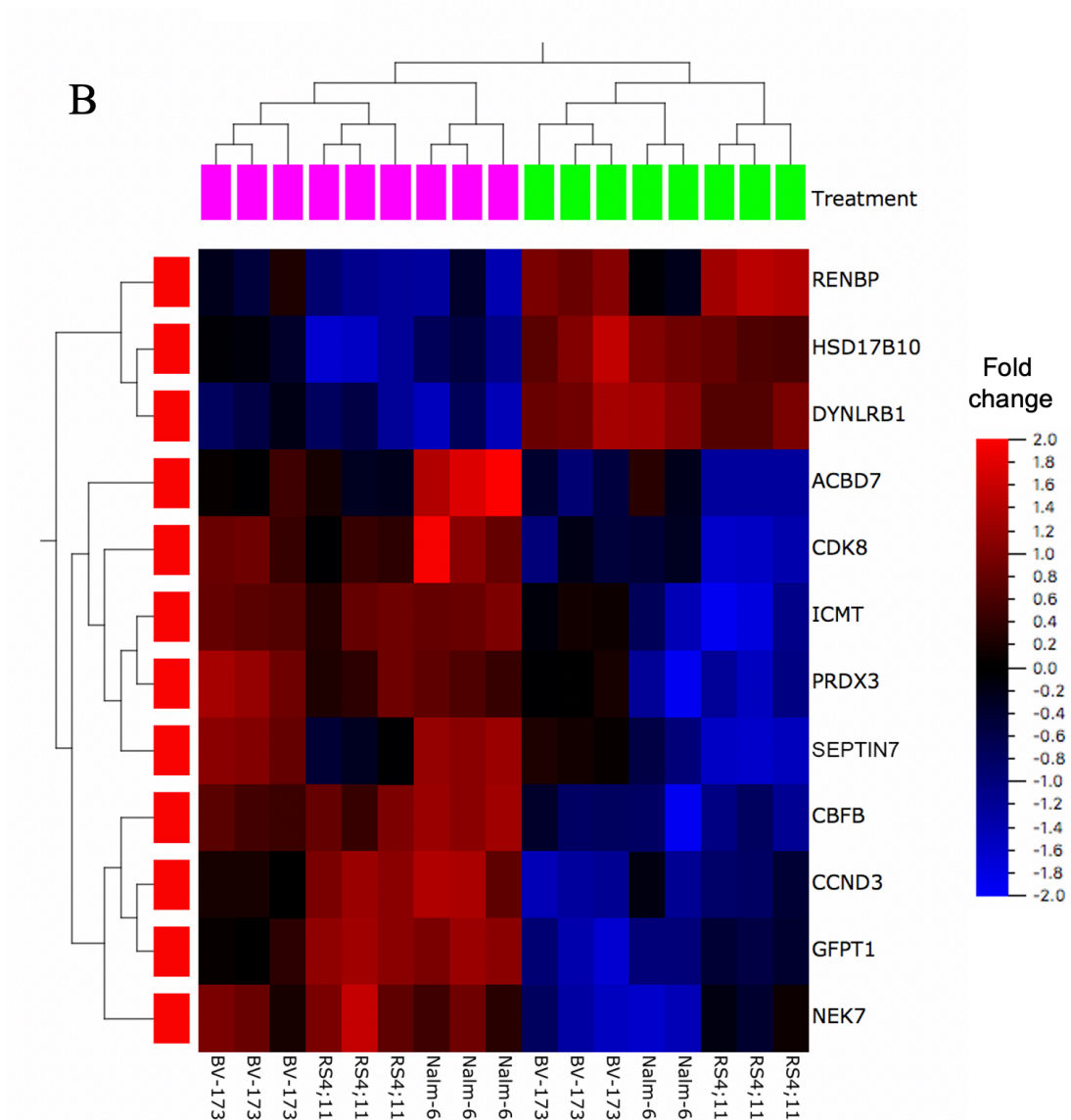
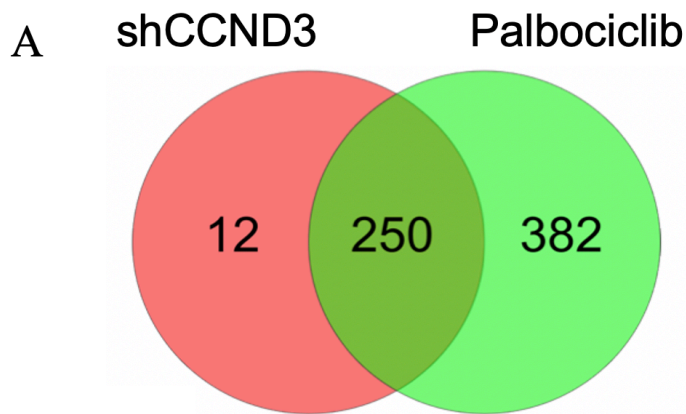


Figure 39: Genes exclusively regulated after *CCND3* knockdown

(A) Venn analysis of differentially expressed genes after shCCND3 (red) and palbociclib (red) was performed with Qlucore Omics Explorer. (B) Significantly modulated genes exclusively after CCND3 knockdown depicted by hierarchical clustering, performed with Qlucore Omics Explorer. Fold change > 1.5, $q < 0.1$, $p < 0.001$. Ketzner et al. (2022)

Of the genes discovered, *ICMT*, *CBFB*, and *CDK8* stood out as well studied factors in oncogenic signaling and potential candidates of *CCND3* knockdown induced cytotoxicity in B-ALL. However, I could not confirm the downregulation of *ICMT* on protein level after *CCND3* knockdown. Conversely, protein expression of *ICMT* in all three cell lines after *CCND3* knockdown was consistently up- but not downregulated (Figure 40A). *CBFB* expression on the other hand was only reduced in BV-173 but not in NALM-6 and RS4;11 (Figure 40B).

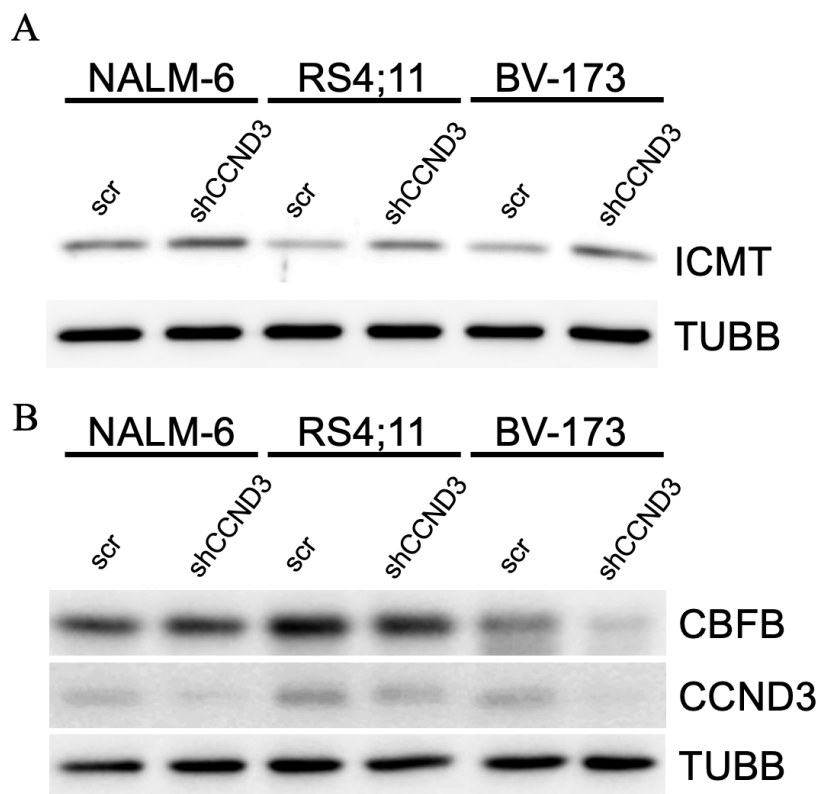


Figure 40: *CCND3* depletion does not reduce protein expression of *ICMT* and *CBFB*

Protein expression of *ICMT* (A) and *CBFB* (B) in NALM-6, RS4;11, and BV-173 after lentiviral transduction with either an shRNA targeting *CCND3* or a scrambled control. *ICMT* protein expression is upregulated in all cell lines while *CBFB* is only reduced in BV-173. Immunoblot was performed with 100 % RFP⁺ cells that were sorted 4 days after transduction. Image is representative of n = 2.

3.6 CDK8 downregulation partially mediates the cytotoxic effect of CCND3 depletion

Among the genes identified to be exclusively downregulated after CCND3 depletion but not inhibition of its associated kinases CDK4/6 by palbociclib, the non-canonical cyclin-dependent kinase CDK8 stood out as a potential gene of interest. Since CDK8 has recently been identified as a putative target in BCR-ABL1⁺ B-ALL (Menzl et al., 2019), I aimed to investigate the role of CDK8 in the cytotoxicity of *CCND3* knockdown and whether it is indeed only regulated after CCND3 depletion but not CDK4/6 inhibition. Additionally, I addressed the question of whether CDK8 expression is essential in other subtypes of B-ALL besides BCR-ABL1⁺ B-ALL.

3.6.1 CDK8 expression is decreased only by CCND3 knockdown but not CDK4/6 inhibition

First, I repeated the treatments of the three B-ALL cell lines NALM-6, RS4;11, and BV-173 as done for the RNA-sequencing analysis in order to confirm the observed decrease of CDK8 transcription on protein level (Ketzer et al., 2022). Cells were either treated with 1 μ M palbociclib for 3 days or lentivirally transduced with either an shRNA against CCND3 or a scrambled control and then analyzed by immunoblot. In accordance with the RNA-sequencing results, CDK8 protein expression was reduced in all three cell lines only after CCND3 knockdown but not after treatment with palbociclib (Figure 41).

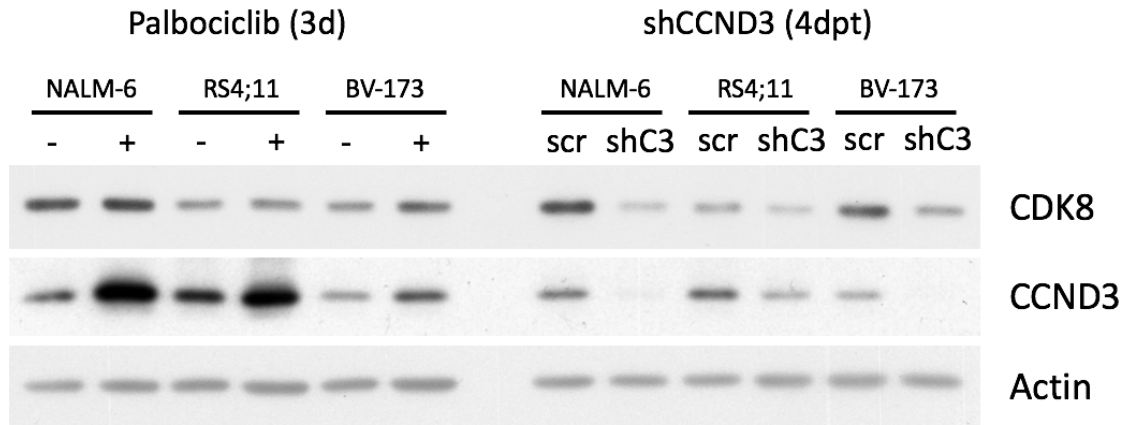


Figure 41: CDK8 is only downregulated after *CCND3* depletion but not CDK4/6 inhibition

Immunoblot of NALM-6, RS4;11, and BV-173 either after treatment with 1 μ M palbociclib for 3 days or 4 days after transduction with either an shRNA against *CCND3* or a scrambled control. CDK8 protein expression reduced in every cell line after *CCND3* knockdown but not after treatment with palbociclib. Image representative of n = 3. Ketzer et al. (2022)

Since *CCND3* downregulation is a consequence of loss of FOXO1, I additionally analyzed *Cdk8* expression after *Foxo1* deletion in the murine BCR-ABL1⁺ B-ALL model. RNA-sequencing data indicate significant downregulation of *Cdk8* mRNA expression two days after *Foxo1* deletion. Indeed, two days after induction of *Foxo1* deletion, a decrease of CDK8 protein expression became visible as well (Figure 42).

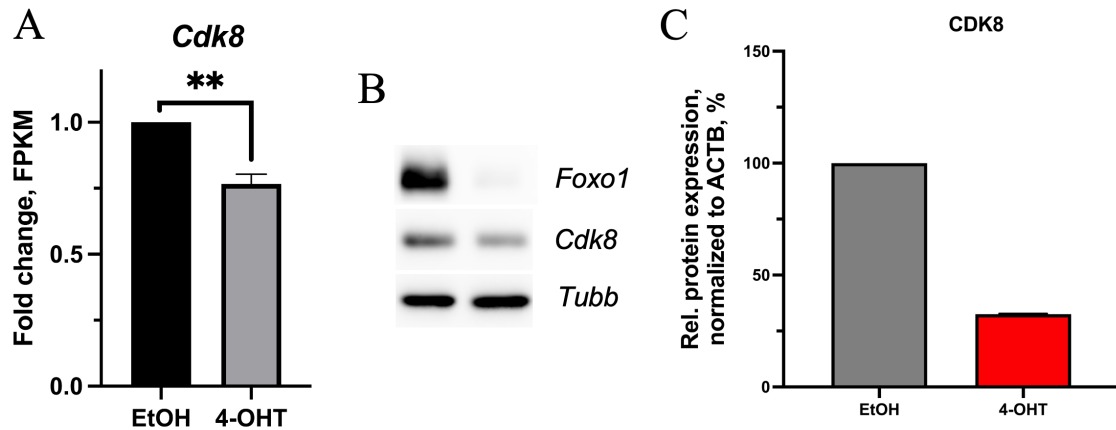


Figure 42: Loss of *Foxo1* decreases *Cdk8* expression

(A) RNA-sequencing of murine *Foxo1*^{fl/fl} BCR-ABL1 transformed pre-B-cells two days after induction of *Foxo1* deletion with 200 nM 4-OHT. The cells significantly downregulate *Cdk8* mRNA expression. Data shown as mean \pm SD, n = 3. Statistical analysis was performed with Students t-test. ** = p < 0.01 (B) Immunoblot of murine *Foxo1*^{fl/fl} BCR-ABL1 transformed pre-B-cells 2 days after induction of *Foxo1* deletion with 200 nM 4-OHT shows decreased CDK8 expression. Image representative of n = 2 (C) Quantification of immunoblots of CDK8 after *Foxo1* deletion. Data shown as mean \pm SD, n = 2.

3.6.2 Genetic depletion of *CDK8* is toxic in B-ALL cells of different underlying driver mutations

Since it has been demonstrated that BCR-ABL1⁺ B-ALL is sensitive to depletion of CDK8 protein but not to enzymatic inhibition (Menzl et al., 2019), I set to investigate whether this is also the case in B-ALL of different genotypes. First, I determined the IC₅₀ values for the CDK8 kinase inhibitor SEL120 in the three B-ALL cell lines NALM-6, RS4;11, and BV-173 (Ketzner et al., 2022). In line with prior findings (Menzl et al., 2019), the BCR-ABL1⁺ cell line BV-173 was insensitive to enzymatic inhibition of CDK8 (Figure 43). Interestingly, this was also the case for the ETV6-PDGFRB cell line NALM-6 and the MLLr cell line RS4;11. These results indicate a kinase-independent role of CDK8 not only in BCR-ABL1⁺ B-ALL.

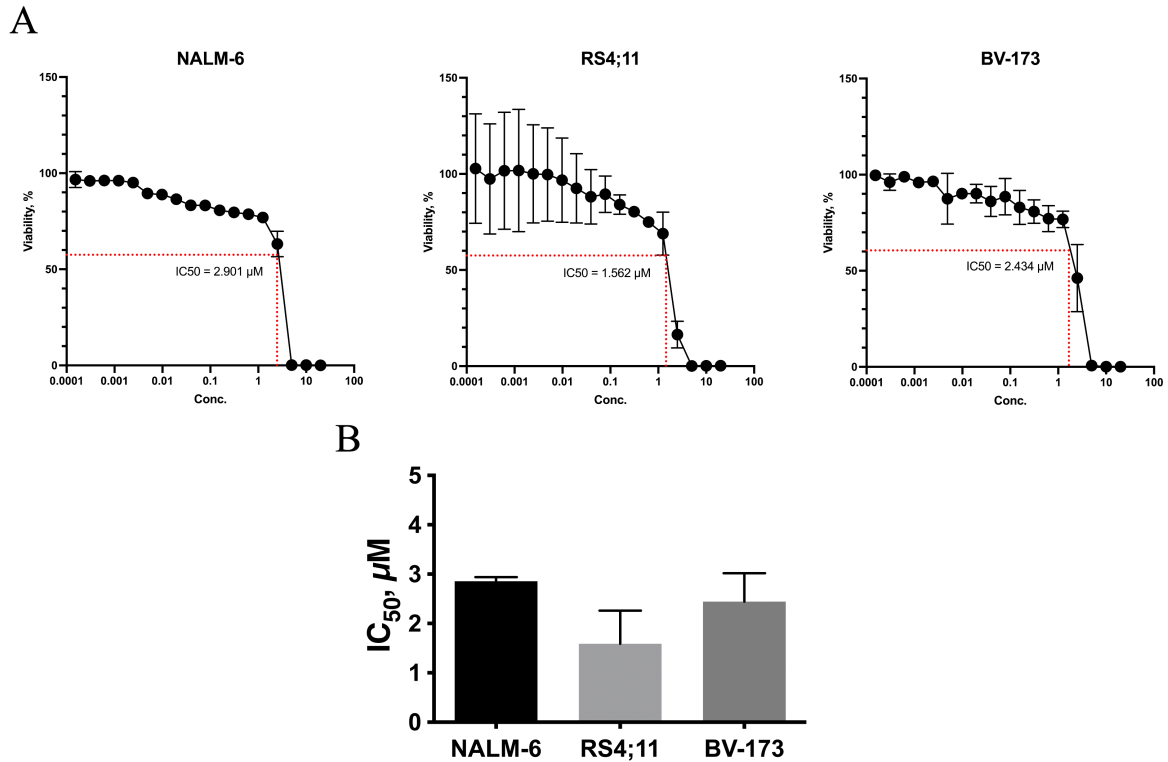
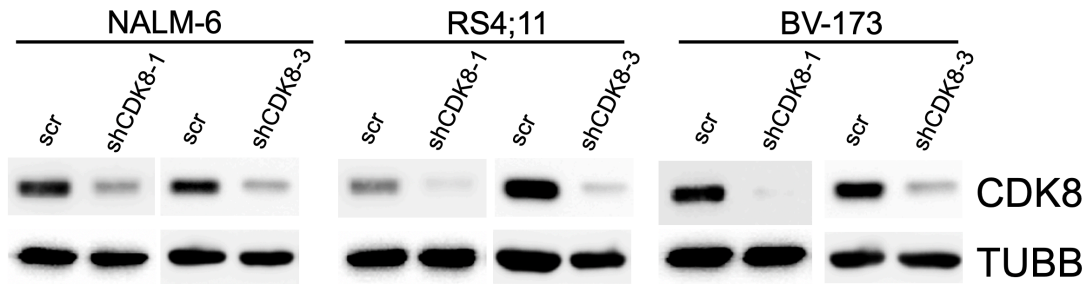


Figure 43: B-ALL cells are not sensitive to enzymatic inhibition of CDK8 by SEL120

(A) IC₅₀ of the B-ALL cell lines NALM-6, RS4;11, and BV-173 for the CDK8 kinase inhibitor SEL120 was determined by MTT assay and non-linear regression curve fit with GraphPad Prism 9. Data shown as mean ± SD, n=2. (B) Direct comparison of the measured IC₅₀ values of all three cell lines. Data shown as mean ± SD, n=2. Ketzer et al. (2022)

Next, in order to investigate whether the depletion of *CDK8* contributes to *CCND3* knockdown-induced cytotoxicity or was just a bystander effect, I lentivirally transduced the BCR-ABL1⁺ cell line BV-173 and the BCR-ABL1⁻ NALM-6 and RS4;11 B-ALL cells with either one of two shRNAs targeting *CDK8* or a scrambled (scr) control (Ketzer et al., 2022). Knockdown efficiency was demonstrated by immunoblot (Figure 44A). Both shRNAs significantly decreased the growth performance of NALM-6 cells, while the growth of RS4;11 and BV-173 cells was only significantly impaired by one shRNA (Figure 44B).

A



B

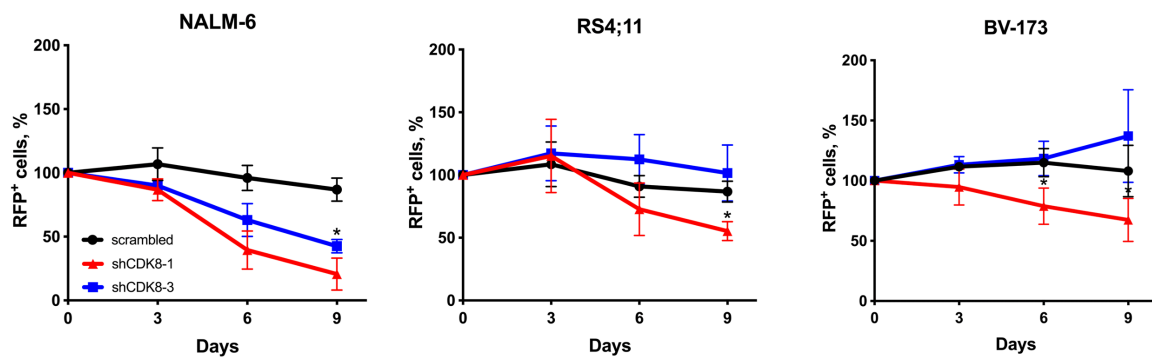


Figure 44: Genetic depletion of *CDK8* is toxic for B-ALL cells

(A) Immunoblot of NALM-6 and RS4;11 four days after lentiviral transduction of either one of two shRNAs targeting *CDK8* or a scrambled control. Image is representative of $n = 3$. (B) shRNA knockdown of *CDK8* decreases performance of NALM-6, RS4;11, and BV-173 in a competitive growth assay. Data shown as mean \pm SD, $n = 3$. * = $p < 0.05$. Ketzner et al. (2022)

It has previously been described that the cytotoxic effect of *CDK8* depletion in BV-173 and BCR-ABL1⁺ B-ALL, in general, is mediated by apoptosis. Hence, I set to analyze the effects of *CDK8* knockdown-induced reduced growth performance in the BCR-ABL1⁻ B-ALL cell lines NALM-6 and RS4;11. First, I analyzed the effects of *CDK8* knockdown on the cell cycle. NALM-6 cells were significantly decreased in the G0/G1 phase, whereas in RS4;11, no effect on the cell cycle became visible (Figure 45A). However, *CDK8* knockdown induced significant apoptosis in both cell lines (Ketzner et al., 2022) (Figure 45B).

These results demonstrate that *CCND3* knockdown-induced downregulation of *CDK8* mRNA and protein expression is partially responsible for the cytotoxic effects of *CCND3* depletion. Furthermore, I showed that *CDK8* depletion is a promising approach not only for targeting BCR-ABL1⁺ B-ALL but also B-ALL harboring other driver mutations.

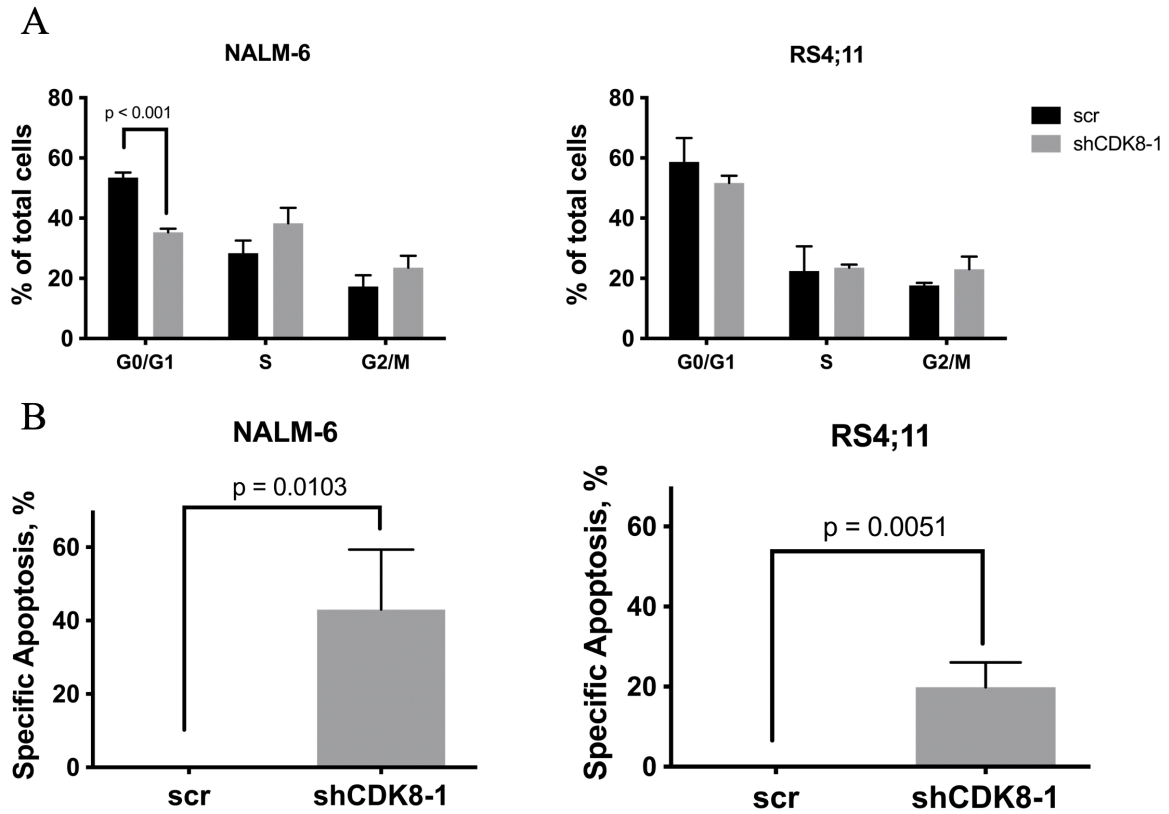


Figure 45: Genetic depletion of *CDK8* induces apoptosis in B-ALL cells

(A) NALM-6 and RS4;11 cells were lentivirally transduced with either an shRNA against CDK8 (shCDK8-1) or a non-targeting (scr) control, both co-expressing RFP. Cells were sorted for 100% RFP⁺ cells four days after transduction and cultured for three more days before fixed and stained with PI. Analysis was done by flow cytometry. Data shown as mean \pm SD, n = 3. Statistical analysis was performed with student's t-test. (B) NALM-6 and RS4;11 cells were lentivirally transduced with either an shRNA against CDK8 (shCDK8-1) or a non-targeting (scr) control, both co-expressing RFP. Cells were sorted for 100% RFP⁺ cells four days after transduction and cultured for three more days before staining with Annexin-V-FITC and PI. Analysis was done by flow cytometry. Data shown as mean \pm SD, n = 3. Statistical analysis was performed with student's t-test. Ketzner et al. (2022)

Chapter 4

Discussion

4.1 CCND3 is the highest expressed D-type Cyclin in B-ALL

In order to characterize the importance of CCND3 in B-ALL, I first mined RNA-expression data from a publicly available database and analyzed the expression levels of the three D-type Cyclins throughout the most common genetic B-ALL subgroups. It became apparent that CCND3 is expressed at the highest mRNA and protein levels, while CCND2 expression is always lower and in some subtypes, like MLLr B-ALL, not expressed at all, while CCND1 is not detectable in any B-ALL subgroup.

In accordance with my data, CCND1 is not regarded as an important factor in B-cell malignancies, apart from its frequent IGH-translocation in mantle cell lymphoma, and has been shown to play no role in B-cell lymphopoiesis (Cooper et al., 2006). However, rare cases of BCR-ABL1⁺ B-ALL show increased expression of CCND1, which has been correlated with a worse clinical outcome (Fernandes et al., 2018). Dogmatically, pro-/pre-B-cell proliferative expansion is governed by the MYC-induced expression of CCND2 (Buchner and Müschen, 2014). However, this dogma was established in healthy B-cells and carried over to B-ALL, largely supported by BCR-ABL1⁺ B-ALL models with particularly high CCND2 expression, and was further inferred because MYC was shown to be essential in B-ALL (de Barrios et al., 2020). Accordingly, I also observed high CCND2 expression in primary BCR-ABL1⁺ B-ALL patient data and cell lines. Yet, even in this genetic subgroup, CCND3 is the highest expressed D-type Cyclin but was largely disregarded in the context of B-ALL, because of

generally accepted redundancy of D-Cyclins (Choi and Anders, 2014). Conversely, it has been demonstrated that CCND3 is indeed essential, non-redundant, and indispensable for the transition from pre-BCR⁻ to pre-BCR⁺ pre-B-cells (Cooper et al., 2006). Additionally, CCND3 protein is found in compartments that do not overlap with CCND2 within the nucleus of early B-lymphoblasts, restricting the access to a large part of the *IgK* variable segments by binding to the nuclear matrix (Powers et al., 2012). Furthermore, CCND3 has been found to play a key role in the germinal center reaction, cannot be substituted by another D-type Cyclin and is regulated post-translationally by GSK3 (Cato et al., 2011). Lastly, previous data from our lab (Wang et al., 2018) has shown that FOXO1 depletion and pharmacological inhibition induces decreased CCND3 mRNA and protein expression and ectopic expression of CCND3 ameliorated the cytotoxic effects of FOXO1 inhibition.

Hence, my data in the context of available literature suggests a widely disregarded, important role of CCND3 in B-ALL that warranted deeper analysis.

4.2 CCND3 expression is directly activated by FOXO1

One aim of my thesis was to analyze the regulation and role of CCND3 in B-ALL. Since our previous publication has shown that the cytotoxic effect of FOXO1 inhibition and genetic depletion is mediated by CCND3 (Wang et al., 2018), I set to understand the mechanism behind the interplay of CCND3 and FOXO1. By performing luciferase assay, EMSA and ChIP, I found that FOXO1 indeed binds to the promoter region of *CCND3* and activates its expression. Data mining of ChIP-sequencing data also revealed conserved binding of FOXO1 to the *CCND3* promoter at the same position in pre-leukemic stem cells and mature B-lymphocytes. Although this mechanism has never been shown in B-lymphoid malignancies before, it did not come as a complete surprise since this had already been demonstrated in

murine pancreatic β -cells (Zhang et al., 2016). However, activation of CCND3 by FOXO1 seemed counter-intuitive, particularly in B-ALL, since CCND1 and CCND2 are both repressed by FOXO1, and active FOXO1 in healthy pro-/pre-B-cells is typically associated with the stop of proliferation (Kode et al., 2012; Eswaran et al., 2015). Indeed, my data shows that *Ccnd1*, as well as *Ccnd3* mRNA expression is significantly increased 24 hours after *Foxo1* deletion in a BCR-ABL1⁺ B-ALL mouse model. While inducing growth arrest and VDJ-recombination in early B-cells, FOXO1 is indispensable for the proliferation of B-ALL cells (Wang et al., 2018; Abdelrasoul et al., 2020). However, constitutive activation of FOXO1 via either PI3K hyperactivation or ectopic FOXO1 expression is also toxic for B-ALL cells (Köhler et al., 2016). This "Goldilocks"-like regulation of FOXO1 in B-ALL and Burkitt lymphoma has been demonstrated by our research group (Wang et al., 2018; Gehringer et al., 2019). This phenomenon has been shown for other genes as well, like PI3K, AKT, SYK, and ERK (Müschen, 2018). For FOXO1, this could mean that high expression levels revert its function to the "benign" phenotype by stopping proliferation and inducing apoptosis, while its inactivation would mimic auto-reactive BCR-signaling, also leading to cell death. Furthermore, activity and modulation of transcription factors change through malignant transformation (Bhagwat and Vakoc, 2015). Since the transcriptional regulation of FOXO1 is governed in part by its binding partners, it is feasible that not only FOXO1 itself but also its binding partners are altered through leukemogenesis, explaining its change from a generally anti-proliferative factor in B-cell development to a proliferation gene (Van Der Vos and Coffey, 2008). Finally, since FOXO1 is a tumor suppressor in Hodgkin lymphoma but not in diffuse-large B-cell lymphoma (DLBCL) or Burkitt lymphoma, this change of function of FOXO1 during malignant transformation is not conserved throughout all major B-cell-derived malignancies (Xie et al., 2012; Trinh et al., 2013; Gehringer et al., 2019). Furthermore, I analyzed the role of MYC and E2F in the expression of

CCND3. Available literature has found direct transcriptional activation of CCND3 by E2F, a MYC target (Ma et al., 2003; Coller et al., 2007). E2F is activated by CCND1/2/3-CDK4/6 and was interrogated by CDK4/6 inhibition with palbociclib. Although treatment with palbociclib induced growth arrest in B-ALL cells, CCND3 levels were stable. The same was observed after treatment of BCR-ABL1⁺ B-ALL cells with imatinib, the cells stopped proliferating but CCND3 remained stable. The treatment with imatinib generally stops STAT-MYC signaling, which was found to activate CCND2 and CCND3 (Clark et al., 2014). However, my data indicates that the activation of D-type Cyclins via STAT5 does not play a role in the B-ALL models that I used. Although E2F and MYC are both *bona fide* proliferation genes by inducing G1-S progression, expression of CCND3 seemed to greatly rely on FOXO1 activity, which after both treatments, concurrently with CCND3 expression, remained stable and even slightly increased. Conclusively, I demonstrated a novel function of FOXO1 in B-ALL, the direct transcriptional activation of CCND3 by FOXO1, adding to its recently discovered functions as a pro-survival and pro-proliferative gene in B-ALL.

4.3 CCND3 depletion but not CDK4/6 inhibition is toxic to B-ALL cells

Our group's previous work has indicated a dependency of B-ALL on CCND3 (Wang et al., 2018). However, this was done with only one shRNA in NALM-6 (ETV6-PDGFRB) and RS4;11 (MLLr). I was able to show that CCND3 is an indispensable gene in all major subtypes of B-ALL. This is particularly interesting because my data acquired by data mining, qPCR, and western blot indicated a varying expression of CCND2 and CCND3, suggesting a potential redundancy, depending on the respective genotype. However, I could show that the knockdown of CCND3 is cytotoxic, independently of CCND2 expression levels. Additionally, knockdown of

CCND3 proved to be toxic and induce apoptosis even in a murine BCR-ABL1⁺ and therefore CCND2^{high} B-ALL model. These results suggest that CCND2 cannot substitute for CCND3 in terms of survival of B-ALL cells. I confirmed this data by knockdown of CCND3 in different *ex vivo* PDX models, one with *KRAS*^{G12D} mutation and two PDXs derived from BCR-ABL1⁺. As mentioned before, this contradicts the dogma of CCND2 being the most important D-Cyclin in B-ALL and challenges the largely accepted idea of D-cyclin redundancy in cellular proliferation. Furthermore, since CCND3 cannot be substituted by CCND1 or CCND2 in order to achieve pre-BCR expression in early B-cell development, it seemed feasible that B-ALL cells possess a CCND3 specific dependence (Cooper et al., 2006). Next, in order to interrogate whether CCND3 is essential in B-ALL because of its function as part of the CCND-CDK4/6 holoenzyme, I treated B-ALL cells with the clinically used CDK4/6 inhibitor palbociclib. Both CCND3 knockdown as well as treatment with palbociclib induced G0/G1 arrest. However, I observed that, opposed to CCND3 depletion, CDK4/6 enzymatic inhibition did not result in the induction of apoptosis in all human and murine models used for my study. Indeed, it had been previously reported, that not the inhibition of CDK6, the highest expressed CDK in B-ALL, but the degradation of CDK6 via PROTAC is detrimental in Ph⁺ B-ALL (De Dominici et al., 2020). Subsequently, this indicated a kinase-independent, pro-survival role of the components of the CCND3-CDK6 holoenzyme in B-ALL, additionally to their functions in G1-S progression. Furthermore, ectopic CCND3 expression was sufficient in ameliorating the cell cycle arrest induced by treatment with palbociclib, even in supra-clinical concentrations, indicating that CCND3 drives proliferation independently of CDK4/6.

Furthermore, in B-ALL cells of different genotypes with acquired resistance to palbociclib, I found a strong upregulation of CCND3 protein expression, which I also demonstrated three days after initial treatment with palbociclib. In accordance with my previous observations, the knockdown of CCND3 in

the resistant cells was cytotoxic, supporting my hypothesis of CCND3 contributing to the resistance of B-ALL cells to palbociclib. Additionally, this furthers the idea that CCND3 performs essential tasks outside of the holoenzymatic CCND-CDK4/6 complex. Multiple kinase-independent functions of CCND3 have been previously shown, but none particularly in B-ALL (Hydbring et al., 2016).

Interestingly, I observed that the MLLr cell line RS4;11 lost expression of RB1 after acquiring resistance to palbociclib. This event has been observed in breast cancer cells that became resistant to palbociclib as well (Guarducci et al., 2018). This is particularly intriguing since palbociclib is clinically used for breast cancer therapy and is currently evaluated for the treatment of various cancers (Niesvizky et al., 2015; Zhang et al., 2021). Although I was not able to replicate loss of RB1 expression after the acquisition of resistance to palbociclib, RB1 mutations might pose a common, possibly arbitrary escape mechanism of cancer cells to CDK4/6 inhibition and should be evaluated when clinically testing palbociclib for cancer treatment.

Conclusively, I showed that CCND3 is an essential pro-survival factor of B-ALL cells of different genetic subgroups, acting independently of CDK4/6 kinase activity and protecting B-ALL cells from palbociclib-induced cytotoxic effects independent of cell cycle dysregulation.

4.4 CCND3 regulates gene expression independently of CDK4/6

Since my data demonstrated that CCND3 depletion but not CDK4/6 inhibition induced apoptosis in B-ALL cell lines and *ex vivo* models, I conducted RNA-sequencing with three cell lines of different genotypes after either treatment. I applied a subtractive exclusion approach by first identifying differentially expressed genes after each treatment in all cell lines and then comparing the regulated genes after CCND3 knockdown and

treatment with palbociclib and to isolate the genes exclusively modulated after CCND3 knockdown. I identified 12 genes that were regulated only after CCND3 depletion in all cell lines. After thorough literature research, the most interesting genes that were implicated in tumorigenesis, regulation of apoptosis, or general survival functions particularly in hematopoietic cells, were ICMT, PRDX3, CBFB, and CDK8.

Since RAS activity is associated with highly aggressive B-ALL and ICMT has been shown to be an essential regulator of RAS in many different pre-clinical tumor models, I included it in the list of genes of interest and tried to verify its downregulation after CCND3 knockdown on protein level (Koschut et al., 2021). ICMT catalyzes the last of three steps of RAS oncoprotein prenylation and negatively correlates with aggressiveness and clinical outcome of multiple types of cancer (Xu et al., 2019). The process of prenylation by ICMT anchors CaaX proteins like RAS and its mutant variants to cellular membranes (Brunsveld et al., 2009). However, I was not able to verify its downregulation observed in the RNA-sequencing on protein level. Conversely, protein expression of ICMT was increased in all three cell lines after CCND3 knockdown, which could indicate the involvement of post-translational mechanisms compensating for the loss of transcription. However, although ICMT is an interesting candidate for therapeutic intervention, and the observed reciprocal regulation of mRNA and protein expression could be a very interesting, separate topic to look into, I did not pursue it any further during my thesis.

CBFB was also a very interesting candidate, particularly because of its competition with CCND3 for the binding to RUNX1, modulating the transcription factor's activity (Peterson et al., 2005). By binding to RUNX1, CCND3 decreases its DNA binding affinity, inducing increased proliferation in preclinical AML models. However, apart from its translocation with ETV6, the role of RUNX1 in B-ALL remains unclear and a decrease of CBFB which is a positive regulator of RUNX1 would be of unclear consequences. Hence, I set to validate the downregulation of CBFB but

could only observe decreased protein expression in the BCR-ABL1⁺ cell line BV-173. It is likely that this effect in BV-173 was strong enough and only occurred after CCND3 knockdown, therefore reaching significance in the unsupervised hierarchical clustering of differentially expressed genes of the RNA-sequencing data. However, since there is no literature available exploring the role of CFBF in B-ALL and particularly in BCR-ABL1⁺ B-ALL, future knockdown experiments would be interesting in order to elucidate whether downregulation of CFBF is involved in CCND3 depletion-induced cytotoxicity.

Having already performed an analysis of ROS accumulation after CCND3 knockdown earlier, I was aware that this is not a mechanism occurring after CCND3 depletion in B-ALL. Hence, although PRDX3 is a key enzyme in ROS detoxification and a direct transcriptional target of MYC, I excluded it from further analysis because of a lack of functional evidence after CCND3 knockdown (Wonsey et al., 2002).

The last gene of interest was CDK8, which I could indeed validate by immunoblot and which I will discuss in detail in the next section.

Overall, the main question concerning the RNA-sequencing data was, how CCND3 by itself, a non-enzymatically active protein could regulate the expression of genes at all. As mentioned above, CCND3 has been found to bind to the nuclear matrix, thus regulating access to different genetic loci, modulating gene expression (Powers et al., 2012). Furthermore, its binding or, after knockdown, lack thereof, to RUNX1 could lead to modulation of gene expression (Peterson et al., 2005). However, none of the genes modulated exclusively after CCND3 knockdown are direct transcriptional targets of RUNX1, according to publicly available ChIP-sequencing data (Oki et al., 2018). Moreover, interactions of CCND3 with other, yet undiscovered binding partners could be responsible for the transcriptional changes observed after CCND3 depletion.

Additionally, evidence is emerging of different functions of differently composed CCND-CDK4/6 complexes. For example, CCND3-CDK6 was

identified as a metabolic regulator in T-ALL, although CCND2 and CDK4 were also expressed but not implicated in these processes (Wang et al., 2017). Furthermore, during embryonic development, different CCND-CDK4/6 complexes are formed and expressed in a lineage-specific manner (Bryja et al., 2008). Moreover, the knockdown of *Ccnd1* and *Ccnd3* in pancreatic ductal adenocarcinoma (PDAC) cell lines induced different effects on the transcriptome (Radulovich et al., 2010). Depletion of *Ccnd3* in these cells was primarily associated with effects on the cell cycle while knockdown of *Ccnd1* affected nuclear factor 'kappa-light-chain-enhancer' of activated B-cells (NF- κ B) and mitogen-activated protein-kinase (MAPK) signaling. However, the authors did not provide a mechanism by which the different D-type Cyclins regulate different pathways of the cells. Taken together, this could indicate a non-redundancy not only of the components but also of the CCND-CDK4/6 holoenzymatic complexes themselves, all of which fulfill separate tasks in (B-ALL) cells. Elaborating on this idea, it is conceivable that CCND3 particularly steers the observed transcriptional activity and modulation of CDK4/6 in a way that involves the genes that I identified only after CCND3 knockdown but not after CDK4/6 inhibition. Since it was shown that not enzymatic inhibition but most likely transcriptional activity of CDK4/6 is essential in Philadelphia-chromosome positive B-ALL, this could mean that by treatment with palbociclib, the non-essential enzymatic action of CDK4/6 is inhibited while its transcriptional activity remains active and undisturbed (De Dominici et al., 2020). Thus, the only way to eliminate this essential function of CDK4/6 would be by either degrading CDK6, as already done previously, or by depleting the most important D-type Cyclin in B-ALL cells, CCND3. Conclusively, my data suggests that CCND3 influences transcription either by modifying the chromatin accessibility, modulating transcription factors or by steering the CDK4/6 transcriptional program.

4.5 CDK8 contributes to the cytotoxic effects of CCND3 depletion in B-ALL

After isolating transcriptional changes occurring exclusively after CCND3 knockdown but not after CDK4/6 inhibition in all three cell lines, CDK8 emerged as a potential downstream effector. CDK8 was of particular interest because it was recently shown to be essential in pre-clinical BCR-ABL1⁺ B-ALL models (Menzl et al., 2019). The CDK8 module is an important component of the mediator complex, providing energy for RNA-polymerase II-mediated transcription (Uehara et al., 2020). Furthermore, CDK8 is also implicated in transcriptional regulation in complex with p53 and has been shown to phosphorylate STAT1 and STAT5 (Rzymiski et al., 2017; Osman et al., 2021). Because of the latter function, inhibitors for the enzymatic function of CDK8 have been developed and are currently clinically evaluated for the treatment of AML and high-risk myelodysplastic syndrome (Borthakur et al., 2019). However, off-target systemic effects have been reported and are currently critically evaluated (Chen et al., 2019). It has been reported that mixed-lineage leukemia is particularly sensitive to CDK8 inhibition, most likely because MLL1 (KMT2A) is a target of CDK8-mediated transcription (Krivtsov et al., 2017). However, my data showed only a minimally stronger effect of CDK8 inhibition by SEL120 on RS4;11 compared to the other, insensitive cell lines. In accordance with the available literature, my data showed that not enzymatic inhibition of CDK8 but depletion of CDK8 protein induces apoptosis in BCR-ABL1⁺ B-ALL (Menzl et al., 2019). Importantly, I was able to show that CDK8 expression is essential not only in BCR-ABL1⁺ B-ALL but also a Philadelphia-chromosome-like cell line (NALM-6) and a MLLr cell line (RS4;11).

Furthermore, direct binding of CDK8 by CCND3 and subsequent complex formation can be excluded, since the Cyclin-binding site of CDK8 is vastly different from that of CDK4 and CDK6, so no effect of CCND3 knockdown

on CDK8 activity itself should be expected (Wood and Endicott, 2018). How the depletion of CCND3 regulates the expression of CDK8 remains unclear and could be the subject of further research.

4.6 Conclusion

I conclude that CCND3 is the highest expressed D-type Cyclin in all major genetic subgroups of B-ALL. CCND3 expression is directly regulated by FOXO1 and is essential for the survival and proliferation program of B-ALL. Challenging the notion of D-type Cyclin redundancy, I found that CCND3 cannot be substituted by CCND1 or CCND2. Furthermore, CCND3 depletion but not inhibition of CDK4/6 induces apoptosis in B-ALL. The knockdown of CCND3 modulates the expression of a distinct set of genes, independently of CCND3-CDK4/6 holoenzymatic activity. Finally, an important gene regulated by CCND3 in B-ALL is CDK8, which depletion induces apoptosis in B-ALL cell lines harboring different driver mutations, in part mediating the cytotoxic effect of CCND3 knockdown.

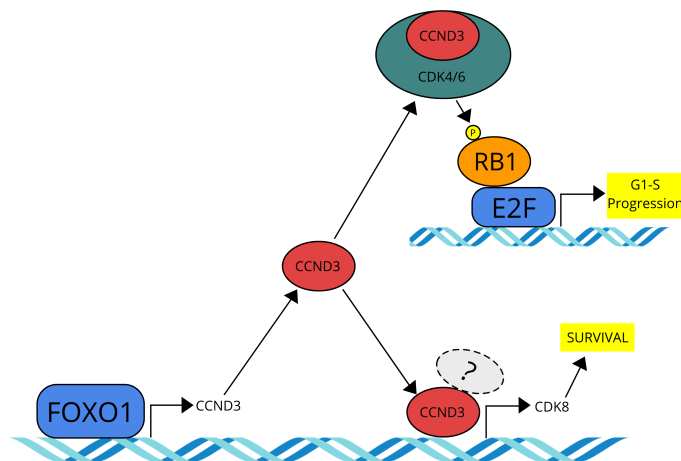


Figure 46: Proposed model of the pro-survival function of CCND3 in B-ALL

Chapter 5

Summary

D-type Cyclins are a well-known and important part of the cell cycle machinery. Interfering with the cell cycle by inhibiting their associated kinases CDK4/6 has been actively studied for decades. These efforts have been successful in certain malignancies, such as breast cancer, but remained futile in B-ALL. Our group has previously shown that down-regulation of FOXO1 leads to a decrease of CCND3 expression, which by itself is toxic to B-ALL cells. This finding came as a surprise, since CCND2 has been previously regarded as the most important D-Cyclin in B-ALL, being a direct transcriptional target of MYC. Intriguingly, targeting CCND3, which by itself is not catalytically active, widely regarded as redundant to other D-Cyclins, and works in a holoenzymatic complex with CDK4/6, has not been explored in B-ALL before. Hence, I set to investigate two main questions: First, how CCND3 is regulated by FOXO1 and second, how the down-regulation of CCND3 exerts cytotoxic effects in B-ALL.

First, I conducted data mining of publicly available gene expression data derived from B-ALL patients, observing that CCND3 is the highest expressed D-type Cyclin throughout all major genetic subgroups of B-ALL. Next, I aimed to elucidate the underlying mechanism of CCND3 activation by FOXO1 using a BCR-ABL1⁺ *Foxo1^{fl/fl}* murine B-ALL model, luciferase reporter assay, EMSA and ChIP. Employing these methods, I indeed observed binding and activation of the *CCND3* promoter by FOXO1.

Based on our group's previous observations of cytotoxic effects by CCND3 knockdown in two B-ALL cell lines, I used a second shRNA against CCND3 to confirm this in more, genetically diverse subgroups of B-ALL. Both shRNAs proved to be toxic in all cell lines tested, inducing cell cycle arrest and apoptosis. I confirmed the growth-inhibitory effects of CCND3

knockdown by additionally employing CRISPR/Cas9 and shRNAs in a murine BCR-ABL1-transformed B-ALL model and three PDXs of different underlying driver mutations and treatment histories. Interestingly, these effects could not be replicated by treating the cells with the clinically used inhibitor of CCND3-associated kinases CDK4/6, palbociclib. Although both treatments induced cell cycle arrest, only knockdown of CCND3 but not CDK4/6 inhibition induced apoptosis in B-ALL cells.

Since the available literature suggested CDK-independent effects of Cyclins, I conducted RNA-sequencing of three B-ALL cell lines of different genotypes either after treatment with palbociclib or after CCND3 knockdown. I subtracted the differentially expressed genes of both groups, which resulted in a compact list of genes that were exclusively regulated after CCND3 knockdown but not after CDK4/6 inhibition. This list included CDK8, which has been shown to fulfill essential functions in BCR-ABL1⁺ B-ALL. First, I confirmed on protein level that CDK8 is exclusively down-regulated after CCND3 knockdown but not after treatment with palbociclib. Furthermore, the shRNA-mediated knockdown of CDK8 in BCR-ABL1⁻ B-ALL cells induced apoptosis. I concluded that CDK8 is an essential gene for the survival B-ALL of different mutational backgrounds, which is regulated by CCND3.

Conclusively, my work presents a mechanistic basis for the regulation of CCND3 by FOXO1, demonstrates an essential role of CCND3 in all major subtypes of B-ALL and provides insight into CDK4/6-independent functions of CCND3 that culminate in the regulation of the essential gene CDK8.

Chapter 6

References

- [1] Chapter 5 - B Cell Development, Activation and Effector Functions. pages 111–142. Academic Cell, Boston, 2014. ISBN 978-0-12-385245-8. doi: <https://doi.org/10.1016/B978-0-12-385245-8.00005-4>.
- [2] Abdelrasoul, H., Vadakumchery, A., Werner, M., Lenk, L., Khadour, A., Young, M., El Ayoubi, O., Vogiatzi, F., Krämer, M., Schmid, V., Chen, Z., Yousafzai, Y., Cario, G., Schrappe, M., Müschen, M., Halsey, C., Mulaw, M. A., Schewe, D. M., Hobeika, E., Alsadeq, A., and Jumaa, H. Synergism between IL7R and CXCR4 drives BCR-ABL induced transformation in Philadelphia chromosome-positive acute lymphoblastic leukemia. *Nature Communications*, 11(1):3194, 2020. ISSN 20411723. doi: 10.1038/s41467-020-16927-w.
- [3] Abou Dalle, I., Jabbour, E., Short, N. J., and Ravandi, F. Treatment of Philadelphia Chromosome-Positive Acute Lymphoblastic Leukemia, jan 2019. ISSN 15346277.
- [4] Aldoss, I. and Stein, A. S. Advances in adult acute lymphoblastic leukemia therapy, 2018. ISSN 10292403.
- [5] Alvarnas, J. C., Brown, P. A., Aoun, P., Ballen, K. K., Barta, S. K., Borate, U., Boyer, M. W., Burke, P. W., Cassaday, R., Castro, J. E., Coccia, P. F., Coutre, S. E., Damon, L. E., De Angelo, D. J., Douer, D., Frankfurt, O., Greer, J. P., Johnson, R. A., Kantarjian, H. M., Klisovic, R. B., Kupfer, G., Litzow, M., Liu, A., Rao, A. V., Shah, B., Uy, G. L., Wang, E. S., Zelenetz, A. D., Gregory, K., and Smith, C. Acute lymphoblastic leukemia, version 2.2015: Clinical practice guidelines in oncology, oct 2015. ISSN 15401413.

- [6] Arber, D. A., Orazi, A., Hasserjian, R., Thiele, J., Borowitz, M. J., Le Beau, M. M., Bloomfield, C. D., Cazzola, M., and Vardiman, J. W. The 2016 revision to the World Health Organization classification of myeloid neoplasms and acute leukemia, may 2016. ISSN 15280020.
- [7] Asma, G. E., Langlois Van Den Bergh, R., and Vossen, J. M. Development of pre-B and B lymphocytes in the human fetus. *Clinical and experimental immunology (Print)*, 56(2):407–414, 1984. ISSN 0009-9104.
- [8] Bhagwat, A. S. and Vakoc, C. R. Targeting Transcription Factors in Cancer, sep 2015. ISSN 24058033.
- [9] Borthakur, G. M., Donnellan, W. B., Solomon, S. R., Abboud, C., Nazha, A., Mazan, M., Mikula, M., Majewska, E., Wiklik, K., Golas, A., Järås, M., Chapellier, M., Polak, A., Bialas, A., Windak, R., Ostrowski, J., Juszczynski, P., Chrom, P., Rzymiski, T., and Brzózka, K. SEL120 - a First-in-Class CDK8/19 Inhibitor As a Novel Option for the Treatment of Acute Myeloid Leukemia and High-Risk Myelodysplastic Syndrome - Data from Preclinical Studies and Introduction to a Phase Ib Clinical Trial. *Blood*, 134(Supplement_1): 2651–2651, nov 2019. ISSN 0006-4971. doi: 10.1182/BLOOD-2019-127835.
- [10] Bracken, A. P., Ciro, M., Cocito, A., and Helin, K. E2F target genes: Unraveling the biology, aug 2004. ISSN 09680004.
- [11] Brunsveld, L., Waldmann, H., and Huster, D. Membrane binding of lipidated Ras peptides and proteins - The structural point of view, jan 2009. ISSN 00052736.
- [12] Bryja, V., Pacherník, J., Vondráček, J., Souček, K., Čajánek, L., Horvath, V., Holubcová, Z., Dvořák, P., and Hampl, A. Lineage specific composition of cyclin D-CDK4/CDK6-p27 complexes reveals

- distinct functions of CDK4, CDK6 and individual D-type cyclins in differentiating cells of embryonic origin. *Cell Proliferation*, 41 (6):875–893, dec 2008. ISSN 09607722. doi: 10.1111/j.1365-2184.2008.00556.x.
- [13] Buchner, M. and Müschen, M. Targeting the B-cell receptor signaling pathway in B lymphoid malignancies. *Current Opinion in Hematology*, 21(4):341–349, jul 2014. ISSN 1065-6251. doi: 10.1097/MOH.0000000000000048.
- [14] Cato, M. H., Chintalapati, S. K., Yau, I. W., Omori, S. A., and Rickert, R. C. Cyclin D3 Is Selectively Required for Proliferative Expansion of Germinal Center B Cells. *Molecular and Cellular Biology*, 31(1): 127–137, jan 2011. ISSN 0270-7306. doi: 10.1128/mcb.00650-10.
- [15] Cerutti, A., Cols, M., and Puga, I. Marginal zone B cells: Virtues of innate-like antibody-producing lymphocytes, feb 2013. ISSN 14741733.
- [16] Chan, L. N., Murakami, M. A., Robinson, M. E., Caeser, R., Sadras, T., Lee, J., Cosgun, K. N., Kume, K., Khairnar, V., Xiao, G., Ahmed, M. A., Aghania, E., Deb, G., Hurtz, C., Shojaee, S., Hong, C., Pölönen, P., Nix, M. A., Chen, Z., Chen, C. W., Chen, J., Vogt, A., Heinäniemi, M., Lohi, O., Wiita, A. P., Izraeli, S., Geng, H., Weinstock, D. M., and Müschen, M. Signalling input from divergent pathways subverts B cell transformation. *Nature*, 583(7818):845–851, 2020. ISSN 14764687. doi: 10.1038/s41586-020-2513-4.
- [17] Chen, M., Li, J., Liang, J., Thompson, Z. S., Kathrein, K., Broude, E. V., and Roninson, I. B. Systemic Toxicity Reported for CDK8/19 Inhibitors CCT251921 and MSC2530818 Is Not Due to Target Inhibition. *Cells*, 8(11), nov 2019. ISSN 20734409. doi: 10.3390/cells8111413.

- [18] Cheng, H., Zheng, Z., and Cheng, T. New paradigms on hematopoietic stem cell differentiation, jan 2020. ISSN 16748018.
- [19] Choi, Y. J. and Anders, L. Signaling through cyclin D-dependent kinases, may 2014. ISSN 14765594.
- [20] Cilloni, D. and Saglio, G. Molecular pathways: BCR-ABL. *Clinical Cancer Research*, 18(4):930–937, feb 2012. ISSN 10780432. doi: 10.1158/1078-0432.CCR-10-1613.
- [21] Clark, M. R., Mandal, M., Ochiai, K., and Singh, H. Orchestrating B cell lymphopoiesis through interplay of IL-7 receptor and pre-B cell receptor signalling, feb 2014. ISSN 14741733.
- [22] Coller, H. A., Forman, J. J., and Legesse-Miller, A. "Myc'ed messages": Myc induces transcription of E2F1 while inhibiting its translation via a microRNA polycistron, aug 2007. ISSN 15537390.
- [23] Collins, A. M. and Watson, C. T. Immunoglobulin light chain gene rearrangements, receptor editing and the development of a self-tolerant antibody repertoire, oct 2018. ISSN 16643224.
- [24] Cooper, A. B., Sawai, C. M., Sicinska, E., Powers, S. E., Sicinski, P., Clark, M. R., and Aifantis, I. A unique function for cyclin D3 in early B cell development. *Nature Immunology*, 7(5):489–497, 2006. ISSN 15292908. doi: 10.1038/ni1324.
- [25] Cui, C., Lin, T., Gong, Z., and Zhu, Y. Relationship between autophagy, apoptosis and endoplasmic reticulum stress induced by melatonin in osteoblasts by septin7 expression. *Molecular Medicine Reports*, 21(6):2427–2434, jun 2020. ISSN 17913004. doi: 10.3892/mmr.2020.11063.
- [26] Dal Porto, J. M., Haberman, A. M., Kelsoe, G., and Shlomchik, M. J. Very low affinity B cells form germinal centers, become

- memory B cells, and participate in secondary immune responses when higher affinity competition is reduced. *Journal of Experimental Medicine*, 195(9):1215–1221, may 2002. ISSN 00221007. doi: 10.1084/jem.20011550.
- [27] de Barrios, O., Meler, A., and Parra, M. MYC's Fine Line Between B Cell Development and Malignancy, feb 2020. ISSN 20734409.
- [28] De Dominici, M., Porazzi, P., Xiao, Y., Chao, A., Tang, H. Y., Kumar, G., Fortina, P., Spinelli, O., Rambaldi, A., Peterson, L. F., Petruk, S., Barletta, C., Mazo, A., Cingolani, G., Salvino, J. M., and Calabretta, B. Selective inhibition of Ph-positive ALL cell growth through kinase-dependent and -independent effects by CDK6-specific PROTACs. *Blood*, 135(18):1560–1573, apr 2020. ISSN 15280020. doi: 10.1182/BLOOD.2019003604.
- [29] DeKoter, R. P., Lee, H. J., and Singh, H. PU.1 regulates expression of the interleukin-7 receptor in lymphoid progenitors. *Immunity*, 16(2):297–309, feb 2002. ISSN 10747613. doi: 10.1016/S1074-7613(02)00269-8.
- [30] Donner, A. J., Szostek, S., Hoover, J. M., and Espinosa, J. M. CDK8 Is a Stimulus-Specific Positive Coregulator of p53 Target Genes. *Molecular Cell*, 27(1):121–133, jul 2007. ISSN 10972765. doi: 10.1016/j.molcel.2007.05.026.
- [31] Eswaran, J., Sinclair, P., Heidenreich, O., Irving, J., Russell, L. J., Hall, A., Calado, D. P., Harrison, C. J., and Vormoor, J. The pre-B-cell receptor checkpoint in acute lymphoblastic leukaemia, aug 2015. ISSN 14765551.
- [32] Etichetti, C. B., Benedetto, C. D., Rossi, C., Baglioni, M. V., Bicciato, S., Sal, G. D., Menacho-Marquez, M., and Girardini, J. Isoprenylcysteine carboxy methyltransferase (ICMT) is associated

- with tumor aggressiveness and its expression is controlled by the p53 tumor suppressor. *Journal of Biological Chemistry*, 294(13):5060–5073, mar 2019. ISSN 1083351X. doi: 10.1074/jbc.RA118.006037.
- [33] Ezhevsky, S. A., Nagahara, H., Vocero-Akbani, A. M., Gius, D. R., Wei, M. C., and Dowdy, S. F. Hypo-phosphorylation of the retinoblastoma protein (pRb) by cyclin D:Cdk4/6 complexes results in active pRb. *Proceedings of the National Academy of Sciences of the United States of America*, 94(20):10699–10704, sep 1997. ISSN 00278424. doi: 10.1073/pnas.94.20.10699.
- [34] Fernandes, J. C., Rodrigues Alves, A. P. N., Coelho-Silva, J. L., Scopim-Ribeiro, R., Fenerich, B. A., Simões, B. P., Rego, E. M., Machado-Neto, J. A., and Traina, F. Increased levels of cyclin D1 negatively impacts on acute lymphoblastic leukemia overall survival. *Applied Cancer Research*, 38(1):7, 2018. ISSN 1980-5578. doi: 10.1186/s41241-018-0058-8.
- [35] Fielding, A. K., Rowe, J. M., Buck, G., Foroni, L., Gerrard, G., Litzow, M. R., Lazarus, H., Luger, S. M., Marks, D. I., McMillan, A. K., Moorman, A. V., Patel, B., Paietta, E., Tallman, M. S., and Goldstone, A. H. UKALLXII/ECOG2993: Addition of imatinib to a standard treatment regimen enhances long-term outcomes in Philadelphia positive acute lymphoblastic leukemia. *Blood*, 123(6): 843–850, feb 2014. ISSN 00064971. doi: 10.1182/blood-2013-09-529008.
- [36] Fry, D. W., Harvey, P. J., Keller, P. R., Elliott, W. L., Meade, M. A., Trachet, E., Albassam, M., Zheng, X. X., Leopold, W. R., Pryer, N. K., and Toogood, P. L. Specific inhibition of cyclin-dependent kinase 4/6 by PD 0332991 and associated antitumor activity in human tumor xenografts. *Molecular Cancer Therapeutics*, 3(11):1427–1437, nov 2004. ISSN 15357163.

- [37] Fry, E. A. and Inoue, K. c-MYB and DMTF1 in Cancer, jan 2019. ISSN 15324192.
- [38] Galili, N., Davis, R. J., Fredericks, W. J., Mukhopadhyay, S., Rauscher, F. J., Emanuel, B. S., Rovera, G., and Barr, F. G. Fusion of a fork head domain gene to PAX3 in the solid tumour alveolar rhabdomyosarcoma. *Nature Genetics*, 5(3):230–235, 1993. ISSN 15461718. doi: 10.1038/ng1193-230.
- [39] Gatto, D. and Brink, R. The germinal center reaction, 2010. ISSN 00916749.
- [40] Gehringer, F., Weissinger, S. E., Swier, L. J., Möller, P., Wirth, T., and Ushmorov, A. FOXO1 confers maintenance of the dark zone proliferation and survival program and can be pharmacologically targeted in burkitt lymphoma. *Cancers*, 11(10), oct 2019. ISSN 20726694. doi: 10.3390/cancers11101427.
- [41] Geng, H., Hurtz, C., Lenz, K. B., Chen, Z., Baumjohann, D., Thompson, S., Goloviznina, N. A., Chen, W. Y., Huan, J., LaTocha, D., Ballabio, E., Xiao, G., Lee, J. W., Deucher, A., Qi, Z., Park, E., Huang, C., Nahar, R., Kweon, S. M., Shojaee, S., Chan, L. N., Yu, J., Kornblau, S. M., Bijl, J. J., Ye, B. H., Mark Ansel, K., Paietta, E., Melnick, A., Hunger, S. P., Kurre, P., Tyner, J. W., Loh, M. L., Roeder, R. G., Druker, B. J., Burger, J. A., Milne, T. A., Chang, B. H., and Müschen, M. Self-Enforcing Feedback Activation between BCL6 and Pre-B Cell Receptor Signaling Defines a Distinct Subtype of Acute Lymphoblastic Leukemia. *Cancer Cell*, 27(3):409–425, mar 2015. ISSN 18783686. doi: 10.1016/j.ccell.2015.02.003.
- [42] Giacinti, C. and Giordano, A. RB and cell cycle progression, aug 2006. ISSN 09509232.
- [43] Gloor, W. Ein fall von geheilter myeloblastenleukämie. *Munch Med Wochenschr*, 77:1096–1098, 1930.

- [44] Goebeler, M. E. and Bargou, R. C. T cell-engaging therapies — BiTEs and beyond, jul 2020. ISSN 17594782.
- [45] Guarducci, C., Bonechi, M., Benelli, M., Biagioni, C., Boccalini, G., Romagnoli, D., Verardo, R., Schiff, R., Osborne, C. K., De Angelis, C., Di Leo, A., Malorni, L., and Migliaccio, I. Cyclin E1 and Rb modulation as common events at time of resistance to palbociclib in hormone receptor-positive breast cancer. *npj Breast Cancer*, 4(1):38, 2018. ISSN 23744677. doi: 10.1038/s41523-018-0092-4.
- [46] Gurnari, C., De Bellis, E., DiVona, M., Ottone, T., Lavorgna, S., and Voso, M. T. When Poisons Cure: The Case of Arsenic in Acute Promyelocytic Leukemia, jul 2020. ISSN 14219794.
- [47] Hanahan, D. and Weinberg, R. A. Hallmarks of cancer: The next generation, mar 2011. ISSN 00928674.
- [48] Hardy, R. R. and Hayakawa, K. B cell development pathways, nov 2001. ISSN 07320582.
- [49] Herzog, S., Reth, M., and Jumaa, H. Regulation of B-cell proliferation and differentiation by pre-B-cell receptor signalling, mar 2009. ISSN 14741733.
- [50] Hosaka, T., Biggs, W. H., Tieu, D., Boyer, A. D., Varki, N. M., Cavenee, W. K., and Arden, K. C. Disruption of forkhead transcription factor (FOXO) family members in mice reveals their functional diversification. *Proceedings of the National Academy of Sciences of the United States of America*, 101(9):2975–2980, mar 2004. ISSN 00278424. doi: 10.1073/pnas.0400093101.
- [51] Hruz, T., Laule, O., Szabo, G., Wessendorp, F., Bleuler, S., Oertle, L., Widmayer, P., Gruissem, W., and Zimmermann, P. Genevestigator V3: A Reference Expression Database for the Meta-Analysis of

- Transcriptomes. *Advances in Bioinformatics*, 2008:1–5, jul 2008. ISSN 1687-8027. doi: 10.1155/2008/420747.
- [52] Huang, F. L., Liao, E. C., Li, C. L., Yen, C. Y., and Yu, S. J. Pathogenesis of pediatric B-cell acute lymphoblastic leukemia: Molecular pathways and disease treatments (Review). *Oncology Letters*, 20(1):448–454, jul 2020. ISSN 17921082. doi: 10.3892/ol.2020.11583.
- [53] Hunger, S. P. and Raetz, E. A. How I treat relapsed acute lymphoblastic leukemia in the pediatric population. *Blood*, 136(16):1803–1812, oct 2020. ISSN 15280020. doi: 10.1182/BLOOD.2019004043.
- [54] Hurtz, C., Chan, L. N., Geng, H., Ballabio, E., Xiao, G., Deb, G., Khoury, H., Chen, C. W., Armstrong, S. A., Chen, J., Ernst, P., Melnick, A., Milne, T., and Müschen, M. Rationale for targeting BCL6 in MLL-rearranged acute lymphoblastic leukemia. *Genes and Development*, 33(17-18):1265–1279, aug 2019. ISSN 15495477. doi: 10.1101/gad.327593.119.
- [55] Hydbring, P., Malumbres, M., and Sicinski, P. Non-canonical functions of cell cycle cyclins and cyclin-dependent kinases. *Nature Reviews Molecular Cell Biology*, 17(5):280–292, apr 2016. ISSN 14710080. doi: 10.1038/nrm.2016.27.
- [56] Hyun Kim, D., Zhang, T., Ringquist, S., and Henry Dong, H. Targeting FoxO1 for Hypertriglyceridemia. *Current Drug Targets*, 12(9):1245–1255, 2011. ISSN 13894501. doi: 10.2174/138945011796150262.
- [57] Igarashi, H., Gregory, S. C., Yokota, T., Sakaguchi, N., and Kincade, P. W. Transcription from the RAG1 locus marks the earliest lymphocyte progenitors in bone marrow. *Immunity*, 17(2):117–130, aug 2002. ISSN 10747613. doi: 10.1016/S1074-7613(02)00366-7.

- [58] Jabbour, E., O'Brien, S., Konopleva, M., and Kantarjian, H. New insights into the pathophysiology and therapy of adult acute lymphoblastic leukemia, aug 2015. ISSN 10970142.
- [59] Jabbour, E. J., Faderl, S., and Kantarjian, H. M. Adult acute lymphoblastic leukemia. In *Mayo Clinic Proceedings*, volume 80, pages 1517–1527. Mayo Clin Proc, 2005. doi: 10.4065/80.11.1517.
- [60] Jackson, T. R., Ling, R. E., and Roy, A. The Origin of B-cells: Human Fetal B Cell Development and Implications for the Pathogenesis of Childhood Acute Lymphoblastic Leukemia, feb 2021. ISSN 16643224.
- [61] Jonsson, H. and Peng, S. L. Forkhead transcription factors in immunology, feb 2005. ISSN 1420682X.
- [62] Juliusson, G. and Hough, R. Leukemia. *Progress in Tumor Research*, 43:87–100, 2016. ISSN 22961887. doi: 10.1159/000447076.
- [63] Kapali, J., Kabat, B. E., Schmidt, K. L., Stallings, C. E., Tippy, M., Jung, D. O., Edwards, B. S., Nantie, L. B., Raetzman, L. T., Navratil, A. M., and Ellsworth, B. S. Foxo1 is required for normal somatotrope differentiation. *Endocrinology*, 157(11):4351–4363, nov 2016. ISSN 19457170. doi: 10.1210/en.2016-1372.
- [64] Karimian, A., Ahmadi, Y., and Yousefi, B. Multiple functions of p21 in cell cycle, apoptosis and transcriptional regulation after DNA damage, jun 2016. ISSN 15687856.
- [65] Katikaneni, D. S. and Jin, L. B cell MHC class II signaling: A story of life and death, jan 2019. ISSN 18791166.
- [66] Kelly, T. N., Li, C., Hixson, J. E., Gu, D., Rao, D. C., Huang, J., Rice, T. K., Chen, J., Cao, J., Li, J., Anderson, C. E., and He, J. Resequencing study identifies rare renin-angiotensin-aldosterone system variants associated with blood pressure salt-sensitivity: The

- gensalt study. *American Journal of Hypertension*, 30(5):495–501, may 2017. ISSN 19417225. doi: 10.1093/ajh/hpx004.
- [67] Ketzner, F., Abdelrasoul, H., Vogel, M., Marienfeld, R., Müschen, M., Jumaa, H., Wirth, T., and Ushmorov, A. CCND3 is indispensable for the maintenance of B-cell acute lymphoblastic leukemia. *Oncogenesis* 2022 11:1, 11(1):1–12, jan 2022. ISSN 2157-9024. doi: 10.1038/s41389-021-00377-0.
- [68] Klein, S., McCormick, F., and Levitzki, A. Killing time for cancer cells. *Nature Reviews Cancer*, 5(7):573–580, jun 2005. ISSN 1474175X. doi: 10.1038/nrc1651.
- [69] Kode, A., Mosialou, I., Silva, B. C., Rached, M. T., Zhou, B., Wang, J., Townes, T. M., Hen, R., DePinho, R. A., Guo, X. E., and Kousteni, S. FOXO1 orchestrates the bone-suppressing function of gut-derived serotonin. *Journal of Clinical Investigation*, 122(10):3490–3503, oct 2012. ISSN 00219738. doi: 10.1172/JCI64906.
- [70] Köhrer, S., Havranek, O., Seyfried, F., Hurtz, C., Coffey, G. P., Kim, E., Ten Hacken, E., Jäger, U., Vanura, K., O’Brien, S., Thomas, D. A., Kantarjian, H., Ghosh, D., Wang, Z., Zhang, M., Ma, W., Jumaa, H., Debatin, K. M., Müschen, M., Meyer, L. H., Davis, R. E., and Burger, J. A. Pre-BCR signaling in precursor B-cell acute lymphoblastic leukemia regulates PI3K/AKT, FOXO1 and MYC, and can be targeted by SYK inhibition. *Leukemia*, 30(6):1246–1254, 2016. ISSN 14765551. doi: 10.1038/leu.2016.9.
- [71] Koschut, D., Ray, D., Li, Z., Giarin, E., Groet, J., Alić, I., Kham, S. K. Y., Chng, W. J., Ariffin, H., Weinstock, D. M., Yeoh, A. E. J., Basso, G., and Nižetić, D. RAS-protein activation but not mutation status is an outcome predictor and unifying therapeutic target for high-risk acute lymphoblastic leukemia. *Oncogene*, 40(4):746–762, nov 2021. ISSN 14765594. doi: 10.1038/s41388-020-01567-7.

- [72] Krivtsov, A. V., Hoshii, T., and Armstrong, S. A. Mixed-lineage leukemia fusions and chromatin in leukemia. *Cold Spring Harbor Perspectives in Medicine*, 7(11), nov 2017. ISSN 21571422. doi: 10.1101/cshperspect.a026658.
- [73] Kudo, A. and Melchers, F. A second gene, VpreB in the lambda 5 locus of the mouse, which appears to be selectively expressed in pre-B lymphocytes. *The EMBO journal*, 6(8):2267–2272, 1987. ISSN 02614189. doi: 10.1002/j.1460-2075.1987.tb02500.x.
- [74] Kuraoka, M., McWilliams, L., and Kelsoe, G. AID expression during B-cell development: Searching for answers, dec 2011. ISSN 0257277X.
- [75] Lanfray, D. and Richard, D. Emerging Signaling Pathway in Arcuate Feeding-Related Neurons: Role of the Acbd7. *Frontiers in Neuroscience*, 11(JUN):328, jun 2017. ISSN 1662-453X. doi: 10.3389/FNINS.2017.00328.
- [76] Lanfray, D., Caron, A., Roy, M. C., Laplante, M., Morin, F., Leprince, J., Tonon, M. C., and Richard, D. Involvement of the Acyl-CoA binding domain containing 7 in the control of food intake and energy expenditure in mice. *eLife*, 5(FEBRUARY2016), feb 2016. ISSN 2050084X. doi: 10.7554/eLife.11742.
- [77] Lebien, T. W. and Tedder, T. F. B lymphocytes: How they develop and function. *Blood*, 112(5):1570–1580, sep 2008. ISSN 00064971. doi: 10.1182/blood-2008-02-078071.
- [78] Leoni, V. and Biondi, A. Tyrosine kinase inhibitors in BCR-ABL positive acute lymphoblastic leukemia. *Haematologica*, 100(3):295, mar 2015. ISSN 15928721. doi: 10.3324/haematol.2015.124016.
- [79] Licht, J. D. Oncogenesis by E2A-PBX1 in ALL: RUNX and more, jul 2020. ISSN 15280020.

- [80] Lin, Y. C., Jhunjhunwala, S., Benner, C., Heinz, S., Welinder, E., Mansson, R., Sigvardsson, M., Hagman, J., Espinoza, C. A., Dutkowsky, J., Ideker, T., Glass, C. K., and Murre, C. A global network of transcription factors, involving E2A, EBF1 and Foxo1, that orchestrates B cell fate. *Nature Immunology*, 11(7):635–643, jul 2010. ISSN 15292908. doi: 10.1038/ni.1891.
- [81] Ma, J., Matkar, S., He, X., and Hua, X. FOXO family in regulating cancer and metabolism, 2018. ISSN 10963650.
- [82] Ma, Y., Yuan, J., Huang, M., Jove, R., and Cress, W. D. Regulation of the cyclin D3 promoter by E2F1. *Journal of Biological Chemistry*, 278(19):16770–16776, may 2003. ISSN 00219258. doi: 10.1074/jbc.M212702200.
- [83] MacDonald, J. I. and Dick, F. A. Posttranslational modifications of the retinoblastoma tumor suppressor protein as determinants of function, nov 2012. ISSN 19476027.
- [84] Malumbres, M. and Barbacid, M. Cell cycle, CDKs and cancer: A changing paradigm, mar 2009. ISSN 1474175X.
- [85] Martin, M. P., Endicott, J. A., and Noble, M. E. Structure-based discovery of cyclin-dependent protein kinase inhibitors, nov 2017. ISSN 00711365.
- [86] Matthias, P. and Rolink, A. G. Transcriptional networks in developing and mature B cells, jun 2005. ISSN 14741733.
- [87] Meier, M., Möller, G., and Adamski, J. Perspectives in Understanding the Role of Human 17 β -Hydroxysteroid Dehydrogenases in Health and Disease. *Annals of the New York Academy of Sciences*, 1155(1):15–24, feb 2009. ISSN 1749-6632. doi: 10.1111/J.1749-6632.2009.03702.X.
- [88] Menzl, I., Zhang, T., Berger-Becvar, A., Grausenburger, R., Heller, G., Prchal-Murphy, M., Edlinger, L., Knab, V. M., Uras, I. Z.,

- Grundschober, E., Bauer, K., Roth, M., Skucha, A., Liu, Y., Hatcher, J. M., Liang, Y., Kwiatkowski, N. P., Fux, D., Hoelbl-Kovacic, A., Kubicek, S., Melo, J. V., Valent, P., Weichhart, T., Grebien, F., Zuber, J., Gray, N. S., and Sexl, V. A kinase-independent role for CDK8 in BCR-ABL1+ leukemia. *Nature Communications*, 10(1):4741, 2019. ISSN 20411723. doi: 10.1038/s41467-019-12656-x.
- [89] Miyazaki, S., Minamida, R., Furuyama, T., Tashiro, F., Yamato, E., Inagaki, S., and Miyazaki, J. I. Analysis of Foxo1-regulated genes using Foxo1-deficient pancreatic β cells. *Genes to Cells*, 17(9):758–767, sep 2012. ISSN 13569597. doi: 10.1111/j.1365-2443.2012.01625.x.
- [90] Monroe, J. G. ITAM-mediated tonic signalling through pre-BCR and BCR complexes, apr 2006. ISSN 14741733.
- [91] Morales, F. and Giordano, A. Overview of CDK9 as a target in cancer research, feb 2016. ISSN 15514005.
- [92] Moser, J., Miller, I., Carter, D., and Spencer, S. L. Control of the restriction point by rb and p21. *Proceedings of the National Academy of Sciences of the United States of America*, 115(35):E8219–E8227, aug 2018. ISSN 10916490. doi: 10.1073/pnas.1722446115.
- [93] Mschen, M. Autoimmunity checkpoints as therapeutic targets in B cell malignancies. *Nature Reviews Cancer*, 18(2):103–116, jan 2018. ISSN 14741768. doi: 10.1038/nrc.2017.111.
- [94] Nemazee, D. Mechanisms of central tolerance for B cells, apr 2017. ISSN 14741741.
- [95] Niesvizky, R., Badros, A. Z., Costa, L. J., Ely, S. A., Singhal, S. B., Stadtmauer, E. A., Haideri, N. A., Yacoub, A., Hess, G., Lentzsch, S., Spicka, I., Chanan-Khan, A. A., Raab, M. S., Tarantolo, S., Vij, R., Zonder, J. A., Huang, X., Jayabalan, D., Di Liberto, M., Huang, X.,

- Jiang, Y., Kim, S. T., Randolph, S., and Chen-Kiang, S. Phase 1/2 study of cyclin-dependent kinase (CDK)4/6 inhibitor palbociclib (PD-0332991) with bortezomib and dexamethasone in relapsed/refractory multiple myeloma. *Leukemia and Lymphoma*, 56(12):3320–3328, dec 2015. ISSN 10292403. doi: 10.3109/10428194.2015.1030641.
- [96] Nuñez, C., Nishimoto, N., Gartland, G. L., Billips, L. G., Burrows, P. D., Kubagawa, H., and Cooper, M. D. B cells are generated throughout life in humans. *Journal of immunology (Baltimore, Md. : 1950)*, 156(2):866–72, 1996. ISSN 0022-1767.
- [97] Obsil, T. and Obsilova, V. Structure/function relationships underlying regulation of FOXO transcription factors, apr 2008. ISSN 09509232.
- [98] Ohnishi, K. and Melchers, F. The nonimmunoglobulin portion of λ 5 mediates cell-autonomous pre-B cell receptor signalling. *Nature Immunology*, 4(9):849–856, aug 2003. ISSN 15292908. doi: 10.1038/ni959.
- [99] Oki, S., Ohta, T., Shioi, G., Hatanaka, H., Ogasawara, O., Okuda, Y., Kawaji, H., Nakaki, R., Sese, J., and Meno, C. Ch IP \square Atlas: a data \square mining suite powered by full integration of public Ch IP \square seq data. *EMBO reports*, 19(12):e46255, dec 2018. ISSN 1469-221X. doi: 10.15252/embr.201846255.
- [100] Osman, S., Mohammad, E., Lidschreiber, M., Stuetzer, A., Bazsó, F. L., Maier, K. C., Urlaub, H., and Cramer, P. The Cdk8 kinase module regulates interaction of the mediator complex with RNA polymerase II. *The Journal of Biological Chemistry*, 296, jan 2021. doi: 10.1016/J.JBC.2021.100734.
- [101] Otero, D. C. and Rickert, R. C. CD19 Function in Early and Late B Cell Development. II. CD19 Facilitates the Pro-B/Pre-B Transition. *The Journal of Immunology*, 171(11):5921–5930, dec 2003. ISSN 0022-1767. doi: 10.4049/jimmunol.171.11.5921.

- [102] Pang, S. H. M., de Graaf, C. A., Hilton, D. J., Huntington, N. D., Carotta, S., Wu, L., and Nutt, S. L. PU.1 is required for the developmental progression of multipotent progenitors to common lymphoid progenitors. *Frontiers in Immunology*, 9(JUN):1264, jun 2018. ISSN 16643224. doi: 10.3389/fimmu.2018.01264.
- [103] Paulsson, K. and Johansson, B. High hyperdiploid childhood acute lymphoblastic leukemia, aug 2009. ISSN 10452257.
- [104] Pelanda, R. and Torres, R. M. Central B-Cell tolerance: Where selection begins. *Cold Spring Harbor Perspectives in Biology*, 4(4):a007146, apr 2012. ISSN 19430264. doi: 10.1101/cshperspect.a007146.
- [105] Peterson, L. F., Boyapati, A., Ranganathan, V., Iwama, A., Tenen, D. G., Tsai, S., and Zhang, D.-E. The Hematopoietic Transcription Factor AML1(RUNX1) Is Negatively Regulated by the Cell Cycle ProteinCyclinD3. *Molecular and Cellular Biology*, 25(23):10205–10219, dec 2005. ISSN 0270-7306. doi: 10.1128/mcb.25.23.10205-10219.2005.
- [106] Peterson, L. F., Boyapati, A., Ranganathan, V., Iwama, A., Tenen, D. G., Tsai, S., and Zhang, D.-E. The Hematopoietic Transcription Factor AML1(RUNX1) Is Negatively Regulated by the Cell Cycle ProteinCyclinD3. *Molecular and Cellular Biology*, 25(23):10205–10219, dec 2005. ISSN 0270-7306. doi: 10.1128/mcb.25.23.10205-10219.2005.
- [107] Pieper, K., Grimbacher, B., and Eibel, H. B-cell biology and development, apr 2013. ISSN 00916749.
- [108] Powers, S. E., Mandal, M., Matsuda, S., Miletic, A. V., Cato, M. H., Tanaka, A., Rickert, R. C., Koyasu, S., and Clark, M. R. Subnuclear cyclin D3 compartments and the coordinated regulation of

- proliferation and immunoglobulin variable gene repression. *Journal of Experimental Medicine*, 209(12):2199–2213, nov 2012. ISSN 00221007. doi: 10.1084/jem.20120800.
- [109] Powers, S. E., Mandal, M., Matsuda, S., Miletic, A. V., Cato, M. H., Tanaka, A., Rickert, R. C., Koyasu, S., and Clark, M. R. Subnuclear cyclin D3 compartments and the coordinated regulation of proliferation and immunoglobulin variable gene repression. *Journal of Experimental Medicine*, 209(12):2199–2213, nov 2012. ISSN 00221007. doi: 10.1084/jem.20120800.
- [110] Radulovich, N., Pham, N.-A., Strumpf, D., Leung, L., Xie, W., Jurisica, I., and Tsao, M.-S. Differential roles of cyclin D1 and D3 in pancreatic ductal adenocarcinoma. *Molecular Cancer*, 9(1):24, 2010. ISSN 1476-4598. doi: 10.1186/1476-4598-9-24.
- [111] Raza, A., Pandey, M. S., Jin, Q., and Mulder, K. M. km23-1/DYNLRB1 regulation of MEK/ERK signaling and R-Ras in invasive human colorectal cancer cells. *Cell Biology International*, 44(1):155–165, jan 2020. ISSN 1095-8355. doi: 10.1002/CBIN.11215.
- [112] Razavipour, S. F., Harikumar, K. B., and Slingerland, J. M. P27 as a transcriptional regulator: New roles in development and cancer, sep 2020. ISSN 15387445.
- [113] Ren, B., Cam, H., Takahashi, Y., Volkert, T., Terragni, J., Young, R. A., and Dynlacht, B. D. E2F integrates cell cycle progression with DNA repair, replication, and G2/M checkpoints. *Genes and Development*, 16(2):245–256, jan 2002. ISSN 08909369. doi: 10.1101/gad.949802.
- [114] Ren, S. and Rollins, B. J. Cyclin C/Cdk3 promotes Rb-dependent G0 exit. *Cell*, 117(2):239–251, apr 2004. ISSN 00928674. doi: 10.1016/S0092-8674(04)00300-9.

- [115] Richter, A., Schoenwaelder, N., Sender, S., Junghanss, C., and Maletzki, C. Cyclin-dependent kinase inhibitors in hematological malignancies—current understanding, (Pre-)clinical application and promising approaches, may 2021. ISSN 20726694.
- [116] Rickert, R. C. New insights into pre-BCR and BCR signalling with relevance to B cell malignancies, jul 2013. ISSN 14741733.
- [117] Roberts, K. G., Li, Y., Payne-Turner, D., Harvey, R. C., Yang, Y.-L., Pei, D., McCastlain, K., Ding, L., Lu, C., Song, G., Ma, J., Becksfort, J., Rusch, M., Chen, S.-C., Easton, J., Cheng, J., Boggs, K., Santiago-Morales, N., Iacobucci, I., Fulton, R. S., Wen, J., Valentine, M., Cheng, C., Paugh, S. W., Devidas, M., Chen, I.-M., Reshmi, S., Smith, A., Hedlund, E., Gupta, P., Nagahawatte, P., Wu, G., Chen, X., Yergeau, D., Vadodaria, B., Mulder, H., Winick, N. J., Larsen, E. C., Carroll, W. L., Heerema, N. A., Carroll, A. J., Grayson, G., Tasian, S. K., Moore, A. S., Keller, F., Frei-Jones, M., Whitlock, J. A., Raetz, E. A., White, D. L., Hughes, T. P., Guidry Auvil, J. M., Smith, M. A., Marcucci, G., Bloomfield, C. D., Mrózek, K., Kohlschmidt, J., Stock, W., Kornblau, S. M., Konopleva, M., Paietta, E., Pui, C.-H., Jeha, S., Relling, M. V., Evans, W. E., Gerhard, D. S., Gastier-Foster, J. M., Mardis, E., Wilson, R. K., Loh, M. L., Downing, J. R., Hunger, S. P., Willman, C. L., Zhang, J., and Mullighan, C. G. Targetable Kinase-Activating Lesions in Ph-like Acute Lymphoblastic Leukemia. *New England Journal of Medicine*, 371(11):1005–1015, sep 2014. ISSN 0028-4793. doi: 10.1056/nejmoa1403088.
- [118] Rodríguez-Hernández, G., Opitz, F. V., Delgado, P., Walter, C., Álvarez-Prado, Á. F., González-Herrero, I., Auer, F., Fischer, U., Janssen, S., Bartenhagen, C., Raboso-Gallego, J., Casado-García, A., Orfao, A., Blanco, O., Alonso-López, D., Rivas, J. D. L., de Tena-Dávila, S. G., Müschen, M., Dugas, M., Criado, F. J. G., Cenador, M. B. G., Vicente-Dueñas, C., Hauer, J., Ramiro, A. R., Sanchez-

- Garcia, I., and Borkhardt, A. Infectious stimuli promote malignant B-cell acute lymphoblastic leukemia in the absence of AID. *Nature Communications*, 10(1):1–10, dec 2019. ISSN 20411723. doi: 10.1038/s41467-019-13570-y.
- [119] Roskoski, R. Cyclin-dependent protein kinase inhibitors including palbociclib as anticancer drugs. *Pharmacological Research*, 107:249–275, may 2016. ISSN 10961186. doi: 10.1016/j.phrs.2016.03.012.
- [120] Rudin, S., Marable, M., and Huang, R. S. The Promise of Pharmacogenomics in Reducing Toxicity During Acute Lymphoblastic Leukemia Maintenance Treatment, apr 2017. ISSN 22103244.
- [121] Rzymiski, T., Mikula, M., Zylkiewicz, E., Dreas, A., Wiklik, K., Golas, A., Wójcik, K., Masiejczyk, M., Wróbel, A., Dolata, I., Kitlinska, A., Statkiewicz, M., Kuklinska, U., Goryca, K., Sapala, L., Grochowska, A., Cabaj, A., Szajewska-Skuta, M., Gabor-Worwa, E., Kucwaj, K., Bialas, A., Radzimierski, A., Combik, M., Woyciechowski, J., Mikulski, M., Windak, R., Ostrowski, J., and Brzózka, K. SEL120-34A is a novel CDK8 inhibitor active in AML cells with high levels of serine phosphorylation of STAT1 and STAT5 transactivation domains. *Oncotarget*, 8(20):33779–33795, 2017. ISSN 19492553. doi: 10.18632/oncotarget.16810.
- [122] Safavi, S., Forestier, E., Golovleva, I., Barbany, G., Nord, K. H., Moorman, A. V., Harrison, C. J., Johansson, B., and Paulsson, K. Loss of chromosomes is the primary event in near-haploid and low-hypodiploid acute lymphoblastic leukemia, jan 2013. ISSN 08876924.
- [123] Sakaguchi, N. and Melchers, F. $\lambda 5$, a new light-chain-related locus selectively expressed in pre-B lymphocytes. *Nature*, 324(6097):579–582, 1986. ISSN 00280836. doi: 10.1038/324579a0.
- [124] Salas, S., Jézéquel, P., Champion, L., Deville, J.-L., Chibon, F., Bartoli, C., Gentet, J.-C., Charbonnel, C., Gouraud, W., Voutsinos-Porche,

- B., Bouchet, A., Duffaud, F., Figarella-Branger, D., and Bouvier, C. Molecular characterization of the response to chemotherapy in conventional osteosarcomas: Predictive value of HSD17B10 and IFITM2. *International Journal of Cancer*, 125(4):851–860, aug 2009. ISSN 1097-0215. doi: 10.1002/IJC.24457.
- [125] Sarruf, D. A., Iankova, I., Abella, A., Assou, S., Miard, S., and Fajas, L. Cyclin D3 Promotes Adipogenesis through Activation of Peroxisome Proliferator-Activated Receptor γ . *Molecular and Cellular Biology*, 25(22):9985–9995, nov 2005. ISSN 0270-7306. doi: 10.1128/mcb.25.22.9985-9995.2005.
- [126] Schmitz, R., Young, R. M., Ceribelli, M., Jhavar, S., Xiao, W., Zhang, M., Wright, G., Shaffer, A. L., Hodson, D. J., Buras, E., Liu, X., Powell, J., Yang, Y., Xu, W., Zhao, H., Kohlhammer, H., Rosenwald, A., Kluin, P., Müller-Hermelink, H. K., Ott, G., Gascoyne, R. D., Connors, J. M., Rimsza, L. M., Campo, E., Jaffe, E. S., Delabie, J., Smeland, E. B., Ogowang, M. D., Reynolds, S. J., Fisher, R. I., Braziel, R. M., Tubbs, R. R., Cook, J. R., Weisenburger, D. D., Chan, W. C., Pittaluga, S., Wilson, W., Waldmann, T. A., Rowe, M., Mbulaiteye, S. M., Rickinson, A. B., and Staudt, L. M. Burkitt lymphoma pathogenesis and therapeutic targets from structural and functional genomics. *Nature*, 490(7418):116–120, aug 2012. ISSN 00280836. doi: 10.1038/nature11378.
- [127] Serra, S. and Chetty, R. p16. *Journal of Clinical Pathology*, 71(10): 853–858, oct 2018. ISSN 0021-9746. doi: 10.1136/JCLINPATH-2018-205216.
- [128] Shin, D. J., Joshi, P., Hong, S. H., Mosure, K., Shin, D. G., and Osborne, T. F. Genome-wide analysis of FoxO1 binding in hepatic chromatin: Potential involvement of FoxO1 in linking retinoid

- signaling to hepatic gluconeogenesis. *Nucleic Acids Research*, 40(22): 11499–11509, dec 2012. ISSN 03051048. doi: 10.1093/nar/gks932.
- [129] Shojaee, S., Chan, L. N., Buchner, M., Cazzaniga, V., Cosgun, K. N., Geng, H., Qiu, Y. H., Von Minden, M. D., Ernst, T., Hochhaus, A., Cazzaniga, G., Melnick, A., Kornblau, S. M., Graeber, T. G., Wu, H., Jumaa, H., and Müschen, M. PTEN opposes negative selection and enables oncogenic transformation of pre-B cells. *Nature Medicine*, 22 (4):379–387, apr 2016. ISSN 1546170X. doi: 10.1038/nm.4062.
- [130] Sicinska, E., Aifantis, I., Le Cam, L., Swat, W., Borowski, C., Yu, Q., Ferrando, A. A., Levin, S. D., Geng, Y., Von Boehmer, H., and Sicinski, P. Requirement for cyclin D3 in lymphocyte development and T cell leukemias. *Cancer Cell*, 4(6):451–461, dec 2003. ISSN 15356108. doi: 10.1016/S1535-6108(03)00301-5.
- [131] Stavnezer, J., Guikema, J. E., and Schrader, C. E. Mechanism and regulation of class switch recombination, 2008. ISSN 07320582.
- [132] Subramanian, A., Tamayo, P., Mootha, V. K., Mukherjee, S., Ebert, B. L., Gillette, M. A., Paulovich, A., Pomeroy, S. L., Golub, T. R., Lander, E. S., and Mesirov, J. P. Gene set enrichment analysis: A knowledge-based approach for interpreting genome-wide expression profiles. *Proceedings of the National Academy of Sciences*, 102(43): 15545 LP – 15550, oct 2005. doi: 10.1073/pnas.0506580102.
- [133] Sung, H., Ferlay, J., Siegel, R. L., Laversanne, M., Soerjomataram, I., Jemal, A., and Bray, F. Global Cancer Statistics 2020: GLOBOCAN Estimates of Incidence and Mortality Worldwide for 36 Cancers in 185 Countries. *CA: A Cancer Journal for Clinicians*, 71(3):209–249, may 2021. ISSN 0007-9235. doi: 10.3322/caac.21660.
- [134] Suski, J. M., Braun, M., Strmiska, V., and Sicinski, P. Targeting cell-cycle machinery in cancer, jun 2021. ISSN 18783686.

- [135] Szilagy, Z. and Gustafsson, C. M. Emerging roles of Cdk8 in cell cycle control. *Biochimica et Biophysica Acta - Gene Regulatory Mechanisms*, 1829(9):916–920, sep 2013. ISSN 18749399. doi: 10.1016/j.bbagr.2013.04.010.
- [136] Tamura, K., Mukai, H., Naito, Y., Yonemori, K., Kodaira, M., Tanabe, Y., Yamamoto, N., Osera, S., Sasaki, M., Mori, Y., Hashigaki, S., Nagasawa, T., Umeyama, Y., and Yoshino, T. Phase I study of palbociclib, a cyclin-dependent kinase 4/6 inhibitor, in Japanese patients. *Cancer Science*, 107(6):755–763, jun 2016. ISSN 13497006. doi: 10.1111/cas.12932.
- [137] Tavian, M., Biasch, K., Sinka, L., Vallet, J., and Péault, B. Embryonic origin of human hematopoiesis, jul 2010. ISSN 02146282.
- [138] Tebbi, C. K. Etiology of acute leukemia: A review, may 2021. ISSN 20726694.
- [139] Teh, J. T., Zhu, W. L., Ilkayeva, O. R., Li, Y., Gooding, J., Casey, P. J., Summers, S. A., Newgard, C. B., and Wang, M. Isoprenylcysteine carboxylmethyltransferase regulates mitochondrial respiration and cancer cell metabolism. *Oncogene*, 34(25):3296–3304, 2015. ISSN 14765594. doi: 10.1038/onc.2014.260.
- [140] Teramoto, N., Pokrovskaja, K., Szekely, L., Polack, A., Yoshino, T., Akagi, T., and Klein, G. EXPRESSION OF CYCLIN D2 AND D3 IN LYMPHOID LESIONS. Technical report, 1999.
- [141] Terwilliger, T. and Abdul-Hay, M. Acute lymphoblastic leukemia: a comprehensive review and 2017 update. *Blood cancer journal*, 7(6): e577, jun 2017. ISSN 20445385. doi: 10.1038/bcj.2017.53.
- [142] Trinh, D. L., Scott, D. W., Morin, R. D., Mendez-Lago, M., An, J., Jones, S. J., Mungall, A. J., Zhao, Y., Schein, J., Steidl, C., Connors, J. M., Gascoyne, R. D., and Marra, M. A. Analysis of FOXO1

- mutations in diffuse large B-cell lymphoma. *Blood*, 121(18):3666–3674, may 2013. ISSN 15280020. doi: 10.1182/blood-2013-01-479865.
- [143] Ubersax, J. A. and Ferrell, J. E. Mechanisms of specificity in protein phosphorylation, 2007. ISSN 14710080.
- [144] Uehara, T., Abe, K., Oginuma, M., Ishitani, S., Yoshihashi, H., Okamoto, N., Takenouchi, T., Kosaki, K., and Ishitani, T. Pathogenesis of CDK8-associated disorder: two patients with novel CDK8 variants and in vitro and in vivo functional analyses of the variants. *Scientific Reports*, 10(1):1–7, oct 2020. ISSN 20452322. doi: 10.1038/s41598-020-74642-4.
- [145] Ushmorov, A. and Wirth, T. FOXO in B-cell lymphopoiesis and B cell neoplasia. *Seminars in Cancer Biology*, 50:132–141, jun 2018. ISSN 10963650. doi: 10.1016/j.semcancer.2017.07.008.
- [146] Van Der Vos, K. E. and Coffey, P. J. FOXO-binding partners: It takes two to tango, apr 2008. ISSN 09509232.
- [147] Van Dongen, J. J., Van Der Velden, V. H., Brüggemann, M., and Orfao, A. Minimal residual disease diagnostics in acute lymphoblastic leukemia: Need for sensitive, fast, and standardized technologies. *Blood*, 125(26):3996–4009, jun 2015. ISSN 15280020. doi: 10.1182/blood-2015-03-580027.
- [148] Vogel, M. J., Xie, L., Guan, H., Tooze, R. M., Maier, T., Kostezka, U., Maier, H. J., Holzmann, K., Chan, F. C., Steidl, C., Reichel, J. B., Weitzer, C. D., Gehringer, F., Kick, A. B., Cesarman, E., Roshal, M., Gascoyne, R. D., Möller, P., Wirth, T., and Ushmorov, A. FOXO1 repression contributes to block of plasma cell differentiation in classical Hodgkin lymphoma. *Blood*, 124(20):3118–3129, nov 2014. ISSN 0006-4971. doi: 10.1182/blood-2014-07-590570.

- [149] Wang, F., Demir, S., Gehringer, F., Osswald, C. D., Seyfried, F., Enzenmüller, S., Eckhoff, S. M., Maier, T., Holzmann, K., Debatin, K. M., Wirth, T., Meyer, L. H., and Ushmorov, A. Tight regulation of FOXO1 is essential for maintenance of B-cell precursor acute lymphoblastic leukemia. *Blood*, 131(26):2929–2942, jun 2018. ISSN 15280020. doi: 10.1182/blood-2017-10-813576.
- [150] Wang, H., Nicolay, B. N., Chick, J. M., Gao, X., Geng, Y., Ren, H., Gao, H., Yang, G., Williams, J. A., Suski, J. M., Keibler, M. A., Sicinska, E., Gerdemann, U., Haining, W. N., Roberts, T. M., Polyak, K., Gygi, S. P., Dyson, N. J., and Sicinski, P. The metabolic function of cyclin D3-CDK6 kinase in cancer cell survival. *Nature*, 546(7658): 426–430, jun 2017. ISSN 14764687. doi: 10.1038/nature22797.
- [151] Weigel, D., Jürgens, G., Küttner, F., Seifert, E., and Jäckle, H. The homeotic gene fork head encodes a nuclear protein and is expressed in the terminal regions of the *Drosophila* embryo. *Cell*, 57(4):645–658, may 1989. ISSN 00928674. doi: 10.1016/0092-8674(89)90133-5.
- [152] Wiemels, J. L., Cazzaniga, G., Daniotti, M., Eden, O. B., Addison, G. M., Masera, G., Saha, V., Biondi, A., and Greaves, M. F. Prenatal origin of acute lymphoblastic leukaemia in children. *Lancet*, 354 (9189):1499–1503, oct 1999. ISSN 01406736. doi: 10.1016/S0140-6736(99)09403-9.
- [153] Wonsey, D. R., Zeller, K. I., and Dang, C. V. The c-Myc target gene PRDX3 is required for mitochondrial homeostasis and neoplastic transformation. *Proceedings of the National Academy of Sciences of the United States of America*, 99(10):6649–6654, may 2002. ISSN 00278424. doi: 10.1073/pnas.102523299.
- [154] Wood, D. J. and Endicott, J. A. Structural insights into the functional diversity of the CDK–cyclin family, sep 2018. ISSN 20462441.

- [155] Xiao, G., Chan, L. N., Klemm, L., Braas, D., Chen, Z., Geng, H., Zhang, Q. C., Aghajani-refah, A., Cosgun, K. N., Sadras, T., Lee, J., Mirzapoiiazova, T., Salgia, R., Ernst, T., Hochhaus, A., Jumaa, H., Jiang, X., Weinstock, D. M., Graeber, T. G., and Müschen, M. B-Cell-Specific Diversion of Glucose Carbon Utilization Reveals a Unique Vulnerability in B Cell Malignancies. *Cell*, 173(2):470–484.e18, apr 2018. ISSN 10974172. doi: 10.1016/j.cell.2018.02.048.
- [156] Xie, L., Ushmorov, A., Leithäuser, F., Guan, H., Steidl, C., Färbing, J., Pelzer, C., Vogel, M. J., Maier, H. J., Gascoyne, R. D., Möller, P., and Wirth, T. FOXO1 is a tumor suppressor in classical Hodgkin lymphoma. *Blood*, 119(15):3503–3511, apr 2012. ISSN 00064971. doi: 10.1182/blood-2011-09-381905.
- [157] Xie, Z., Zhang, Y., Guliaev, A. B., Shen, H., Hang, B., Singer, B., and Wang, Z. The p-benzoquinone DNA adducts derived from benzene are highly mutagenic. *DNA Repair*, 4(12):1399–1409, dec 2005. ISSN 1568-7864. doi: 10.1016/J.DNAREP.2005.08.012.
- [158] Xu, J., Zhu, Y., Wang, F., Zhou, Y., Xia, G., and Xu, W. ICMT contributes to hepatocellular carcinoma growth, survival, migration and chemoresistance via multiple oncogenic pathways. *Biochemical and Biophysical Research Communications*, 518(3):584–589, oct 2019. ISSN 10902104. doi: 10.1016/j.bbrc.2019.08.094.
- [159] Xu, Y., Fairfax, K., Light, A., Huntington, N. D., and Tarlinton, D. M. CD19 differentially regulates BCR signalling through the recruitment of PI3K. *Autoimmunity*, 47(7):430–437, nov 2014. ISSN 1607842X. doi: 10.3109/08916934.2014.921810.
- [160] Yi, M., Zhou, L., Li, A., Luo, S., and Wu, K. Global burden and trend of acute lymphoblastic leukemia from 1990 to 2017. *Aging*, 12(22):22869–22891, nov 2020. ISSN 19454589. doi: 10.18632/aging.103982.

- [161] Zarkowska, T. and Mitnacht, S. Differential phosphorylation of the retinoblastoma protein by G1/S cyclin-dependent kinases. *Journal of Biological Chemistry*, 272(19):12738–12746, may 1997. ISSN 00219258. doi: 10.1074/jbc.272.19.12738.
- [162] Zhang, C., Lian, H., Xie, L., Yin, N., and Cui, Y. LncRNA ELFN1-AS1 promotes esophageal cancer progression by up-regulating GFPT1 via sponging miR-183-3p. *Biological Chemistry*, 401(9):1053–1061, aug 2020. ISSN 14374315. doi: 10.1515/hsz-2019-0430.
- [163] Zhang, K., Li, L., Qi, Y., Zhu, X., Gan, B., DePinho, R. A., Averitt, T., and Guo, S. Hepatic suppression of Foxo1 and Foxo3 causes hypoglycemia and hyperlipidemia in mice. *Endocrinology*, 153(2): 631–646, feb 2012. ISSN 00137227. doi: 10.1210/en.2011-1527.
- [164] Zhang, M., Zhang, L., Hei, R., Li, X., Cai, H., Wu, X., Zheng, Q., and Cai, C. CDK inhibitors in cancer therapy, an overview of recent development. *American journal of cancer research*, 11(5):1913–1935, 2021. ISSN 2156-6976.
- [165] Zhang, N., Liu, L., Fan, N., Zhang, Q., Wang, W., Zheng, M., Ma, L., Li, Y., Shi, L., Zhang, N., Liu, L., Fan, N., Zhang, Q., Wang, W., Zheng, M., Ma, L., Li, Y., and Shi, L. The requirement of SEPT2 and SEPT7 for migration and invasion in human breast cancer via MEK/ERK activation. *Oncotarget*, 7(38):61587–61600, aug 2016. ISSN 1949-2553. doi: 10.18632/ONCOTARGET.11402.
- [166] Zhang, T., Kim, D. H., Xiao, X., Lee, S., Gong, Z., Muzumdar, R., Calabuig-Navarro, V., Yamauchi, J., Harashima, H., Wang, R., Bottino, R., Alvarez-Perez, J. C., Garcia-Ocaña, A., Gittes, G., and Dong, H. H. Foxo1 plays an important role in regulating β -cell compensation for insulin resistance in male mice. *Endocrinology*, 157(3):1055–1070, mar 2016. ISSN 19457170. doi: 10.1210/en.2015-1852.

- [167] Zhang, X., Rastogi, P., Shah, B., and Zhang, L. B lymphoblastic leukemia/lymphoma: New insights into genetics, molecular aberrations, subclassification and targeted therapy, 2017. ISSN 19492553.
- [168] Zheng, Q., Jiang, C., Liu, H., Hao, W., Wang, P., Huang, H., Li, Z., Qian, J., Qian, M., and Zhang, H. Down-Regulated FOXO1 in Refractory/Relapse Childhood B-Cell Acute Lymphoblastic Leukemia. *Frontiers in Oncology*, 10:579673, nov 2020. ISSN 2234943X. doi: 10.3389/fonc.2020.579673.

Chapter 7

Statutory Declaration

I hereby declare that I wrote the present dissertation with the topic:

Cyclin D3 is essential for the maintenance of B-cell acute lymphoblastic leukemia

independently and used no other aids than those cited.

In each individual case, I have clearly identified the source of the passages that are taken word for word or paraphrased from other works.

I also hereby declare that I have carried out my scientific work according to the principles of good scientific practice in accordance with the current „Satzung der Universität Ulm zur Sicherung guter wissenschaftlicher Praxis“ [Rules of the University of Ulm for Assuring Good Scientific Practice].

Ulm,

Franz Ketzer